The Pennsylvania State University

The Graduate School

Department of Chemistry

MOLECULAR SELF-ASSEMBLY FOR BIOLOGICAL INVESTIGATIONS AND NANOSCALE LITHOGRAPHY

A Dissertation in

Chemistry

by

Sarawut Cheunkar

Submitted in Partial Fulfillment
of the Requirements
for the Degree of

Doctor of Philosophy

May 2013

The dissertation of Sarawut Cheunkar was reviewed and approved* by the following:

Christine D. Keating
Professor of Chemistry
Chair of Committee

Anne M. Andrews
Professor of Psychiatry & Biobehavioral Sciences
Dissertation Co-Advisor

Paul S. Weiss
Distinguished Professor of Chemistry & Biochemistry
Dissertation Co-Advisor

John Asbury
Associate Professor of Chemistry
Major Program Committee

David Vandenbergh
Associate Professor of Biobehavioral Health
Outside Field Committee

Barbara J. Garrison
Shapiro Professor of Chemistry
Head of the Department of Chemistry

*Signatures are on file in the Graduate School

ABSTRACT

Small, diffusible molecules when recognized by their binding partners, such as proteins and antibodies, trigger enzymatic activity, cell communication, and immune response. Progress in analytical methods enabling detection, characterization, and visualization of biological dynamics at the molecular level will advance our exploration of complex biological systems. In this dissertation, analytical platforms were fabricated to capture membrane-associated receptors, which are essential proteins in cell signaling pathways. The neurotransmitter serotonin and its biological precursor were immobilized on gold substrates coated with self-assembled monolayers (SAMs) of oligo(ethylene glycol)alkanethiols and their reactive derivatives. The SAM-coated substrates present the biologically selective affinity of immobilized molecules to target native membrane-associated receptors. These substrates were also tested for biospecificity using antibodies.

In addition, small-molecule-functionalized platforms, expressing neurotransmitter pharmacophores, were employed to examine kinetic interactions between G-protein-coupled receptors and their associated neurotransmitters. The binding interactions were monitored using a quartz crystal microbalance equipped with liquid-flow injection. The interaction kinetics of G-protein-coupled serotonin 1A receptor and 5-hydroxytyptophan-functionalized surfaces were studied in a real-time, label-free environment. Key binding parameters, such as equilibrium dissociation constants, binding rate constants, and dissociative half-life, were extracted. These parameters are critical for understanding and comparing biomolecular interactions in modern biomedical research.

By integrating self-assembly, surface functionalization, and nanofabrication, small-molecule microarrays were created for high-throughput screening. A hybrid soft-lithography, called microcontact insertion printing, was used to pattern small molecules at the dilute scales necessary for highly selective biorecognition. By carefully tuning the polar surface energy of polymeric stamps, problems associated with patterning hydrophilic tether molecules inserted into hydrophilic preformed SAMs are surmounted. The patterned substrates presenting neurotransmitter precursors selectively capture membrane-associated receptors. These advances provide new avenues for fabricating small-molecule arrays.

Furthermore, a novel strategy based on a conventional microcontact printing, called chemical lift-off lithography, was invented to overcome the micrometer-scale resolution limits of molecular ink diffusion in soft lithography. Self-assembled monolayers of hydroxyl-terminated alkanethiols, preformed on gold substrates, were selectively removed by oxygen-plasma-treated polymeric stamps in a subtractive stamping process with high pattern fidelity. The covalent interactions formed at the stamp-substrate interface are believed to be responsible for removing not only alkanethiol molecules but also a monolayer of gold atoms from the substrates. A variety of high-resolution patterned features were fabricated, and stamps were cleaned and reused many times without feature deterioration. The remaining SAMs acted as resists for etching exposed gold features. Monolayer backfilling into lifted-off areas enabled patterned protein capture, and 40-nanometer chemical patterns were achieved.

TABLE OF CONTENTS

LIST OF FIGURES

LIST OF TABLES

LIST OF ABBREVIATIONS

Chemicals

5-HT	5-hydroxytryptamine, serotonin
5-HT$_{1A}$	Serotonin 1A receptors
5-HT$_{2C}$	Serotonin 2C receptors
5-HT$_{7}$	Serotonin 7 receptors
AEG	Amine-terminated hexa(ethylene glycol)undecanethiol
Ag	Silver
Au	Gold
BEG	Biotin-terminated hexa(ethylene glycol)undecanethiol
BSA	Bovine serum albumin
Cr	Chromium
Cu	Copper
D1	Dopamine 1 receptors
D12	Perdeuterated 1-dodecanethiol
DA	Dopamine
DIC	Diisopropylcarbodiimide
DNA	Deoxyribonucleic acid
EtOH	Ethanol, ethyl alcohol
FMOC-L-5-HTP	9-fluorenylmethoxycarbonyl-L-5-hydroxytryptophan
FTIC	Fluorescein isothiocyanate
GABA	γ-aminobutyric acid
Ge	Germanium
GPCR	G-protein-coupled receptor
HEG	Carboxyl-terminated hexa(ethylene glycol)undecanethiol
HHEG	Hydrazide-terminated hexa(ethylene glycol)undecanethiol

L-5-HTP	L-5-hydroxytryptophan
LGIC	Ligand-gated ion channel
mAb	Monoclonal antibody
OEG	Oligo(ethylene glycol)
pAb	Polyclonal antibody
PBS	Phosphate buffered saline
Pd	Palladium
PDMS	Polydimethylsiloxane
PEG	Poly(ethylene glycol)
Pt	Platinum
RNA	Ribonucleic acid
Si	Silicon
TEG	Hydroxyl-terminated tri(ethylene glycol)undecanethiol
Tris	Tris(hydroxymethyl)aminomethane, Trizma

Characterization Tools

AFM	Atomic force microscopy
CV	Cyclic voltammetry
HREELS	High resolution electron energy loss spectroscopy
IRRAS	Infrared reflection absorption spectroscopy
PM-IRRAS	Polarization modulation infrared reflection absorption spectroscopy
QCM	Quartz crystal microbalance
SPR	Surface plasmon resonance
STM	Scanning tunneling microscopy
XPS	X-ray photoelectron spectroscopy

Technical Terms

μCIP	Microcontact insertion printing
ANOVA	One way analysis of variance
CLL	Chemical lift-off lithography
DI	Deionized
IR	Infrared
PM	Photoelastic modulator
PZT	Piezoelectric transducer
RF	Radio frequency
RIE	Reactive ion etching
SAM	Self-assembled monolayer
VDW	van der Waals

ACKNOWLEDGMENTS

My journey in graduate school would not have been possible without the love, support, patience, and expertise of so many wonderful people. I would like to take this opportunity to express my gratitude to all these people.

First and foremost, I would like to thank my graduate advisor Prof. Paul Weiss and my co-advisor Prof. Anne Andrews for giving me the opportunity and resources to fulfill the work in this dissertation. I feel very fortunate to experience double professional guidance and perspective from both of you, and I am glad to be called a "hybrid" student. I would also like to thank my committee members: Prof. Christine Keating, Prof. John Asbury, and Prof. David Vandenbergh, for their valuable opinions and comments. I am thankful to Prof. Nicholas Winograd for serving as my former committee member.

To the former and current Weiss group members that I have worked with and learned from, I am very thankful for their generosity and contributions: especially, the colleagues who guided me at the start of the project, Dr. Mitchell Shuster, Dr. Amit Vaish, Dr. Nathan Hohman, Dr. Moonhee Kim, Dr. Ajeet Kumar, and Dr. Shelley Claridge. I sincerely want to thank members of the "Neurochip" project, Dr. Wei-ssu Liao and Huan Cao for working with me through the hard and good time. For the fellows in Young hall basement, I thank Jeffrey Schwartz, Yuxi Zhao, and Andrew Guttentag for your wonderful friendship. I also appreciate Steve Bumbarger and David McMillan for keeping our lab running smoothly. I wish the best of luck for those who come after me.

I would like to dedicate this dissertation to my parents and sister. I very much appreciate their love, encouragement, and endless support. To my mom “Jae Lek” and dad “Por”, who are the most wonderful parents, I am so proud to be your son. You have been pushing me from the beginning to the present, and I couldn’t have become the person I am today without you both in my life.

To Meow, I can’t thank you enough for being a part of my life. You are everything to me for now and for the future. You have been on my side when I have a difficult time. Your love and support will be in my memory forever.

Finally, I gratefully acknowledge support from the Royal Thai Government for providing me a full scholarship to pursue my Ph.D. in United States. Thank you to all staffs who work at the office of Education Affairs, Royal Thai Embassy, in Washington D.C. for their kind help and suggestion, as well as the National Science Foundation, the Kavli Foundation, the Penn State Department of Chemistry, the UCLA Department of Chemistry and Biochemistry, and the California NanoSystems Institute.

Chapter 1

Molecular Self-Assembly for Biological Investigations and Nanoscale Printing

1.1 Introduction

Over the past two decades, our understanding of self-assembly has impacted the development of a broad spectrum of science disciplines including biology, pharmacology, food sciences, engineering, and neuroscience [*1-5*]. State-of-the-art designs at the nano- and micrometer scales have enabled the creation of systems with precisely controlled surface properties that are specific for systems of interest [*6-15*]. These capabilities have been driven, in large part, by advances in instrumentation and new experimental techniques for the self-assembly chemistry and characterization of surfaces comprising "nanoscale building blocks." [*16-23*]. Moreover, significance advances in chemical synthesis offer a wide variety of these building blocks, resulting in the construction of practical models in many applications [*24-28*].

Bioactive surfaces, which have been found to be powerful tools in biological investigations, are one application of self-assembly [*29-31*]. Generally, a bioactive surface is a substrate that has a specific affinity for biological targets such as proteins, peptides, antibodies, DNA, carbohydrates, neurotransmitters, etc [*32-36*]. An underlying principle of bioactive surfaces relies on the immobilization of biomolecules on the surfaces and the recognition of their binding partners in solution at the solid-liquid interface [*37-40*]. Due to the constrained environments and steric hindrance of the

binding partners on the surfaces, the effects of orientation and size of both biorecognition elements become important [*41, 42*]. In addition, the biological environment can complicate investigations due to background noise from non-specific adsorption. Therefore, the type of building blocks used for bioactive surfaces is a crucial factor for surface preparation and biological studies.

When integrated with transducers, bioactive surfaces can be used as "biosensors" for detection and differentiation of biomolecular interactions [*43, 44*]. Materials possessing plasmonic, piezoelectric, or electrochemical properties are common types of transducers. These property arrays offer the advantage of label-free, real-time investigation, leading to the interpretation of physicochemical parameters relevant to the binding interactions [*37, 40, 45-47*]. When combined with soft lithography, bioactive surfaces can be used as platforms, called "biochips" for visualizing and screening the biomolecular targets and even within biological membranes [*12, 48-54*].

Self-assembled monolayers (SAMs) played a crucial role in this dissertation due to their roles in biological investigations and nano- and microscale patterning. Kinetics and thermodynamics of binding interactions of small-molecule neurotransmitters and their biomacromolecule partners were studied by immobilizing their neurotransmitter analogs on SAM-modified substrates. The functionalized substrates, integrated with mass-sensitive devices, were used to monitor biomolecular recognition interactions in a real-time, label-free manner. In addition to biologically-relevant studies, self-assembled monolayers were used as a starting material for fabricating patterned surfaces. The interfacial interactions between an elastomeric stamp and SAMs were found to be key factors for successful patterning.

1.2 Dissertation Overview

The objective of this dissertation is to develop and to utilize substrates with immobilized small molecules to study the biomolecular interactions of membrane-associated proteins, relevant to molecular pharmacology and neuroscience. Chapter 1 focuses the background chemistry knowledge of self-assembled monolayers and their applications, and explains the main experimental techniques used in these studies. Chapter 2 provides a review of the significant literature on the topics of small-molecule signaling in neuroscience, small-molecule neurotransmitter including serotonin (5-HT), and challenges of small-molecule immobilization. The development of small-molecule-functionalized surfaces is discussed. In Chapter 3, 5-hydroxytryptophan (5-HTP)-functionalized surfaces are utilized to study the kinetic aspects of the molecular interactions of G-protein-coupled receptors (GPCRs). These kinetic studies use ligand-bound substrates with label-free, real-time methods. Chapter 4 presents an approach based on surface wettability to fabricate small-molecule arrays for multiplexed screening. Microcontact-insertion printing (μCIP) is utilized to transfer alkanethiol inks from oxygen-plasma-treated polydimethylsiloxane (PDMS) stamps to existing SAM matrices. The relation of treatment time from oxygen plasma and surface wettability is studied to optimize printing conditions. Chapter 5 describes the invention of a new printing technique, chemical lift-off lithography (CLL). In CLL, a PDMS stamp, chemically treated with oxygen plasma, is used to remove alkanethiolates at the conformal contact area. Detail studies were performed to understand the parameters that

lead to subtractive printing. Chapter 6 summarizes all works done in this dissertation, and outlines possible future work.

1.3 Background

1.3.1 Self-Assembly

Whitesides and Grzybowski beautifully define self-assembly as "the autonomous organization of components into patterns or structures without human intervention" [*55*]. Self-assembled patterns and structures can be found in both living and non-living organisms, from the molecular-cluster (10^{-9} m) to the galaxy scales (10^{21} m) [*56-58*]. For instance, cells are examples of self-assembly in biological systems [*59*]. Each individual unit is encapsulated by cell membranes, which are dynamic self-assembled bilayers of phospholipid molecules. These molecules are held together with weak intermolecular forces such as van der Waals, electrostatic, and hydrogen-bonding interactions. The concept of self-assembly has been expanded into a wide range of disciplines from basic research to engineering applications [*60-62*].

1.3.2 Self-Assembled Monolayers

Self-assembled monolayers of organic surfactant molecules on substrates represent a principal subdivision of self-assembled systems. Intrinsic physical properties of individual molecules are responsible for energetically favorable interactions, resulting in the formation of crystalline nanostructures with single-molecule thicknesses [*1, 2*]. The most well-known, highly characterized SAM is based on the assembly of *n*-alkanethiols on gold (Au) substrates (

Figure **1-1**) [*63*]. Interestingly, gold/thiolate SAM system is prototypical for other fields because they are easy to prepare, highly reproducible, notably stable in ambient conditions and flexible for tuning of interfacial properties including wettability, reactivity, conductivity, and resistance [*1, 64-66*]. Although gold is the standard platform for SAM formation due to its inertness, SAMs can be formed on a variety of metal substrates such as platinum (Pt), copper (Cu), silver (Ag), germanium (Ge), etc, making them highly attractive for engineering applications [*67-72*].

In the most general case, an *n*-alkanethiol comprises an alkyl backbone with the n-1 number of methylene units (-CH_2-), a thiol head group (-SH), and a methyl tail group (CH_3-) at the other end. Each molecular component plays a different role in SAM formation and its surface properties. After immersion, the chemisorption of *n*-alkanethiols on Au substrates is kinetically favorable occurred due to the strong gold-sulfur (Au-S) bond formation at ~40 kcal/mol (compared to ~1.5 kcal/mol of heat required for boiling water) [*1, 2*]. The result of fast and strong bond formation quickly leads to nearly full surface coverage (>90%) in approximately 10 s with quasi-ordered structures. The phenomenon involves the thermodynamic-favorable maximization of weak van der Waals interactions between alkyl backbones, favoring the formation of an ordered crystalline lattice with a tilt angle at ~30˚ to the surface normal [*71*]. Further chemisorption increases both the surface coverage and crystallinity. Intensive studies by scanning tunneling microscopy (STM) have shown that alkanethiolate SAMs have several structural features, including domain boundaries, step edges, and vacancy islands (Figure 1-2) [*73, 74*].

In addition to STM techniques, a variety of surface analyses have been utilized to characterize SAMs, such as atomic force microscopy (AFM) [*75-79*], X-ray photoelectron spectroscopy (XPS) [*71, 77, 80-86*], high-resolution electron energy loss spectroscopy (HREELS) [*87*], infrared reflection absorption spectroscopy (IRRAS) [*88-94*], contact angle goniometry, surface plasmon resonance (SPR) [*45, 95*], ellipsometry [*96, 97*], cyclic voltammetry (CV) [*98-100*], and others. These techniques provide additional information, such as composition, structure, and formation energy.

Usually, absorption of *n*-alkanethiol SAMs on metal substrates is done via solution deposition. In some cases, vapor deposition is used as a stand-alone and/or supplementary procedure [*101, 102*]. The most practical solvent for preparing SAMs is ethanol because: it dissolves a variety of alkanethiols, it is inexpensive, it is available in high purity, and it has low toxicity. Others such as tetrahydrofuran, dimethyformamide, methanol, and toluene, etc, can also be used, depending on the solubility of individual adsorbates [*25*]. Research has been carried out to determine the experimental factors that govern the SAM qualities and properties, such as solvent, temperature, concentration, deposition time, purity, chain length, chemical structures, and head and tail groups [*80, 103-107*].

1.3.3 Mixed Self-Assembled Monolayers

Much of the work in this dissertation involves SAMs containing two or more absorbates, called mixed SAMs (Figure 1-3). Mixed SAMs used in many applications requires non-phase segregation [*10, 11, 41*]. Mixed SAMs can be prepared by several methods including codeposition from solution mixtures, adsorption of asymmetric

disulfides, asymetric diakylsulfides, and insertion-directed self-assembly [*1, 23, 108, 109*]. Two main methods that will be employed here involve codeposition and insertion-directed self-assembly. Codeposition allows SAM formation with a wide range of compositions. The surface mole fraction of each component can be adjusted for an individual application by varying the solution mole fraction of each component. However, the solution mole fraction does not proportionally reflect the surface mole fraction, and depends on several factors such as solubility, chain length, and functional group [*42*]. Moreover, these parameters play roles in the homogeneity of the local surface composition of SAMs.

In insertion-directed self-assembly, secondary adsorbate molecules are inserted into existing SAM matrices formed from primary thiol molecules, creating a low-density and non-phase separated mixed SAMs. The quality of mixed SAMs can be controlled by manipulating the defect sizes and density, which are governed by many factors such as formation time, concentrations, temperature, and post- preparation treatment. This method provides a convenient platform to study single-molecule properties and fabrication of biologically-active surfaces.

1.3.4 Self-Assembled Monolayers for Biological Studies

The biological system consists of countless macromolecules ranging from small oligosaccharides to large proteins. The interactions of an individual component influence many processes in living organisms, such as growth, division, communication, and reproduction, leading to the diversity of biochemical and biomedical investigations. A challenge in biological studies is the non-specific interference from the compositional

complexity, making certain fundamental aspects difficult to study. Self-assembled monolayers have become a powerful tool for biological studies. The principle of SAM formation enables the structure and properties of surfaces to be precisely controlled sufficient in order to prevent non-specific protein adsorption [*80, 107, 110-114*].

Surfaces coated with SAMs of ω-functionalized poly-, or oligo-(ethylene glycol) [-$(CH_2CH_2O)_n$-, (PEG, OEG)] alkanethiols on Au substrates are the most common systems that exhibit anti-biofouling properties from other biomolecules (Figure 1-4A) [*113, 115-122*]. Generally, alkanethiols are modified with tri-, tetra-, or hexa-(ethylene glycol) groups. Structurally, the alkyl backbones of PEG-terminated alkanethiols form densely packed, ordered monolayers with nominally all-trans conformation tilted at 30º to surface normal, similar to that of *n*-alkanethiols. The peculiar van der Waals interactions of the (ethylene glycol) tail group influence the SAM structures, forming either in helical or amorphous conformations. The helical structures give quasi-crystalline surfaces, while the amorphous structures produce liquid-like phases [*29, 94, 113*]. Comprehensive studies suggest that both helical and amorphous PEG structures exhibit protein resistance, but not *all-trans* conformations [*113*]. This result supports the hypothesis that the incorporation of interfacial water with PEG moieties may contribute to their ability to resist protein adsorption, however, this is still an open area of investigations [*123*]. Moreover, experimental observations show that PEG SAMs formed on different metal substrates, such as silver (Ag), exhibit distinct PEG structures, thus altering bio-resistance [*113*].

Besides protein resistance, mixed SAMs containing two or more PEG-terminated alkanethiols provide a practical experimental platform to tailor the ligands or

biomolecules of interest for investigations of ligand-protein, protein-protein, protein-carbohydrates, and DNA-protein interactions [*10-13, 114, 124-127*]. One widely used system comprises shorter chain tri(ethylene glycol)-terminated alkanethiols (TEG) and longer, reactive, hexa(ethylene glycol)-terminated alkanethiols, so-called tethers (Figure 1-4B). While the shorter chain resists protein adsorption, the tether, containing reactive terminal groups such as amine (NH_2), carboxyl (COOH), azide (N_3), or hydrazide ($CONH_2$), is responsible for coupling reactions.

1.3.5 Self-Assembled Monolayers for Nano- and Microscale Patterning

Self-assembled monolayers enable the production of deliberate nanostructures with well-defined surface properties. By combining these characteristics with lithography technologies, SAMs can be patterned into sophisticated small-feature architectures, extending their capabilities to a wide range of applications such as high-throughput screening, microfluidic networks, and micro-well arrays [*49, 51, 128*]. Soft lithography, introduced by Whitesides and coworkers in the early 1990's, has been a means for patterning SAMs. The key strategy involves the use of flexible, elastomeric polymer stamp made of PDMS [*2, 21, 129*]. In general (Figure 1-5), a PDMS stamp is molded onto a silicon master containing physical features, resulting in a bas-relief pattern on the PDMS stamp. The SAM features are fabricated by transferring alkanethiols, as molecular inks, from the featured PDMS stamp onto Au substrates only in the conformally contact areas. There are many subfamilies of soft lithography such as microcontact printing (μCP), microcontact displacement printing, and microcontact-insertion printing (μCIP) [*2, 21-23, 108, 130, 131*]. Although exhibiting great success for small-scale patterning,

these techniques are also limited by many factors such as chemical compatibility of inks, stamps, and substrates. Furthermore, pattern fidelity is reduced by lateral diffusion and gas-phase deposition of ink molecules, resulting in a practical resolution limit of <100 nm for alkanethiols on Au when conventional μCP is used.

Later in this dissertation, small-molecule arrays were fabricated using μCIP. By using an oxygen-plasma treatment, hydrophilic alkanethiol molecules were be able to be inked on hydrophobic stamps. This technique allows different types of molecular inks on the PDMS stamp to be inserted into existing SAM matrices at contact areas. The new printing technique, CLL, was developed based on conventional soft lithography [*132*]. By treating a PDMS stamp with oxygen plasma, specific alkanethiols can be withdrawn from Au substrates, creating nano- and microscale features. This technique significantly improves the resolution limit at 100 nm of conventional printing techniques.

1.4 Experimental Techniques

1.4.1 Atomic Force Microscopy

Atomic force microscopy, a scanning probe technique, measures surface profiles with nanometer-scale resolution by measuring intermolecular forces between a probe (tip, <10 nm radius) and surfaces at proximal distances (0.2-10 nm) [*133, 134*]. An advantage of AFM is the sample compatibility with both conductive and non-conductive materials. Therefore, AFM is a versatile tool in a broad range of applications, such as electronics, semiconductors, materials, and biology [*27, 135-139*]. Information given by AFM measurements tremendously advances our understanding of the surface chemistry of materials.

The key concept of AFM relies on the detection of the differential van der Waals interactions between the tip and the surface, which manifests itself as attractive and repulsive forces. The force depends on the spring constant of the cantilever and the distance between the probe and the sample surface. The force can be approximated to be linearly proportional to the cantilever displacement, as described by Hooke's law;

$$F = -kx, \tag{1-1}$$

where F is the force, k is the spring constant, and x is the cantilever deflection. The spring constant of the cantilever typically ranges from 0.1 to 200 N/m, resulting in forces from 10^{-6} to 10^{-13} N.

In general, an atomic force microscope consists of five components, including a piezoelectronic actuator (PZT), a laser source, a position-sensitive photodiode detector, a

feedback controller, and a micro-machined sharp tip (Figure 1-6). The principle of AFM operation is to move the tip laterally over (rasterizing) the surface with feedback mechanisms that enable the PZT scanner to maintain the tip-sample system at constant force, or constant separation. As a result of feedback compensation, the PZT scanner moves vertically causing the deviation of laser intensity on the photodiode detector, which is used to construct the differential surface profiles.

Typically, AFM is operated in one of three modes; non-contact mode, contact mode, and tapping mode [*133*]. In non-contact mode (Figure 1-6A), the tip is maintained at about 0.1 to 10 nm away from the surface and is oscillated at near its natural resonance frequency. By maintain its resonance frequency due to varied sample-tip VDW interactions, surface information can be extracted. However, the oscillating tip in native or simulated, biological environment, such as aqueous solutions, causes tremendous signal interference, making the surface information difficult to interpret. Alternatively, in contact mode (<0.5 nm) (Figure 1-6B), the forces between the tip and the surface remain constant by maintaining a constant cantilever deflection. Contact mode measurement offers the advantages of fast scanning and high resolution, provides surface friction analysis, and is suitable for rough samples. Yet, the strong repulsive force exerted by the tip can damage or deform soft samples. Another popular mode of AFM operation is an intermittently contact mode (0.5-2.0 nm), tapping mode, which is the combination of those two techniques (Figure 1-6C). While scanning, the oscillating tip periodically touches, "taps", on the sample surface at constant tip-sample interactions by maintaining its oscillation amplitudes. This mode allows for high resolution measurements to be made on sample surfaces, in particular soft biological specimens. In this work, extensive AFM

measurements are used to acquire surface topography, analyze protein binding, and examine chemical lift-off lithography.

1.4.2 Quartz Crystal Microbalance

In this work, the quartz crystal microbalance (QCM) is utilized as a label-free biosensor for qualitative and quantitative detection of protein binding on small-molecule-functionalized substrates. The quartz crystal microbalance is a mechanical sensor that has been used in many research fields and industrial instruments [*37, 140*]. Its operating principle relies on the piezoelectric property of a quartz crystal. Applying an alternating potential to metal electrodes on the crystal faces causes a mechanical strain in a shear direction, and thus a crystal oscillation. A number of physical parameters of the quartz crystal including cut plane, density, shear modulus, and thickness govern the oscillating frequency of the quartz crystal. This frequency is called the resonance frequency, f_0, which is described by

$$f_0 = \frac{\sqrt{\mu_q/\rho_q}}{2t_q}, \tag{1-2}$$

where μ_q is the shear modulus, ρ_q is the density, and t_q is the crystal thickness. Another crucial factor to determine its applications is the crystal cut plane. The AT-cut, the most common cut of a quartz crystal, has a cut plane at about 35˚ from the optical z axis. At this angle, a quartz crystal has low temperature coefficient at room temperature, resulting in applications over a wide temperature range [*37*].

For our system, an Au electrode deposited on the quartz crystal is used as a substrate for surface modification with thiol SAMs (Figure 1-7). The binding of proteins

on the SAM-modified quartz crystals cause decreases in frequency, which can be directly correlated to the increase in mass, as described by the Sauerbrey's equation:

$$\Delta f = -\frac{2f_0^2 \Delta m n}{A\sqrt{\mu_q \rho_q}}, \tag{1-3}$$

where Δm is the change in mass, and n is the harmonic number (n = 1, for this system), A is the active measurement area. In this system, f_0 = 10 MHz, A = 0.2 cm^2, μ_q = 2.648 g/cm^3, and ρ_q = 2.947 x 10^{11} g/cm.s^2. Because these values are constant throughout the experiment, the eq.3 can be simplified as:

$$\Delta f = -C_f \Delta m \tag{1-4}$$

where C_f is the calibration constant, equal to 1.1 x 10^9 Hz/g. From this equation, the reduction in the oscillating frequency is directly proportional to the mass bound on the crystal substrate. With the constant calibration number, this translates to 0.88 ng of mass uptake for every 1 Hz change in frequency. The frequency change is measured through an oscillator circuit that consists of a surface-mounted oscillator and an external frequency counter.

1.4.3 Infrared Reflection Absorption Spectroscopy

Infrared reflection absorption spectroscopy and polarization-modulation reflection absorption spectroscopy (PM-IRRAS) are used throughout this dissertation to characterize the surface functional groups and molecular conformation of SAM-functionalized substrates. These techniques are forms of infrared (IR) spectroscopy, differing only instrument configurations. In conventional IR spectroscopy, a molecule absorbs IR light only when its molecular vibration changes internal dipole moments (a

standard selection rule). The absorption causes the depletion of IR intensity at a specific wavelength that depends on molecular vibrations of each functional group. However, conventional IR measurements are limited to systems containing very thin films (< 200 nm) or monolayers, in which the number of molecules on the surface are far less than those in the bulk sample [*90*]. Moreover, diluting the molecule of interest in thin films (mixed SAMs) also decreased the measured adsorption peaks [*10*]. As a result, it is extremely difficult to draw definitive conclusions from IR data due to low signal-to-noise ratios due in part to atmospheric background absorption.

By taking advantages of the surface polarization selectivity, some of the difficulties in the IR measurement can be circumvented. At grazing angle of incidence (~80º from the surface normal), the absorption of *p*-polarized light by a thin film on a metal surface is enhanced, while that of *s*-polarized light is negligible [*90*]. This polarization selectivity results in the IR absorption only when vibrational modes having transition dipole moments perpendicular to the surface. This rule only applies to good conductors such as Au. As a consequence, this particular instrument setup, called IRRAS, is sensitive to the surface functional groups and molecular orientation on metal surfaces. A practical concern of this technique is that the measurement of background references on the separate sample can produce baseline artifacts.

This can be overcome by integrating the IRRAS setup with a photoelastic modulator (PM). The PM device produces both *s*- and *p*-polarized light that are alternated at a high frequency (~50 kHz). Using the same sample, the *p*-polarized light is used to measure the total IR intensity, while *s*-polarized light is effectively used as a baseline

collection of atmospheric background. Subtraction of these light outputs results in the IR spectra that are free from the baseline artifacts.

1.5 Figures

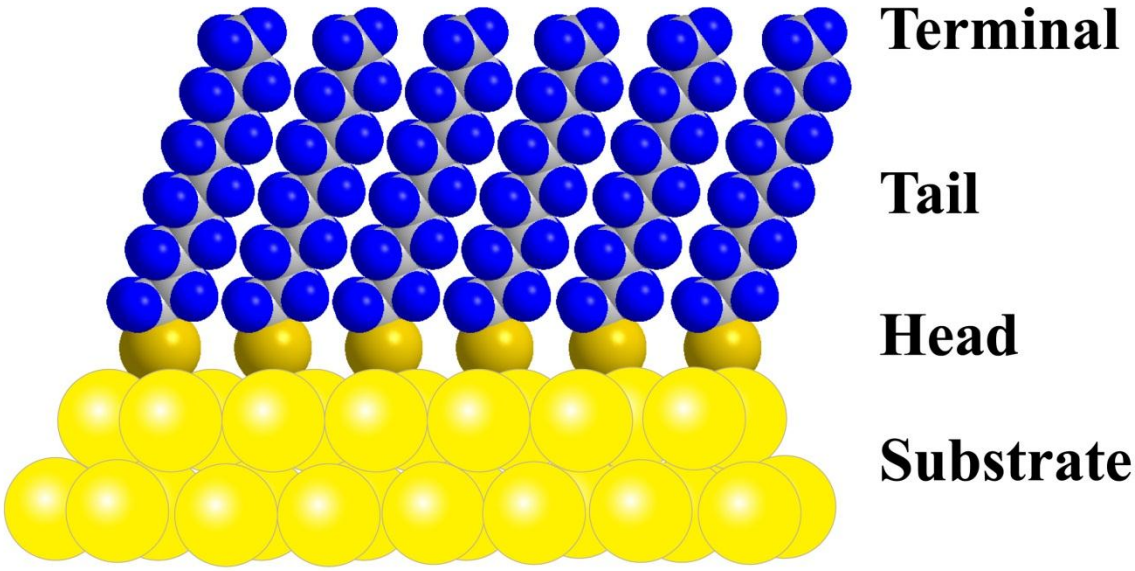

Figure 1-1. A cross-sectional view of a 1-dodecanethiolate self-assembled monolayer (SAM) on a Au{111} substrate. The thiolate head groups (dark yellow) rapidly adsorb on the gold surface with high affinity, leading to nearly complete coverage. Weaker intermolecular forces between the hydrocarbon backbones (blue) drive the ordered SAM lattice. This chemical interaction occurs spontaneously when a gold substrate is exposed to alkanethiol molecules, resulting in one-molecule-thick crystalline nanostructures. Moreover, the surface properties of SAM-modified substrates can be engineered with a wide range of terminal functional groups.

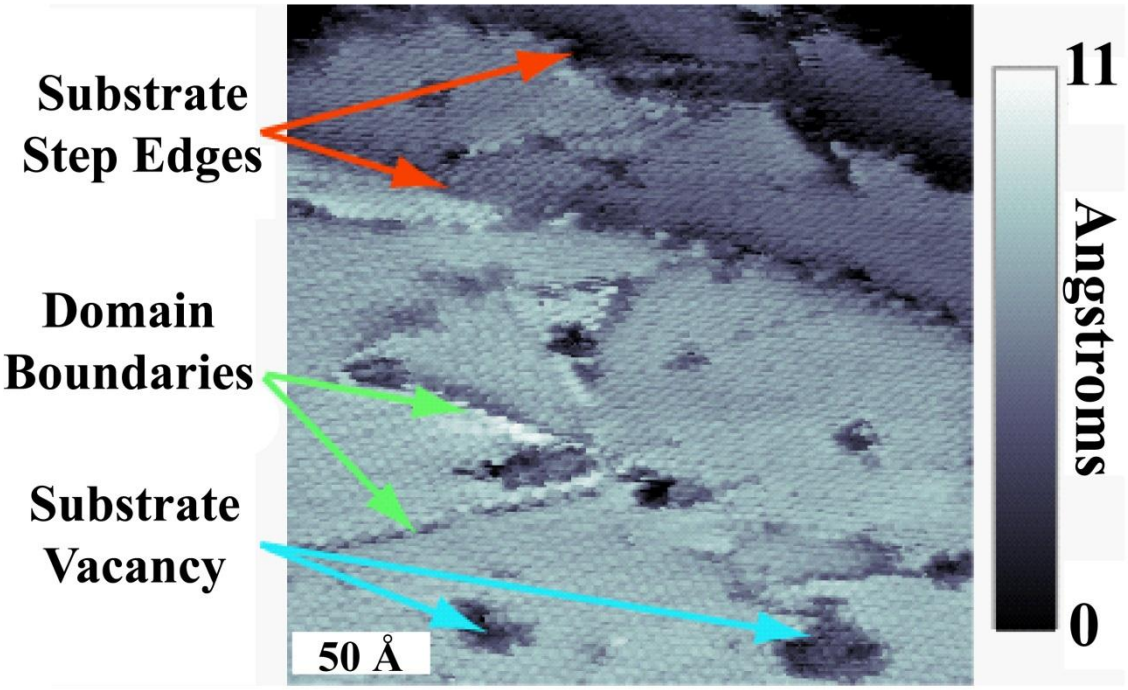

Figure 1-2. A STM image of a 1-dodecanthiolate self-assembled monolayer on Au{111} to illustrate characteristic defects. Defects within the monolayer are inherent to assembly and include substrate step edges (red arrows), domain boundaries (green arrows), and substrate vacancy sites (blue arrows). Substrate step edges occur at the boundary between gold terraces that differ by a single atomic layer. Domain boundaries result from two domains (a domain is a lattice structure with the same tilt direction) of alkanethiolates at the interface. Substrate vacancy islands are believed to be formed as a result of reorganization of gold atoms removed during deposition.

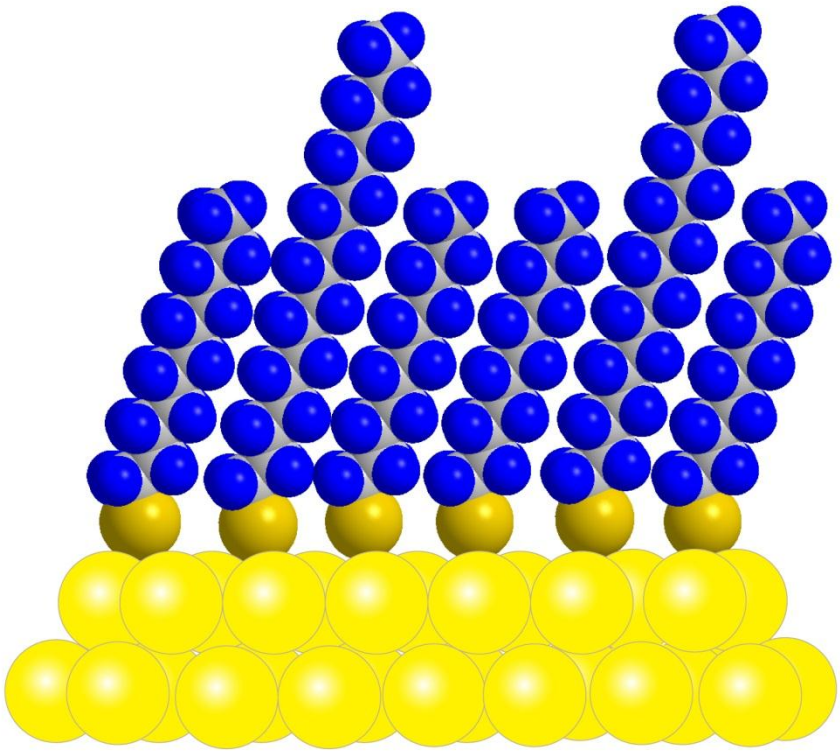

Figure 1-3. Schematic illustration of mixed self-assembled monolayers consisting of two types of alkanethiols with different chain lengths. The surface mole fraction of two molecules on the substrates depends nonlinearly on the solution mole fraction of these molecules. Mixed SAMs can be prepared by several methods such as solution codeposition and solution insertion.

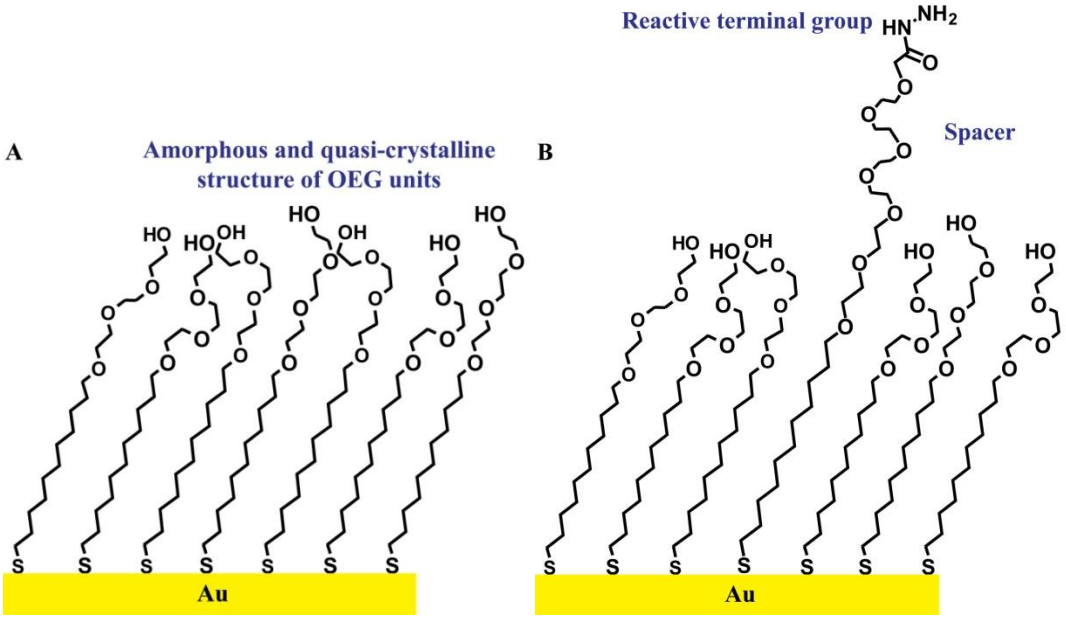

Figure 1-4. Schematic illustration of self-assembled monolayers for biological studies. (A) Self-assembled monolayers functionalized with oligo(ethylene glycol) units (OEG-SAMs) can resist non-specific protein adsorption. Similar to alkanethiols, the thiol head groups and the hydrocarbon backbones are responsible for SAM formation on Au substrates. van der Waals interactions in the OEG backbones cause amorphous and quasi-crystalline helical structures that exhibit protein resistance. (B) Mixed SAMs of different types of OEG molecules present the reactive functional groups, called tethers, in a controllable manner. In general, the tethers contain spacer units (longer OEG) and are spaced away from each other to facilitate the biomolecular recognition of large biomolecules. Various reactive terminal groups may be used as tethers for biomolecule captures, including hydrazide ($CONH_2$ as shown in the figure B), carboxyl (COOH), and amine (NH_2).

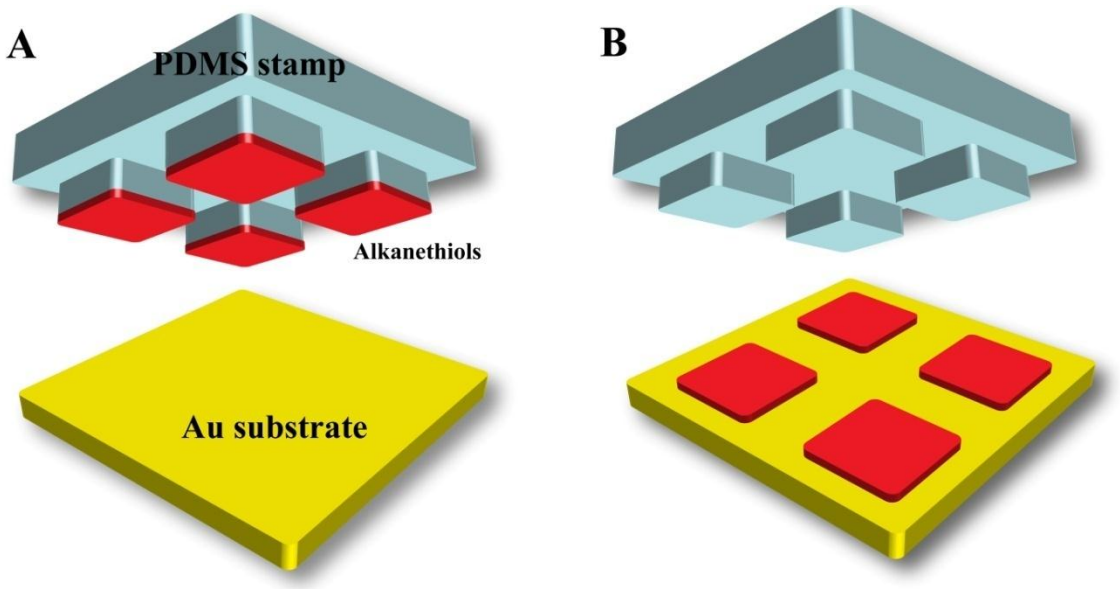

Figure 1-5. Overview of soft lithography for SAM patterning. An elastomeric stamp is made by using polydimethylsiloxane (PDMS) molded from a silicon master containing features, resulting in a bas-relief pattern in the PDMS stamp. (A) Before stamping, alkanethiols are coated on the PDMS stamp as molecular inks. (B) After stamping, the molecular inks are transferred onto Au substrates in conformally contacted areas, resulting in a patterned SAM that replicates the stamp feature. This figure is adapted with permission from reference 225.

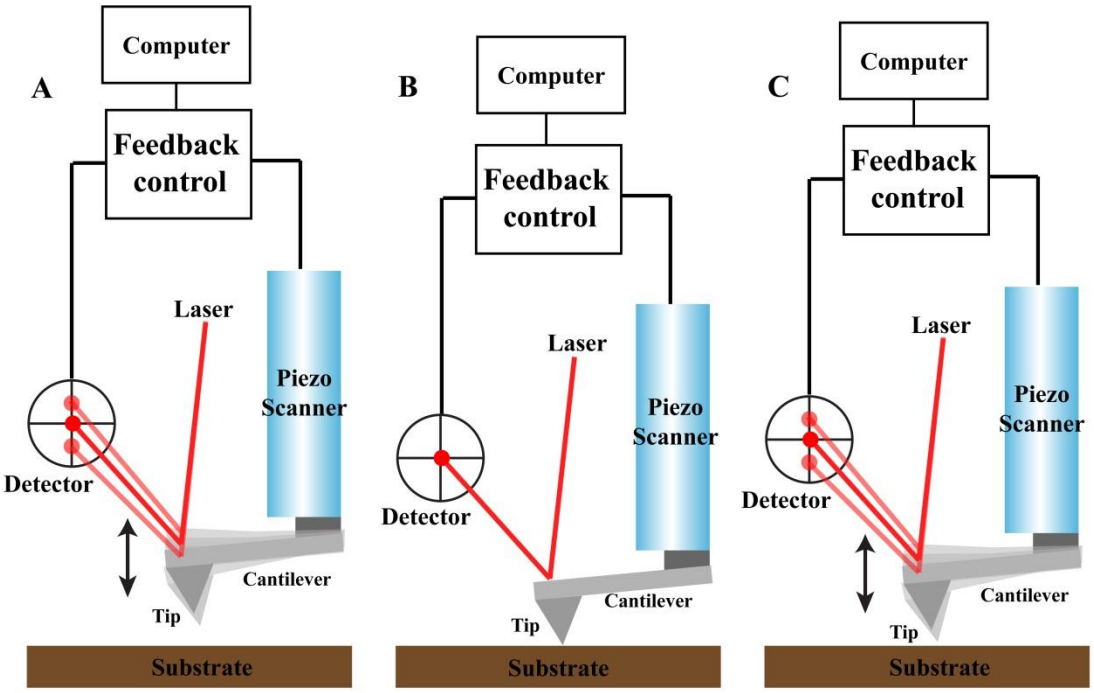

Figure 1-6. Schematic illustrations of AFM in three operating modes. (A) In non-contact mode, the tip-surface distance is maintained while the tip is oscillated at near its resonant frequency. The variations in intermolecular forces between the tip and the surface are monitored to produce surface profiles. (B) In contact mode, the tip is in contact with the substrate. While scanning, the forces between the tip and surface are kept constant by feedback mechanisms, resulting in high-resolution topographic information. (C) A tapping mode AFM, a combination of two previous modes, is operated by bringing the oscillating tip into intermittent contact with the substrate. As a result of oscillation, the tip is periodically tapped on the surface at its resonance frequency. The surface information is acquired by maintaining the oscillation amplitude.

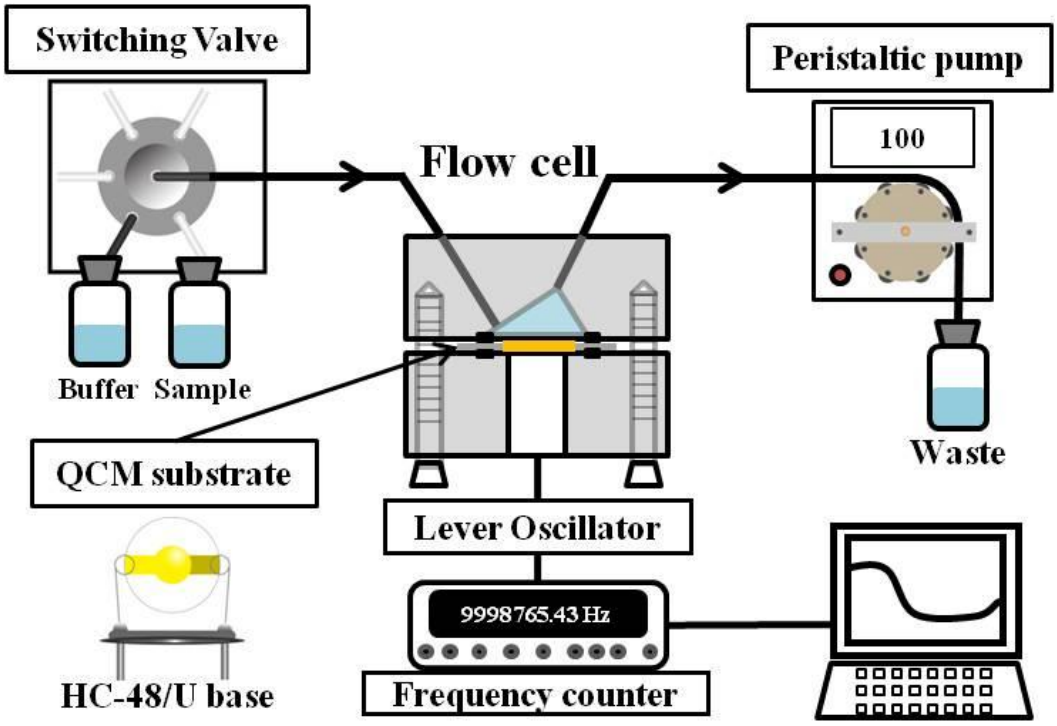

Figure 1-7. Schematic illustration of a QCM instrument. A quartz crystal is coated with Au electrodes on both sides and is attached electrically. Generally, in a biomolecule binding experiment, the quartz crystal is integrated in a liquid flow cell and sealed with a rubber O-ring. The crystal is oscillated by a lever oscillator. While an analyte is flowing over the oscillating crystal, any mass adsorbed on the surface causes reduction in the oscillating frequency. The frequency change is monitored by a frequency counter and recorded for further binding analysis.

1.6 References

1. Love, J. C., Estroff, L. A., Kriebel, J. K., Nuzzo, R. G., and Whitesides, G. M. Self-Assembled Monolayers of Thiolates on Metals as a Form of Nanotechnology. *Chem. Rev.* **2005**, *105*, 1103-1169.
2. Smith, R. K., Lewis, P. A., and Weiss, P. S. Patterning Self-Assembled Monolayers. *Prog. Surf. Sci.* **2004**, *75*, 1-68.
3. Mastrangeli, M., Abbasi, S., Varel, C., Van Hoof, C., Celis, J. P., and Bohringer, K. F. Self-Assembly from Milli- to Nanoscales: Methods and Applications. *J. Micromech. Microeng.* **2009**, *19*, 83001-83073.
4. Whitesides, G. M., Mathias, J. P., and Seto, C. T. Molecular Self-Assembly and Nanochemistry: A Chemical Strategy for the Synthesis of Nanostructures. *Science* **1991**, *254*, 1312-1319.
5. Kovtyukhova, N. I., Martin, B. R., Mbindyo, J. K. N., Mallouk, T. E., Cabassi, M., and Mayer, T. S. Layer-by-Layer Self-Assembly Strategy for Template Synthesis of Nanoscale Devices. *Mater. Sci. Eng. C* **2002**, *19*, 255-262.
6. Blattler, T., Huwiler, C., Ochsner, M., Stadler, B., Solak, H., Voros, J., and Grandin, H. M. Nanopatterns with Biological Functions. *J. Nanosci. Nanotechnol.* **2006**, *6*, 2237-2264.
7. Piner, R. D., Zhu, J., Xu, F., Hong, S. H., and Mirkin, C. A. "Dip-Pen" Nanolithography. *Science* **1999**, *283*, 661-663.

8. Hampton, J. R., Dameron, A. A., and Weiss, P. S. Double-Ink Dip-Pen Nanolithography Studies Elucidate Molecular Transport. *J. Am. Chem. Soc.* **2006**, *128*, 1648-1653.

9. Anderson, M. E., Smith, R. K., Donhauser, Z. J., Hatzor, A., Lewis, P. A., Tan, L. P., Tanaka, H., Horn, M. W., and Weiss, P. S. Exploiting Intermolecular Interactions and Self-Assembly for Ultrahigh Resolution Nanolithography. *J. Vac. Sci. Technol. B* **2002**, *20*, 2739-2744.

10. Shuster, M. J., Vaish, A., Szapacs, M. E., Anderson, M. E., Weiss, P. S., and Andrews, A. M. Biospecific Recognition of Tethered Small Molecules Diluted in Self-Assembled Monolayers. *Adv. Mater.* **2008**, *20*, 164-167.

11. Vaish, A., Shuster, M. J., Cheunkar, S., Singh, Y. S., Weiss, P. S., and Andrews, A. M. Native Serotonin Membrane Receptors Recognize 5-Hydroxytryptophan-Functionalized Substrates: Enabling Small-Molecule Recognition. *ACS Chem. Neurosci.* **2010**, *1*, 495-504.

12. Vaish, A., Shuster, M. J., Cheunkar, S., Weiss, P. S., and Andrews, A. M. Tuning Stamp Surface Energy for Soft Lithography of Polar Molecules to Fabricate Bioactive Small-Molecule Microarrays. *Small* **2011**, *7*, 1471-1479.

13. Shuster, M. J., Vaish, A., Cao, H. H., Guttentag, A. I., McManigle, J. E., Gibb, A. L., Martinez, M. M., Nezarati, R. M., Hinds, J. M., Liao, W. S., Weiss, P. S., and Andrews, A. M. Patterning Small-Molecule Biocapture Surfaces: Microcontact Insertion Printing vs. Photolithography. *Chem. Commun.* **2011**, *47*, 10641-10643.

14. Shuster, M. J., Vaish, A., Gilbert, M. L., Martinez-Rivera, M., Nezarati, R. M., Weiss, P. S., and Andrews, A. M. Comparison of Oligo(Ethylene

Glycol)Alkanethiols Versus *N*-Alkanethiols: Self-Assembly, Insertion, and Functionalization. *J. Phys. Chem. C* **2011**, *115*, 24778-24787.

15. Vaish, A., Liao, W. S., Shuster, M. J., Hinds, J. M., Weiss, P. S., and Andrews, A. M. Thin Gold Film-Assisted Fluorescence Spectroscopy for Biomolecule Sensing. *Anal. Chem.* **2011**, *83*, 7451-7456.

16. Stranick, S. J., Atre, S. V., Parikh, A. N., Wood, M. C., Allara, D. L., Winograd, N., and Weiss, P. S. Nanometer-Scale Phase Separation in Mixed Composition Self-Assembled Monolayers. *Nanotechnology* **1996**, *7*, 438-442.

17. Dunbar, T. D., Cygan, M. T., Bumm, L. A., McCarty, G. S., Burgin, T. P., Reinerth, W. A., Jones, L., Jackiw, J. J., Tour, J. M., Weiss, P. S., and Allara, D. L. Combined Scanning Tunneling Microscopy and Infrared Spectroscopic Characterization of Mixed Surface Assemblies of Linear Conjugated Guest Molecules in Host Alkanethiolate Monolayers on Gold. *J. Phys. Chem. B* **2000**, *104*, 4880-4893.

18. Lewis, P. A., Donhauser, Z. J., Mantooth, B. A., Smith, R. K., Bumm, L. A., Kelly, K. F., and Weiss, P. S. Control and Placement of Molecules via Self-Assembly. *Nanotechnology* **2001**, *12*, 231-237.

19. Lewis, P. A., Smith, R. K., Kelly, K. F., Bumm, L. A., Reed, S. M., Clegg, R. S., Gunderson, J. D., Hutchison, J. E., and Weiss, P. S. The Role of Buried Hydrogen Bonds in Self-Assembled Mixed Composition Thiols on Au{111}. *J. Phys. Chem. B* **2001**, *105*, 10630-10636.

20. Mantooth, B. A., and Weiss, P. S. Fabrication, Assembly, and Characterization of Molecular Electronic Components. *Proceedings of the IEEE* **2003**, *9*, 1785-1802.

21. Dameron, A. A., Hampton, J. R., Smith, R. K., Mullen, T. J., Gillmor, S. D., and Weiss, P. S. Microdisplacement Printing. *Nano Lett.* **2005**, *5*, 1834-1837.

22. Srinivasan, C., Mullen, T. J., Hohman, J. N., Anderson, M. E., Dameron, A. A., Andrews, A. M., Dickey, E. C., Horn, M. W., and Weiss, P. S. Scanning Electron Microscopy of Nanoscale Chemical Patterns. *ACS Nano* **2007**, *1*, 191-201.

23. Mullen, T. J., Srinivasan, C., Hohman, J. N., Gillmor, S. D., Shuster, M. J., Horn, M. W., Andrews, A. M., and Weiss, P. S. Microcontact Insertion Printing. *Appl. Phys. Lett.* **2007**, *90*, 063114-063117.

24. Hohman, J. N., Zhang, P., Morin, E. I., Han, P., Kim, M., Kurland, A. R., McClanahan, P. D., Balema, V. P., and Weiss, P. S. Self-Assembly of Carboranethiol Isomers on Au{111}: Intermolecular Interactions Determined by Molecular Dipole Orientations. *ACS Nano* **2009**, *3*, 527-536.

25. Kim, M., Hohman, J. N., Cao, Y., Houk, K. N., Ma, H., Jen, A. K. Y., and Weiss, P. S. Creating Favorable Geometries for Directing Organic Photoreactions in Alkanethiolate Monolayers. *Science* **2011**, *331*, 1312-1315.

26. Pathem, B. K., Zheng, Y. B., Payton, J. L., Song, T.-B., Yu, B.-C., Tour, J. M., Yang, Y., Jensen, L., and Weiss, P. S. Effect of Tether Conductivity on the Efficiency of Photoisomerization of Azobenzene-Functionalized Molecules on Au{111}. *J. Phys. Chem. Lett.* **2012**, *3*, 2388-2394.

27. Drew, M. E., Chworos, A., Oroudjev, E., Hansma, H., and Yamakoshi, Y. A Tripod Molecular Tip for Single Molecule Ligand-Receptor Force Spectroscopy by AFM. *Langmuir* **2010**, *26*, 7117-7125.

28. Chiang, P. T., Mielke, J., Godoy, J., Guerrero, J. M., Alemany, L. B., Villagomez, C. J., Saywell, A., Grill, L., and Tour, J. M. Toward a Light-Driven Motorized Nanocar: Synthesis and Initial Imaging of Single Molecules. *ACS Nano* **2012**, *6*, 592-597.

29. Schreiber, F. Self-Assembled Monolayers: From Simple Model Systems to Biofunctionalized Interfaces. *J. Phys. Condens. Matter* **2004**, *16*, R881-R900.

30. Samanta, D., and Sarkar, A. Immobilization of Bio-Macromolecules on Self-Assembled Monolayers: Methods and Sensor Applications. *Chem. Soc. Rev.* **2011**, *40*, 2567-2592.

31. Arya, S. K., Solanki, P. R., Datta, M., and Malhotra, B. D. Recent Advances in Self-Assembled Monolayers Based Biomolecular Electronic Devices. *Biosensors Bioelectron.* **2009**, *24*, 2810-2817.

32. Lee, Y. S., and Mrksich, M. Protein Chips: From Concept to Practice. *Trends Biotechnol.* **2002**, *20*, S14-S18.

33. Lee, K. B., Park, S. J., Mirkin, C. A., Smith, J. C., and Mrksich, M. Protein Nanoarrays Generated by Dip-Pen Nanolithography. *Science* **2002**, *295*, 1702-1705.

34. Wang, T. T., and Muthuswamy, J. Immunosensor for Detection of Inhibitory Neurotransmitter Gamma-Aminobutyric Acid Using Quartz Crystal Microbalance. *Anal. Chem.* **2008**, *80*, 8576-8582.

35. Chen, Y., Nakamoto, K., Niwa, O., and Corn, R. M. On-Chip Synthesis of RNA Aptamer Microarrays for Multiplexed Protein Biosensing with SPR Imaging Measurements. *Langmuir* **2012**, *28*, 8281-8285.

36. Funder, E. D., Jensen, A. B., Torring, T., Kodal, A. L. B., Azcargorta, A. R., and Gothelf, K. V. Synthesis of Dopamine and Serotonin Derivatives for Immobilization on a Solid Support. *J. Org. Chem.* **2012**, *77*, 3134-3142.

37. Cheng, C. I., Chang, Y. P., and Chu, Y. H. Biomolecular Interactions and Tools for Their Recognition: Focus on the Quartz Crystal Microbalance and Its Diverse Surface Chemistries and Applications. *Chem. Soc. Rev.* **2012**, *41*, 1947-1971.

38. Heyse, S., Stora, T., Schmid, E., Lakey, J. H., and Vogel, H. Emerging Techniques for Investigating Molecular Interactions at Lipid Membranes. *Biochim. Biophys. Acta: Rev. Biomem.* **1998**, *1376*, 319-338.

39. Cooper, M. A. Optical Biosensors in Drug Discovery. *Nat. Rev. Drug Discov.* **2002**, *1*, 515-528.

40. Homola, J., Yee, S. S., and Gauglitz, G. Surface Plasmon Resonance Sensors: Review. *Sens. Actuat. B-Chem.* **1999**, *54*, 3-15.

41. Lahiri, J., Isaacs, L., Grzybowski, B., Carbeck, J. D., and Whitesides, G. M. Biospecific Binding of Carbonic Anhydrase to Mixed SAMs Presenting Benzenesulfonamide Ligands: A Model System for Studying Lateral Steric Effects. *Langmuir* **1999**, *15*, 7186-7198.

42. Lahiri, J., Isaacs, L., Tien, J., and Whitesides, G. M. A Strategy for the Generation of Surfaces Presenting Ligands for Studies of Binding Based on an Active Ester as a Common Reactive Intermediate: A Surface Plasmon Resonance Study. *Anal. Chem.* **1999**, *71*, 777-790.

43. Marx, K. A. Quartz Crystal Microbalance: A Useful Tool for Studying Thin Polymer Films and Complex Biomolecular Systems at the Solution-Surface Interface. *Biomacromolecules* **2003**, *4*, 1099-1120.

44. de Kloe, G. E., Retra, K., Geitmann, M., Kallblad, P., Nahar, T., van Elk, R., Smit, A. B., van Muijlwijk-Koezen, J. E., Leurs, R., Irth, H., Danielson, U. H., and de Esch, I. J. Surface Plasmon Resonance Biosensor Based Fragment Screening Using Acetylcholine Binding Protein Identifies Ligand Efficiency Hot Spots (Le Hot Spots) by Deconstruction of Nicotinic Acetylcholine Receptor A7 Ligands. *J. Med. Chem.* **2010**, *53*, 7192-7201.

45. Peterlinz, K. A., and Georgiadis, R. In Situ Kinetics of Self-Assembly by Surface Plasmon Resonance Spectroscopy. *Langmuir* **1996**, *12*, 4731-4740.

46. Bailey, K., Bally, M., Leifert, W., Voros, J., and McMurchie, T. G-Protein Coupled Receptor Array Technologies: Site Directed Immobilisation of Liposomes Containing the H1-Histamine or M2-Muscarinic Receptors. *Proteomics* **2009**, *9*, 2052-2063.

47. Mori, T., Toyoda, M., Ohtsuka, T., and Okahata, Y. Kinetic Analyses for Bindings of Concanavalin a to Dispersed and Condensed Mannose Surfaces on a Quartz Crystal Microbalance. *Anal. Biochem.* **2009**, *395*, 211-216.

48. Xia, Y. N., and Whitesides, G. M. Soft Lithography. *Angew. Chem. Int. Ed.* **1998**, *37*, 551-575.

49. Kane, R. S., Takayama, S., Ostuni, E., Ingber, D. E., and Whitesides, G. M. Patterning Proteins and Cells Using Soft Lithography. *Biomaterials* **1999**, *20*, 2363-2376.

50. Michel, B., Bernard, A., Bietsch, A., Delamarche, E., Geissler, M., Juncker, D., Kind, H., Renault, J. P., Rothuizen, H., Schmid, H., Schmidt-Winkel, P., Stutz, R., and Wolf, H. Printing Meets Lithography: Soft Approaches to High-Resolution Printing. *IBM Journal of Research and Development* **2001**, *45*, 697-719.

51. Whitesides, G. M., Ostuni, E., Takayama, S., Jiang, X. Y., and Ingber, D. E. Soft Lithography in Biology and Biochemistry. *Annu. Rev. Biomed. Eng.* **2001**, *3*, 335-373.

52. Ng, J. M. K., Gitlin, I., Stroock, A. D., and Whitesides, G. M. Components for Integrated Poly(Dimethylsiloxane) Microfluidic Systems. *Electrophoresis* **2002**, *23*, 3461-3473.

53. Burridge, K. A., Figa, M. A., and Wong, J. Y. Patterning Adjacent Supported Lipid Bilayers of Desired Composition to Investigate Receptor-Ligand Binding under Shear Flow. *Langmuir* **2004**, *20*, 10252-10259.

54. Christman, K. L., Enriquez-Rios, V. D., and Maynard, H. D. Nanopatterning Proteins and Peptides. *Soft Matter* **2006**, *2*, 928-939.

55. Whitesides, G. M., and Grzybowski, B. Self-Assembly at All Scales. *Science* **2002**, *295*, 2418-2421.

56. Schmidt-Mende, L., Fechtenkotter, A., Mullen, K., Moons, E., Friend, R. H., and MacKenzie, J. D. Self-Organized Discotic Liquid Crystals for High-Efficiency Organic Photovoltaics. *Science* **2001**, *293*, 1119-1122.

57. Nelson, J. Solar Energy-Solar Cells by Self-Assembly? *Science* **2001**, *293*, 1059-1060.

58. Loudet, J. C., Barois, P., and Poulin, P. Colloidal Ordering from Phase Separation in a Liquid-Crystalline Continuous Phase. *Nature* **2000**, *407*, 611-613.

59. Whitesides, G. M. The 'Right' Size in Nanobiotechnology. *Nat. Biotechnol.* **2003**, *21*, 1161-1165.

60. Jakubith, S., Rotermund, H. H., Engel, W., von Oertzen, A., and Ertl, G. Spatiotemporal Concentration Patterns in a Surface Reaction: Propagating and Standing Waves, Rotating Spirals, and Turbulence. *Phys. Rev. Lett.* **1990**, *65*, 3013-3016.

61. Aizenberg, J., Black, A. J., and Whitesides, G. M. Control of Crystal Nucleation by Patterned Self-Assembled Monolayers. *Nature* **1999**, *398*, 495-498.

62. Voigt, N. V., Torring, T., Rotaru, A., Jacobsen, M. F., Ravnsbaek, J. B., Subramani, R., Mamdouh, W., Kjems, J., Mokhir, A., Besenbacher, F., and Gothelf, K. V. Single-Molecule Chemical Reactions on DNA Origami. *Nat. Nanotechnol.* **2010**, *5*, 200-203.

63. Nuzzo, R. G., and Allara, D. L. Adsorption of Bifunctional Organic Disulfides on Gold Surfaces. *J. Am. Chem. Soc.* **1983**, *105*, 4481-4483.

64. Nuzzo, R. G., Zegarski, B. R., and Dubois, L. H. Fundamental-Studies of the Chemisorption of Organosulfur Compounds on Au(111) - Implications for Molecular Self-Assembly on Gold Surfaces. *J. Am. Chem. Soc.* **1987**, *109*, 733-740.

65. Dubois, L. H., Zegarski, B. R., and Nuzzo, R. G. Fundamental-Studies of Microscopic Wetting on Organic-Surfaces. 2. Interaction of Secondary

Adsorbates with Chemically Textured Organic Monolayers. *J. Am. Chem. Soc.* **1990**, *112*, 570-579.

66. Nuzzo, R. G., Dubois, L. H., and Allara, D. L. Fundamental Studies of Microscopic Wetting on Organic Surfaces. 1. Formation and Structural Characterization of a Self-Consistent Series of Polyfunctional Organic Monolayers. *J. Am. Chem. Soc.* **1990**, *112*, 558-569.

67. Hulteen, J. C., Treichel, D. A., Smith, M. T., Duval, M. L., Jensen, T. R., and Van Duyne, R. P. Nanosphere Lithography: Size-Tunable Silver Nanoparticle and Surface Cluster Arrays. *J. Phys. Chem. B* **1999**, *103*, 3854-3863.

68. Hohman, J. N., Kim, M., Bednar, H. R., Lawrence, J. A., McClanahan, P. D., and Weiss, P. S. Simple, Robust Molecular Self-Assembly on Germanium. *Chem. Sci.* **2011**, *2*, 1334-1343.

69. Hohman, J. N., Kim, M., Lawrence, J. A., McClanahan, P. D., and Weiss, P. S. High-Fidelity Chemical Patterning on Oxide-Free Germanium. *J. Phys: Condens. Matter* **2012**, *24*, 164214.

70. Laibinis, P. E., Hickman, J. J., Wrighton, M. S., and Whitesides, G. M. Orthogonal Self-Assembled Monolayers: Alkanethiols on Gold and Alkane Carboxylic Acids on Alumina. *Science* **1989**, *245*, 845-847.

71. Laibinis, P. E., Whitesides, G. M., Allara, D. L., Tao, Y. T., Parikh, A. N., and Nuzzo, R. G. Comparison of the Structures and Wetting Properties of Self-Assembled Monolayers of N-Alkanethiols on the Coinage Metal Surfaces, Copper, Silver, and Gold. *J. Am. Chem. Soc.* **1991**, *113*, 7152-7167.

72. Love, J. C., Wolfe, D. B., Haasch, R., Chabinyc, M. L., Paul, K. E., Whitesides, G. M., and Nuzzo, R. G. Formation and Structure of Self-Assembled Monolayers of Alkanethiolates on Palladium. *J. Am. Chem. Soc.* **2003**, *125*, 2597-2609.

73. Poirier, G. E. Characterization of Organosulfur Molecular Monolayers on Au(111) Using Scanning Tunneling Microscopy. *Chem. Rev.* **1997**, *97*, 1117-1128.

74. Schreiber, F. Structure and Growth of Self-Assembling Monolayers. *Prog. Surf. Sci.* **2000**, *65*, 151-256.

75. Klein, H., Blanc, W., Pierrisnard, R., Fauquet, C., and Dumas, P. Self-Assembled Monolayers of Decanethiol on Au(111)/Mica. *Eur. Phys. J. B* **2000**, *14*, 371-376.

76. Li, Y., Maynor, B. W., and Liu, J. Electrochemical AFM "Dip-Pen" Nanolithography. *J. Am. Chem. Soc.* **2001**, *123*, 2105-2106.

77. Han, S. M., Ashurst, W. R., Carraro, C., and Maboudian, R. Formation of Alkanethiol Monolayer on Ge(111). *J. Am. Chem. Soc.* **2001**, *123*, 2422-2425.

78. Jiang, S. Y. Molecular Simulation Studies of Self-Assembled Monolayers of Alkanethiols on Au(111). *Mol. Phys.* **2002**, *100*, 2261-2275.

79. Giessibl, F. J. Advances in Atomic Force Microscopy. *Rev. Mod. Phys.* **2003**, *75*, 949-983.

80. Pale-Grosdemange, C., Simon, E. S., Prime, K. L., and Whitesides, G. M. Formation of Self-Assembled Monolayers by Chemisorption of Derivatives of Oligo(Ethylene Glycol) of Structure $HS(CH_2)_{11}(OCH_2CH_2)_mOH$ on Gold. *J. Am. Chem. Soc.* **1991**, *113*, 12-20.

81. Laibinis, P. E., Fox, M. A., Folkers, J. P., and Whitesides, G. M. Comparisons of Self-Assembled Monolayers on Silver and Gold: Mixed Monolayers Derived from $HS(CH_2)_{21}X$ and $HS(CH_2)_{10}Y$ (X, Y = CH_3, CH_2OH) Have Similar Properties. *Langmuir* **1991**, *7*, 3167-3173.

82. Bensebaa, F., Yu, Z., Deslandes, Y., Kruus, E., and Ellis, T. H. XPS Study of Metal-Sulfur Bonds in Metal-Alkanethiolate Materials. *Surf. Sci.* **1998**, *405*, L472-L476.

83. Beulen, M. W. J., Bugler, J., Lammerink, B., Geurts, F. A. J., Biemond, E., van Leerdam, K. G. C., van Veggel, F., Engbersen, J. F. J., and Reinhoudt, D. N. Self-Assembled Monolayers of Heptapodant Beta-Cyclodextrins on Gold. *Langmuir* **1998**, *14*, 6424-6429.

84. Rieley, H., Kendall, G. K., Zemicael, F. W., Smith, T. L., and Yang, S. H. X-Ray Studies of Self-Assembled Monolayers on Coinage Metals. 1. Alignment and Photooxidation in 1,8-Octanedithiol and 1-Octanethiol on Au. *Langmuir* **1998**, *14*, 5147-5153.

85. Speller, S., Rauch, T., Bomermann, J., Borrmann, P., and Heiland, W. Surface Structures of S on Pd(111). *Surf. Sci.* **1999**, *441*, 107-116.

86. Zharnikov, M., and Grunze, M. Spectroscopic Characterization of Thiol-Derived Self-Assembling Monolayers. *J. Phys. Condens. Matter* **2001**, *13*, 11333-11365.

87. Duwez, A. S. Exploiting Electron Spectroscopies to Probe the Structure and Organization of Self-Assembled Monolayers: A Review. *J. Electron. Spectrosc. Relat. Phenom.* **2004**, *134*, 97-138.

88. Allara, D. L., and Nuzzo, R. G. The Application of Reflection Infrared and Surface Enhanced Raman-Spectroscopy to the Characterization of Chemisorbed Organic Disulfides on Au. *J. Electron. Spectrosc. Relat. Phenom.* **1983**, *30*, 11.

89. Raddatz, S., Mueller-Ibeler, J., Kluge, J., Wass, L., Burdinski, G., Havens, J. R., Onofrey, T. J., Wang, D., and Schweitzer, M. Hydrazide Oligonucleotides: New Chemical Modification for Chip Array Attachment and Conjugation. *Nucleic Acids Res.* **2002**, *30*, 4793-4802.

90. Brian L. Frey, R. M. C., and Stephen C. Weibel. (2002) Polarization-Modulation Approaches to Reflection-Absorption Spectroscopy In *Handbook of Vibrational Spectroscopy* (Griffiths, C. J. M. a. P., Ed.), p 1042, John Wiley & Sons, Inc.

91. Liu, Z., and Amiridis, M. D. FT-IRRAS Quantitative Analysis of Specific Avidin Adsorption on Biotinylated Au Surfaces. *Surf. Sci.* **2005**, *596*, 117-125.

92. Liu, Z., and Amiridis, M. D. Quantitative FT-IRRAS Spectroscopic Studies of the Interaction of Avidin with Biotin on Functionalized Quartz Surfaces. *J. Phys. Chem. B* **2005**, *109*, 16866-16872.

93. Yang, M., Teeuwen, R. L. M., Giesbers, M., Baggerman, J., Arafat, A., de Wolf, F. A., van Hest, J. C. M., and Zuilhof, H. One-Step Photochemical Attachment of NHS-Terminated Monolayers onto Silicon Surfaces and Subsequent Functionalization. *Langmuir* **2008**, *24*, 7931-7938.

94. Zorn, S., Martin, N., Gerlach, A., and Schreiber, F. Real-Time Pmirras Studies of in Situ Growth of $C_{11}(EG_6)OMe$ on Gold and Immersion Effects. *PCCP* **2010**, *12*, 8986-8991.

95. Nemetz, A., Fischer, T., Ulman, A., and Knoll, W. Surface Plasmon Enhanced Raman Spectroscopy with $HS(CH_2)_{21}OH$ on Different Metals. *J. Chem. Phys.* **1993**, *98*, 5912-5919.

96. Tour, J. M., Jones, L., Pearson, D. L., Lamba, J. J. S., Burgin, T. P., Whitesides, G. M., Allara, D. L., Parikh, A. N., and Atre, S. Self-Assembled Monolayers and Multilayers of Conjugated Thiols, Alpha, Omega-Dithiols, and Thioacetyl-Containing Adsorbates. Understanding Attachments between Potential Molecular Wires and Gold Surfaces. *J. Am. Chem. Soc.* **1995**, *117*, 9529-9534.

97. Valiokas, R., Svedhem, S., Svensson, S. C. T., and Liedberg, B. Self-Assembled Monolayers of Oligo(Ethylene Glycol)-Terminated and Amide Group Containing Alkanethiolates on Gold. *Langmuir* **1999**, *15*, 3390-3394.

98. Caldwell, W. B., Campbell, D. J., Chen, K., Herr, B. R., Mirkin, C. A., Malik, A., Durbin, M. K., and Dutta, P. A Highly Ordered Self-Assembled Monolayer Film of an Azobenzenealkanethiol on Au(111) - Electrochemical Properties and Structural Characterization by Synchrotron X-Ray-Diffraction, Atomic-Force Microscopy, and Surface-Enhanced Raman-Spectroscopy. *J. Am. Chem. Soc.* **1995**, *210*, 6071-6082.

99. Tao, Y. T., Wu, C. C., Eu, J. Y., Lin, W. L., Wu, K. C., and Chen, C. H. Structure Evolution of Aromatic-Derivatized Thiol Monolayers on Evaporated Gold. *Langmuir* **1997**, *13*, 4018-4023.

100. Mullen, T. J., Zhang, P. P., Srinivasan, C., Horn, M. W., and Weiss, P. S. Combining Electrochemical Desorption and Metal Deposition on Patterned Self-Assembled Monolayers. *J. Electroanal. Chem.* **2008**, *621*, 229-237.

101. Donhauser, Z. J., Price, D. W., Tour, J. M., and Weiss, P. S. Control of Alkanethiolate Monolayer Structure Using Vapor-Phase Annealing. *J. Am. Chem. Soc.* **2003**, *125*, 11462-11463.

102. Kumar, A. S., Ye, T., Takami, T., Yu, B. C., Flatt, A. K., Tour, J. M., and Weiss, P. S. Reversible Photo-Switching of Single Azobenzene Molecules in Controlled Nanoscale Environments. *Nano Lett.* **2008**, *8*, 1644-1648.

103. Bain, C. D., Troughton, E. B., Tao, Y. T., Evall, J., Whitesides, G. M., and Nuzzo, R. G. Formation of Monolayer Films by the Spontaneous Assembly of Organic Thiols from Solution onto Gold. *J. Am. Chem. Soc.* **1989**, *111*, 321-335.

104. Nuzzo, R. G., Korenic, E. M., and Dubois, L. H. Studies of the Temperature-Dependent Phase Behavior of Long Chain N-Alkyl Thiol Monolayers on Gold. *J. Chem. Phys.* **1990**, *93*, 767-773.

105. Dubois, L. H., Zegarski, B. R., and Nuzzo, R. G. Temperature Induced Reconstruction of Model Organic-Surfaces. *J. Electron. Spectrosc. Relat. Phenom.* **1990**, *54*, 1143-1152.

106. Laibinis, P. E., Nuzzo, R. G., and Whitesides, G. M. Structure of Monolayers Formed by Coadsorption of 2 Normal-Alkanethiols of Different Chain Lengths on Gold and Its Relation to Wetting. *J. Phys. Chem.* **1992**, *96*, 5097-5105.

107. Prime, K. L., and Whitesides, G. M. Adsorption of Proteins onto Surfaces Containing End-Attached Oligo(Ethylene Oxide): A Model System Using Self-Assembled Monolayers. *J. Am. Chem. Soc.* **1993**, *115*, 10714-10721.

108. Fuchs, D. J., and Weiss, P. S. Insertion of 1,10-Decanedithiol in Decanethiolate Self-Assembled Monolayers on Au{111}. *Nanotechnology* **2007**, *18*, 044021.

109. Jung, C., Dannenberger, O., Xu, Y., Buck, M., and Grunze, M. Self-Assembled Monolayers from Organosulfur Compounds: A Comparison between Sulfides, Disulfides, and Thiols. *Langmuir* **1998**, *14*, 1103-1107.

110. Mrksich, M., and Whitesides, G. M. (1997) Using Self-Assembled Monolayers That Present Oligo(Ethylene Glycol) Groups to Control the Interactions of Proteins with Surfaces, In *Poly(Ethylene Glycol): Chemistry and Biological Applications* (Harris, J. M., and Zalipsky, S., Eds.), pp 361-373.

111. Mrksich, M., Chen, C. S., Xia, Y., Dike, L. E., Ingber, D. E., and Whitesides, G. M. Controlling Cell Attachment on Contoured Surfaces with Self-Assembled Monolayers of Alkanethiolates on Gold. *Proc. Natl. Acad. Sci. USA* **1996**, *93*, 10775-10778.

112. Deng, L., Mrksich, M., and Whitesides, G. M. Self-Assembled Monolayers of Alkanethiolates Presenting Tri(Propylene Sulfoxide) Groups Resist the Adsorption of Protein. *J. Am. Chem. Soc.* **1996**, *118*, 5136-5137.

113. Harder, P., Grunze, M., Dahint, R., Whitesides, G. M., and Laibinis, P. E. Molecular Conformation in Oligo(Ethylene Glycol)-Terminated Self-Assembled Monolayers on Gold and Silver Surfaces Determines Their Ability to Resist Protein Adsorption. *J. Phys. Chem. B* **1998**, *102*, 426-436.

114. Roberts, C., Chen, C. S., Mrksich, M., Martichonok, V., Ingber, D. E., and Whitesides, G. M. Using Mixed Self-Assembled Monolayers Presenting RGD and $(EG)_3OH$ Groups to Characterize Long-Term Attachment of Bovine Capillary Endothelial Cells to Surfaces. *J. Am. Chem. Soc.* **1998**, *120*, 6548-6555.

115. Herrwerth, S., Eck, W., Reinhardt, S., and Grunze, M. Factors That Determine the Protein Resistance of Oligoether Self-Assembled Monolayers: Internal Hydrophilicity, Terminal Hydrophilicity, and Lateral Packing Density. *J. Am. Chem. Soc.* **2003**, *125*, 9359-9366.

116. Wang, R. L. C., Kreuzer, H. J., and Grunze, M. Molecular Conformation and Solvation of Oligo(Ethylene Glycol)-Terminated Self-Assembled Monolayers and Their Resistance to Protein Adsorption. *J. Phys. Chem. B* **1997**, *101*, 9767-9773.

117. Feldman, K., Hähner, G., Spencer, N. D., Harder, P., and Grunze, M. Probing Resistance to Protein Adsorption of Oligo(Ethylene Glycol)-Terminated Self-Assembled Monolayers by Scanning Force Microscopy. *J. Am. Chem. Soc.* **1999**, *121*, 10134-10141.

118. Pertsin, A. J., Grunze, M., Kreuzer, H. J., and Wang, R. L. C. The Effect of Electrostatic Fields on an Oligo(Ethylene Glycol) Terminated Alkanethiol Self-Assembled Monolayer. *PCCP* **2000**, *2*, 1729-1733.

119. Wang, R. L. C., Kreuzer, H. J., Grunze, M., and Pertsin, A. J. The Effect of Electrostatic Fields on an Oligo(Ethylene Glycol) Molecule: Dipole Moments, Polarizabilities, and Field Dissociation. *PCCP* **2000**, *2*, 1721-1727.

120. Zolk, M., Eisert, F., Pipper, J., Herrwerth, S., Eck, W., Buck, M., and Grunze, M. Solvation of Oligo(Ethylene Glycol)-Terminated Self-Assembled Monolayers Studied by Vibrational Sum Frequency Spectroscopy. *Langmuir* **2000**, *16*, 5849-5852.

121. Schwendel, D., Dahint, R., Herrwerth, S., Schloerholz, M., Eck, W., and Grunze, M. Temperature Dependence of the Protein Resistance of Poly- and

Oligo(Ethylene Glycol)-Terminated Alkanethiolate Monolayers. *Langmuir* **2001**, *17*, 5717-5720.

122. Chan, Y. H. M., Schweiss, R., Werner, C., and Grunze, M. Electrokinetic Characterization of Oligo- and Poly(Ethylene Glycol)-Terminated Self-Assembled Monolayers on Gold and Glass Surfaces. *Langmuir* **2003**, *19*, 7380-7385.

123. Skoda, M. W. A., Jacobs, R. M. J., Willis, J., and Schreiber, F. Hydration of Oligo(Ethylene Glycol) Self-Assembled Monolayers Studied Using Polarization Modulation Infrared Spectroscopy. *Langmuir* **2007**, *23*, 970-974.

124. Mirkin, C. A., Letsinger, R. L., Mucic, R. C., and Storhoff, J. J. A DNA-Based Method for Rationally Assembling Nanoparticles into Macroscopic Materials. *Nature* **1996**, *382*, 607-609.

125. Mbindyo, J. K. N., Reiss, B. D., Martin, B. R., Keating, C. D., Natan, M. J., and Mallouk, T. E. DNA-Directed Assembly of Gold Nanowires on Complementary Surfaces. *Adv. Mater.* **2001**, *13*, 249-254.

126. Lange, S. A., Benes, V., Kern, D. P., Horber, J. K. H., and Bernard, A. Microcontact Printing of DNA Molecules. *Anal. Chem.* **2004**, *76*, 1641-1647.

127. Mrksich, M., Grunwell, J. R., and Whitesides, G. M. Biospecific Adsorption of Carbonic Anhydrase to Self-Assembled Monolayers of Alkanethiolates That Present Benzenesulfonamide Groups on Gold. *J. Am. Chem. Soc.* **1995**, *117*, 12009-12010.

128. Zhao, X. M., Xia, Y. N., and Whitesides, G. M. Soft Lithographic Methods for Nano-Fabrication. *J. Mater. Chem.* **1997**, *7*, 1069-1074.

129. Lahiri, J., Ostuni, E., and Whitesides, G. M. Patterning Ligands on Reactive SAMs by Microcontact Printing. *Langmuir* **1999**, *15*, 2055-2060.

130. Mullen, T. J., Srinivasan, C., Shuster, M. J., Horn, M. W., Andrews, A. M., and Weiss, P. S. Hybrid Approaches to Nanometer-Scale Patterning: Exploiting Tailored Intermolecular Interactions. *J. Nanopart. Res.* **2008**, *10*, 1231-1240.

131. Saavedra, H. M., Mullen, T. J., Zhang, P. P., Dewey, D. C., Claridge, S. A., and Weiss, P. S. Hybrid Strategies in Nanolithography. *Rep. Prog. Phys.* **2010**, *73*, 036501.

132. Liao, W. S., Cheunkar, S., Cao, H. H., Bednar, H. R., Weiss, P. S., and Andrews, A. M. Subtractive Patterning via Chemical Lift-Off Lithography. *Science* **2012**, *337*, 1517-1521.

133. Jalili, N., and Laxminarayana, K. A Review of Atomic Force Microscopy Imaging Systems: Application to Molecular Metrology and Biological Sciences. *Mechatronics* **2004**, *14*, 907-945.

134. Dawn, B. A. (2001) *Scanning Probe Microscopy and Spectroscopy: Theory, Techniques, and Applications*, 2nd ed., Wiley-VCH, Inc., New York.

135. Yang, Y., Tsukahara, K., and Sawayama, S. Performance and Methanogenic Community of Rotating Disk Reactor Packed with Polyurethane During Thermophilic Anaerobic Digestion. *Mater. Sci. Eng. C* **2007**, *27*, 767-772.

136. Liang, J., and Scoles, G. Nanografting of Alkanethiols by Tapping Mode Atomic Force Microscopy. *Langmuir* **2007**, *23*, 6142-6147.

137. Salaita, K., Wang, Y., and Mirkin, C. A. Applications of Dip-Pen Nanolithography. *Nat. Nanotechnol.* **2007**, *2*, 145-155.

138. Barrera, N. P., Henderson, R. M., and Edwardson, J. M. Determination of the Architecture of Ionotropic Receptors Using AFM Imaging. *Pflugers Arch.* **2008**, *456*, 199-209.

139. Shim, W., Braunschweig, A. B., Liao, X., Chai, J. N., Lim, J. K., Zheng, G. F., and Mirkin, C. A. Hard-Tip, Soft-Spring Lithography. *Nature* **2011**, *469*, 516-521.

140. Arlett, J. L., Myers, E. B., and Roukes, M. L. Comparative Advantages of Mechanical Biosensors. *Nat. Nanotechnol.* **2011**, *6*, 203-215.

Chapter 2

Small-Molecule-Functionalized Substrates For Biomacromolecule Capture

2.1 Introduction

2.1.1 Significance of Small Molecules in Cell Signaling

In biological systems, small molecules (<700-800 Da) play regulatory roles in both enzymatic activities and signal transmission [*1-6*]. Specifically, in the brain, signal transmission by small, diffusible molecules, called neurotransmitters, enables interneuronal communication, which regulates a wide range of physiological responses, such as cell growth, gene expression, and activation of membrane potential [*7-10*]. Typically, neurotransmitters can be classified as amino acids, monoamines, peptides, and others [*11, 12*]. The signaling process occurs when neurotransmitters are released from presynaptic neurons to an intercellular space between neurons, called a synaptic cleft. The released neurotransmitters, carrying chemical information, are mediated by specific cell surface receptors in postsynaptic neurons, commonly known as membrane-associated receptors, leading to signal transduction into the inside of cells [*13*]. Different types of signal transduction are transmitted through various classes of receptors, including enzyme-linked receptors, ligand-gated ion channels (LGICs), and G-protein-coupled receptors [*14, 15*]. Changing the three-dimensional conformation of these receptors upon neurotransmitter association is the major key for ion channel opening, G-protein activation cycle, and enzyme subunit dimerization [*13*].

2.1.2 G-Protein-Coupled Receptors as Targets for Small-Molecule Drugs

Among three classes of receptors, GPCRs are the largest family of membrane-associated receptors [*16*]. Commonly, their structure consists of an extracellular N-terminal domain, an intracellular C-terminal domain, and seven transmembrane-spanning domains [*13, 17, 18*]. Because GPCRs recognize a number of small molecules, they are implicated in diverse physiological functions, such as vision, smell, taste, and behavior and mood regulation [*10*]. Alterations of GPCR function are thus believed to be relevant in major neuropsychiatric disorders, including anxiety, depression, and Alzheimer's and Parkinson's diseases [*19-21*]. It has been estimated that nearly half of all available drugs on the market target at this class of receptors [*22, 23*].

The pharmacological development of therapeutic agents for these receptors has been driven toward small active compounds (ligands) that modulate GPCR bioactivity [*16, 22*]. This is because they are easy to solubillize, and they diffuse and permeate in biological environments [*24*]. Their advantages are also supported by the Lipinski's rules, which describe the upper limits of molecular weight and/or lipophilicity that increase the risk of both toxicity and cross-reactivity [*25*]. Synthetic ligands are principally designed to yield high selectivity to the "orthosteric site" (the main binding pocket) of some GPCRs [*16, 25*]. These ligands can act as agonists, inverse agonists, and antagonists, which regulate different cellular activities that exhibit specific responses. The binding of an agonist activates GPCR functions, while an inverse agonist reduces receptor activities [*25*]. An antagonist produces a neutral effect to GPCRs by preventing the agonist binding, thus inhibiting GPCR activities [*25*]. This is the basic understanding for

extensive pharmaceutical development, which can be adopted for many types of receptors. However, due to the highly specific interaction at the orthosteric site, only a small fraction of drugs is available in the market [*16*].

In addition to the specific binding at the orthosteric site, some GPCRs can also interact with ligands at different sites, called allosteric sites [*16*]. The binding of ligands at the allosteric binding site has long been known for LGICs, in which their functions can be controlled by two ligands simultaneously [*26, 27*]. A typical mechanism of action of these ligands potentiates or inhibits receptor activation by its natural ligand. Due to the action at a less conserved binding site, allosteric ligands have been attractive targets for drug design. Many GPCRs that have been found to interact with these ligands include adenosine, muscarinic, dopamine, and glutamate receptors [*28-30*]. Benzodiazepines are an example of potentiated allosteric ligands of aminobutyric acid receptors [*31*]. They treat anxiety and sleep disorders without inducing the potentially lethal effects of direct-acting GABA receptor agonists.

An alternative approach for modulating GPCR function is to use ligands containing both orthosteric and allosteric pharmacophores [*32*]. Two active compounds are connected by a chemical linker, yielding bitopic hybrid ligands. These types of molecules are designed to act at two different binding sites on the same receptor [*33*].

2.2 Small-Molecule-Immobilized Substrates as Tools for Biological Investigations

2.2.1 General Considerations of Small-Molecule Immobilization

Besides their significance, mentioned above, small molecules can be used as tools for chemical genetic study and the discovery of orphan receptors in both peripheral and central nervous systems [*4, 34, 35*]. Progress towards elucidating the roles of orphan receptors and functional regulation compounds is supported by advancing in bioanalytical models, allowing studies of these particular aspects. Among analytical models, the immobilization of biologically active compounds on surfaces (bound ligands) to capture their binding partners in solution has been widely recognized [*36-39*].

Small-molecule immobilization on surfaces has several key requirements to achieve suitable platforms for biorecognition studies. The bound ligands must retain bioactivity comparable to that of free molecules in solution [*40, 41*]. This brings a challenge such that some epitopes, limited in number on small molecules, are not available after ligand attachment, resulting in possible bioaffinity alteration [*42, 43*]. In chemical biology, a highly conserved binding site on an individual biomolecule requires all functional groups for site-specific interactions. This difficulty has been seen in pharmacological development when rational drug design relies on few protein models, yielding high failure rates in the clinic [*25, 44*]. In contrast, this challenge is less important for large biomolecules for which many function groups are available for tethering without changing the physicochemical properties of binding sites [*45, 46*].

An additional criterion relates to the accessibility of surface-bound ligands to their large biomolecules. In general, the sizes of biomolecules, such as proteins and antibodies,

are approximately 2 to 10 nm in diameter, which is relatively large compared to small-molecule ligands [*47*]. Besides, due to constrained environments, the size mismatch between large binding partners in solution and small-molecule ligands on surfaces can significantly hinder biomolecular recognition (Figure 2-1). This difficulty can be obviated by controlling the surface density of small-molecule ligands in a manner such that they are not in proximity, providing a sufficient space for interactions [*48*]. Moreover, densely packed ligands with moieties, such as carboxyls and amines, on surfaces can enhance attractive van der Waals and strong hydrogen bonding interactions, leading to non-specific adsorption from biomolecules and other complex components in heterogeneous biological samples. Hence, strategies to achieve dilute surface coverage of bound ligands are necessary to ensure the optimal accessibility and specificity of biomolecular interactions.

Spacing small molecules approximately 5 nm apart due to the sizes of large biomolecule partners, requires an advance surface chemistry. Previously, small-molecule printing was developed using a high-precision robot printer, creating a dense micro-spot array (~200-250 μm) that contains different small-molecule libraries in each spot [*37*, *49*]. However, this technique cannot determine the *spacings* between small molecules within a spot. Recent developments of SAMs on noble metals were applied to insert single molecules by controlling defect sites in a SAM matrix, enabling studies of single-molecule properties such as photoinduced isomerization, mechanical conductivity, and photoinduced conductivity [*50-54*]. Moreover, insertion-based SAMs can be integrated with soft lithography to fabricate patterned SAMs for electronic applications [*55-58*].

In addition to the insertion-based strategy, small molecules can be spatially addressed by using codeposition-based SAMs [*59, 60*]. By using two or more different thiol molecules, the spacings of tether molecules can be stoichiometrically controlled. This method is widely applicable in many experimental studies, such as single-molecule wires, protein biosensors, and cell physiology [*61, 62*]. To overcome the challenges mentioned earlier, our group has performed systematic studies to fabricate small-molecule-functionalized surfaces for biomacromolecule capture. By adjusting self-assembly conditions, such as incubation time and concentration, and more importantly by using ligand analogs, functionalized surfaces can express the endogenous bioactivity and optimal accessibility of small molecules. To begin, the fabrication of surfaces mimicking serotonin bioaffinity was initial goal, as discussed below

2.2.2 Serotonin as a Prototypical System for Small-Molecule Immobilization

In our study, serotonin has been chosen to direct our initial efforts at designing bioselective surfaces. Structurally, serotonin is a monoamine neurotransmitters, consisting of a primary amine separated from an aromatic indole ring by a two carbon aliphatic chain (Figure 2-2) [*63*]. Serotonin is synthesized biologically in two enzymatic steps. The first step includes the aromatic ring hydroxylation of the amino acid L-tryptophan by tryptophan hydroxylase, yielding L-5-hydroxytryptophan (L-5-HTP). In the second step, the carboxyl moiety on L-5-HTP is enzymatically removed by aromatic amino acid decarboxylase, giving serotonin or 5-hydroxytrptamine (5-HT) (Figure 2-2). Serotonin is one of the most ancient signaling molecules, found in both central and peripheral nervous systems, as well as in the gut, cardiovascular system, and blood [*64*].

Brain serotonin has been implicated in physiological functions, including endocrine regulation, cognitive functions, anxiety, sensory functions, appetite, pain, and sleep [*65*]. Alteration in 5-HT signaling is believed to cause neuropsychiatric disorders, disorders, such as depression, panic, Alzheimer's and Parkinson's diseases [*66-68*]. The World Health Organization reported that these diseases comprise about 7% of the global burden of diseases [*22*]. Therefore, discovering better treatments for these diseases is one of the most important targets for biochemical, clinical, and pharmaceutical research and development.

Investigating serotonin neurotransmission has been particularly challenging, however, because serotonin is present in the brain extracellular space at exceptionally low (sub-nanomolar to nanomolar) concentrations that are equal to or significantly less than those of structurally similar precursors, analogs, metabolites, and other electrochemically active neurotransmitters [*69*]. Thus, the detection of serotonin requires ultra-sensitive and selective detection strategies. Insofar as the information content of neurotransmitter signaling is encoded temporally and spatially, development of methods to measure rapid changes in neurotransmitter levels in specific brain regions, subregions and ultimately, in individual synapses is essential for understanding the roles of neurotransmitters in modulating complex behavior [*70*].

A comprehensive understanding of serotonergic function is necessary for advances in the treatment of the abovementioned psychiatric and neurological disorders. The development of *in vitro* analytical tools to discover unknown serotonin-related proteins and to investigate the intermolecular interactions of known serotonin receptors will advance our understanding of cell signaling and thus brain function.

2.2.3 Solution Insertion for Dilute Surface Coverage of Tether Molecules

As mentioned above, surface-derivatized systems require proper distances between small-molecule ligands for optimal accessibility of large-biomolecule capture. Initially, we introduced a strategy using a combination of insertion-directed SAMs and chemical functionalization [*42, 71*]. With this method, oligo(ethylene glycol)alkanethiols containing reactive terminal groups, called tethers, are inserted into a preformed hydroxyl-terminated oligo(ethylene glycol)alkanethiolate SAM, known as a protein-resistant layer. This creates the requisite dilute surface coverage of tether molecules. The reactive terminal group of the tethers is then covalently modified with the selected small neurotransmitter 5-HT, resulting in 5-HT-immobilized surfaces at dilute coverage in biomolecule-resistant matrices (Figure 2-3).

5-HT-functionalized surfaces exhibit specific recognition to antibodies directed against 5-HT molecules, but *not* to those raised against other neurotransmitters, including dopamine and the enzyme tyrosine hydroxylase. Moreover, these derivatized surfaces resist nonspecific protein adsorption from bovine serum albumin (BSA) [*42*].

The assembly and small-molecule immobilization strategy produces surfaces capable of biospecific recognition. This approach can be extended to most neurotransmitters, as well as to many other small molecules of biological importance. In addition to specific interactions, the 5-HT-functionalized surfaces can be used in combination with mass spectrometry to derive biomolecular structures of captured proteins [*72*]. However, immobilizing neurotransmitters with this strategy exploits a primary amine to bind reactive terminal groups covalently on surface tethers. Using an

essential functional group on a neurotransmitter can considerably influence the biological functionality of immobilized ligands. Therefore, we have introduced a novel method for preserving *all* necessary functional groups.

2.2.4 Chemical Functionalization of Small Molecules via Their Biological Analogs

The initial 5-HT-functionalized surfaces were created by utilizing the primary amine group on the 5-HT molecule to couple to surface tethers. Disabling or modifying one functional group on a small molecule may significantly change their binding affinity with endogenous biological targets. To avoid the functionality alteration of immobilized molecules, we have invented the next generation of capture surfaces designed to mimic free small molecules in solution [*43*, *73*]. Here, we exploited 5-hydroxytryptophan (5-HTP), the biological precursor of 5-HT neurotransmitter. By tethering via its extra carboxyl moiety, the immobilized 5-HTP leaves all essential groups associated with 5-HT pharmacophore for biorecognition of endogenous receptors (Figure 2-4).

The binding measurements suggested that 5-HTP-functionalized surfaces show bioselectivity to both 5-HTP antibodies and 5-HT membrane-associated receptors, but 5-HT-functionalized surfaces do not (Figure 2-5). The result from AFM measurements also show that 5-HT_7 receptors bind onto 5-HTP-functionalized surfaces (Figure 2-6). In addition, because the 5-HTP molecule contains a chiral center at the α-carboxyl position, immobilizing L-5-HTP molecules, the biologically active stereoisomers, allows the selective capture of 5-HT receptors (Figure 2-7) to a greater extent than enantiomerically mixed surfaces.

2.3 Conclusions and Prospects

Chemical signaling by small-molecule neurotransmitters is an important biological process enabling intercellular communication. These neurotransmitters carry chemical information and transmit signals through different types of membrane-associated receptors. Thus, the biological activities of small molecules and membrane-associated receptors influence many physiological functions, such as mood, pain, and appetite. Alterations of these biological activities can cause many neurological disorders, including Alzheimer's and Parkinson's diseases. Understanding of cell-signaling mechanisms and receptor function is critical for better treatment of the abovementioned psychiatric and neurological disorders. Hence, the development of *in vitro* analytical tools to discover unknown serotonin proteins and to investigate the molecular interactions of known serotonin receptors enables our comprehension of cell signaling and thus brain function.

Serotonergic neurotransmission is an initial target system for directing the development of small-molecule-functionalized substrates. The critical challenges of immobilizing small molecules on surfaces, including selectivity, accessibility, and bioactivity, were addressed based on insertion-directed self-assembled chemistry of oligo(ethylene glycol)alkanethiols and surface chemical functionalization. Initially, we invented surface-bound 5-HT as protein-capture platforms for studying and detecting 5-HT endogenous membrane-associated receptors. Consuming one functional group on a small molecule raised concerns that the bioaffinity of surface-bound 5-HT may alter and thus reduce biorecognition.

Ultimately, utilizing the 5-HTP molecule, containing a carboxyl auxiliary group, enables the surfaces containing bound ligands that mimic 5-HT functionality. Accordingly, 5-HTP-functionalized surfaces recognize native 5-HTP membrane-associated receptors. In Chapter 3, the 5-HTP-functionalized surfaces will be utilized to investigate biomolecular interactions of GPCRs. Key binding parameters, such as equilibrium dissociation constants, rate constants, and dissociative half-life, will be extracted. This fundamental information is critical in biomedical research and the development of new pharmaceutical strategies to target these important biomolecules.

Some parts of this chapter was adapted with permission from Vaish, A., Shuster, M. J., Cheunkar, S., Singh, Y.S., Weiss, P. S., and Andrews, A. M. Native Serotonin Membrane Receptors Recognize 5-Hydroxytryptophan-Functionalized Substrates: Enabling Small Molecule Recognition. *ACS Chem. Neurosci.* **2010**, 1, 495-504.

2.4 Figures

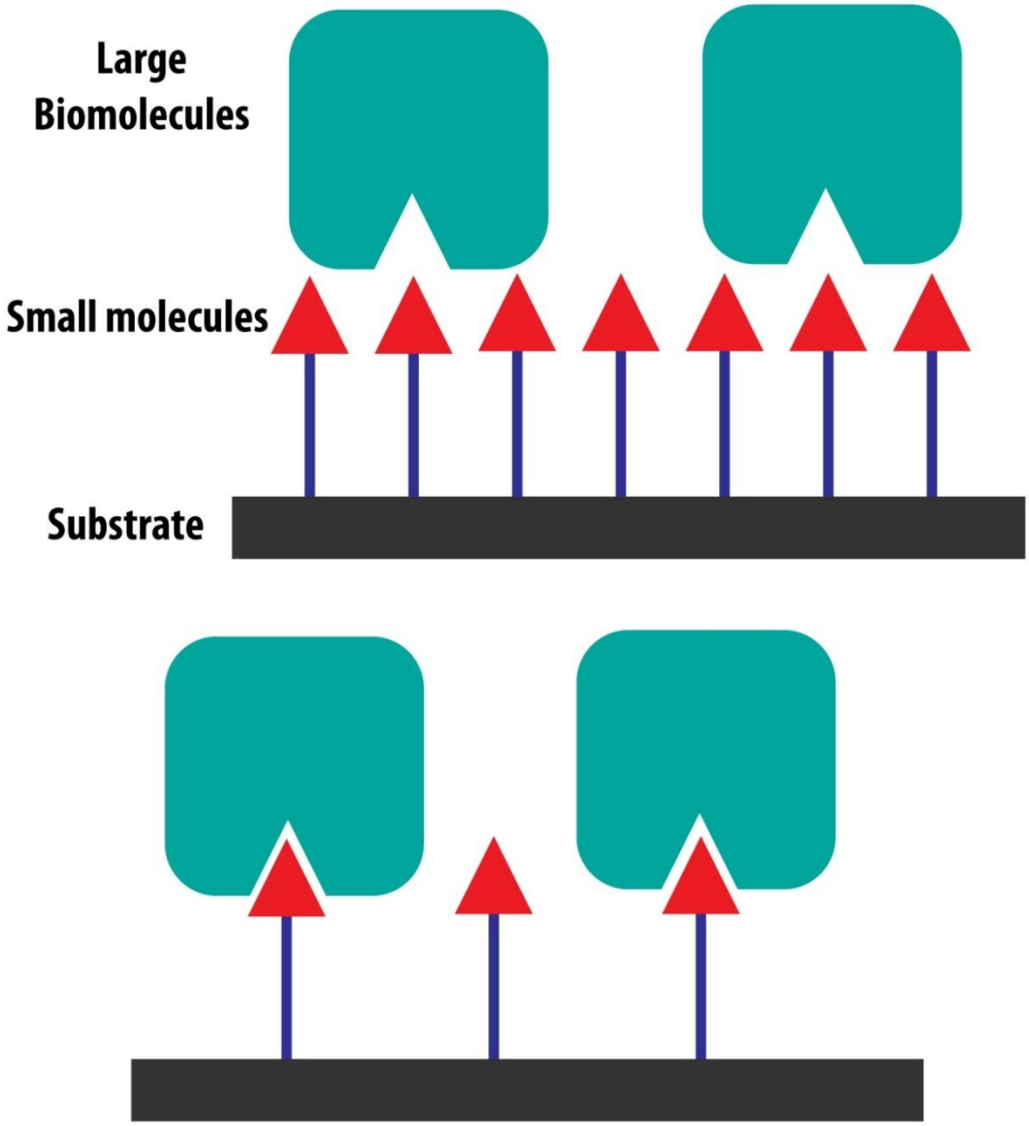

Figure 2-1. **Schematic representation of large biomolecules interacting with a small-molecule-immobilized substrate.** Due to the size mismatch between large biomolecules and immobilized molecules, densely packed molecules on the substrate result in steric hindrance, preventing bioaccessbility of large biomolecules and reducing bioactivity.

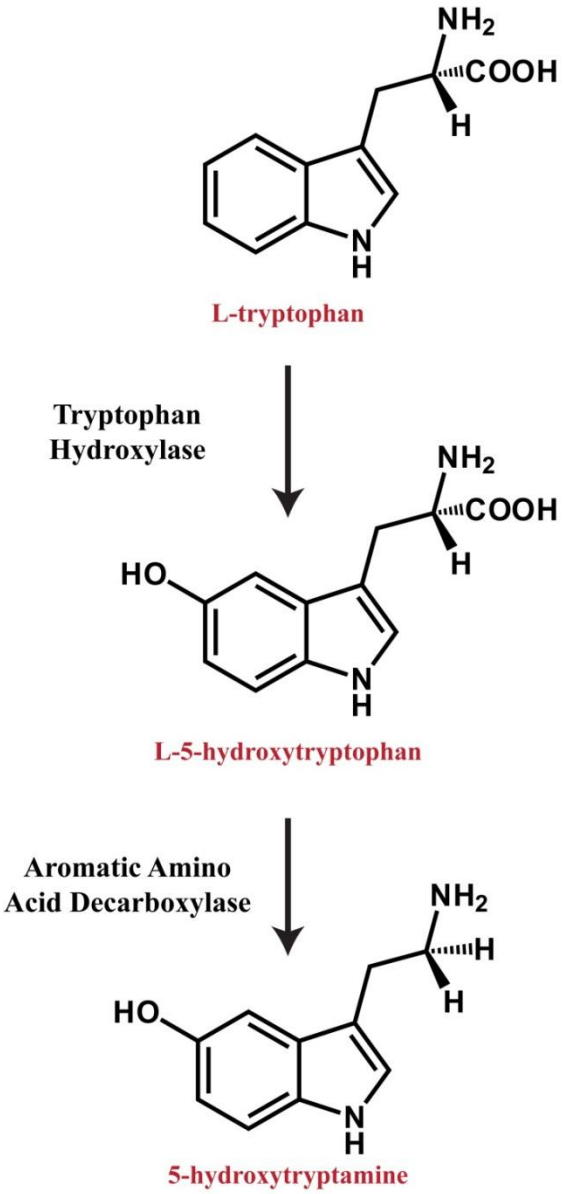

Figure 2-2. **Biosynthesis of serotonin neurotransmitter (5-hydroxytryptamine)**. Serotonin is synthesized in a two-step enzymatic process. First, an enzyme tryptophan hydroxylase converts the amino acid L-tryptophan to L-5-hydroxytryptophan. Second, L-5-hydroxytryptophan is decarboxylated by aromatic amino acid decarboxylase, yielding 5-hydroxytryptamine.

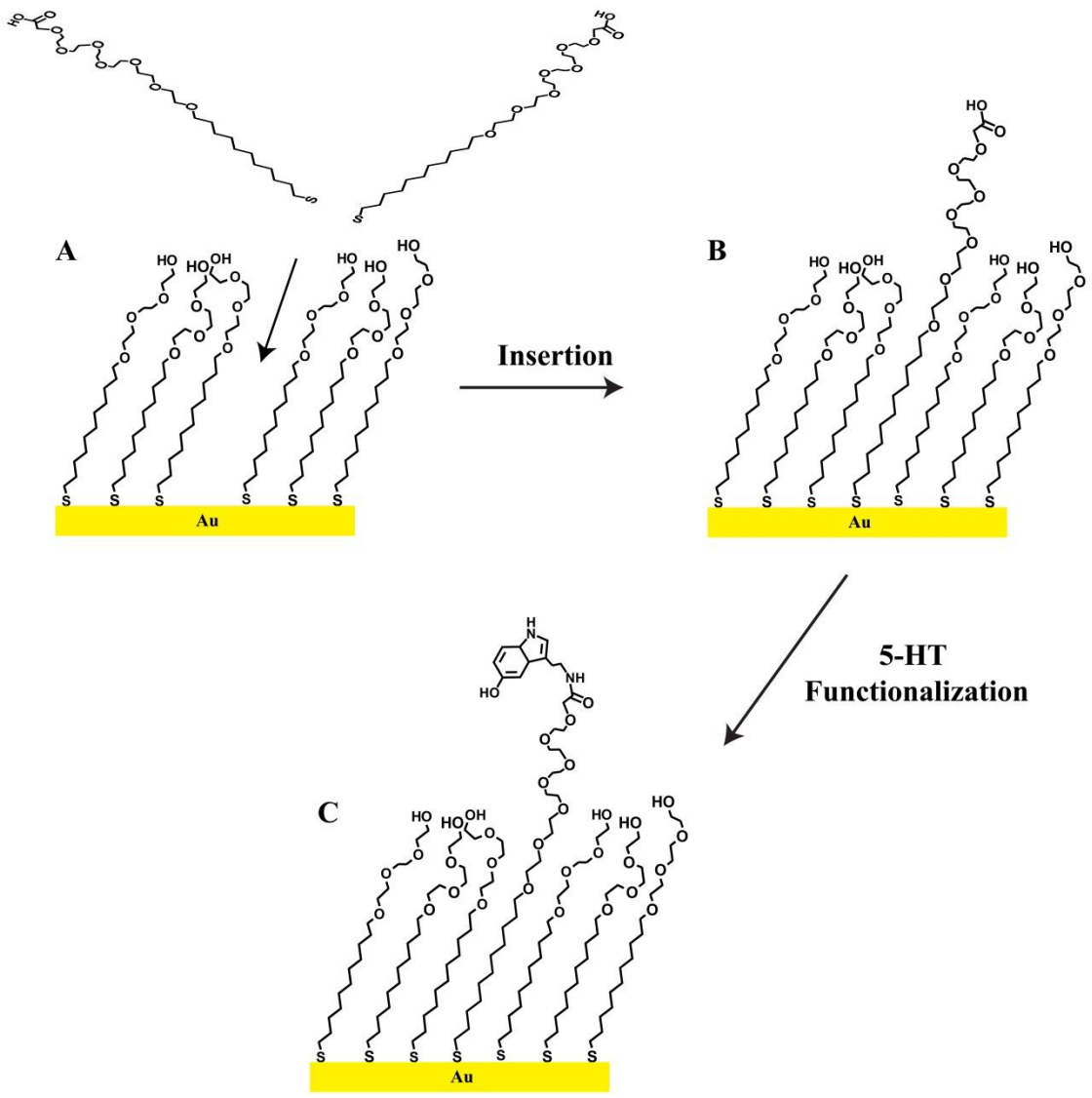

Figure 2-3. **Strategy to fabricate 5-HT-functionalized surfaces**. (A) A Au substrate is coated with self-assembled monolayers of oligo(ethylene glycol)alkanethiols, a protein-resistant layer. (B) Carboxyl-terminated oligo(ethylene glycol)alkanethiols are inserted into defect sites of the preformed SAMs, creating a dilute surface coverage of longer tether molecules. (C) The carboxyl tethers are modified with 5-HT neurotransmitters to produce 5-HT-functionaized surfaces.

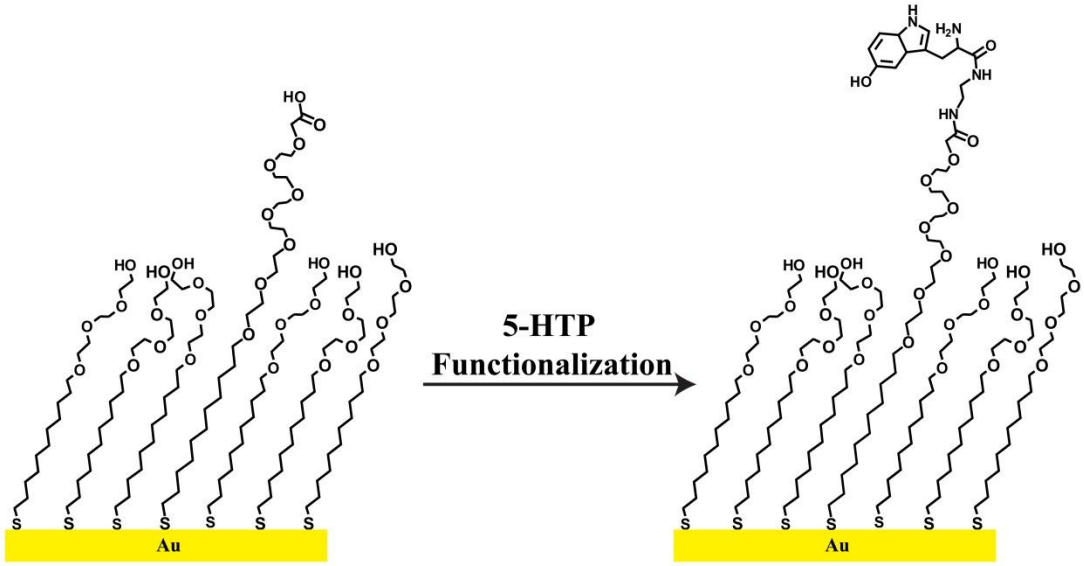

Figure 2-4. **Schematic representation of a 5-HTP functionalization process**. Mixed SAMs of carboxyl- and hydroxyl-terminated oligo(ethylene glycol)alkanethiols are formed on a Au substrate (left). The carboxyl tether is functionalized with 5-HTP molecules (right).

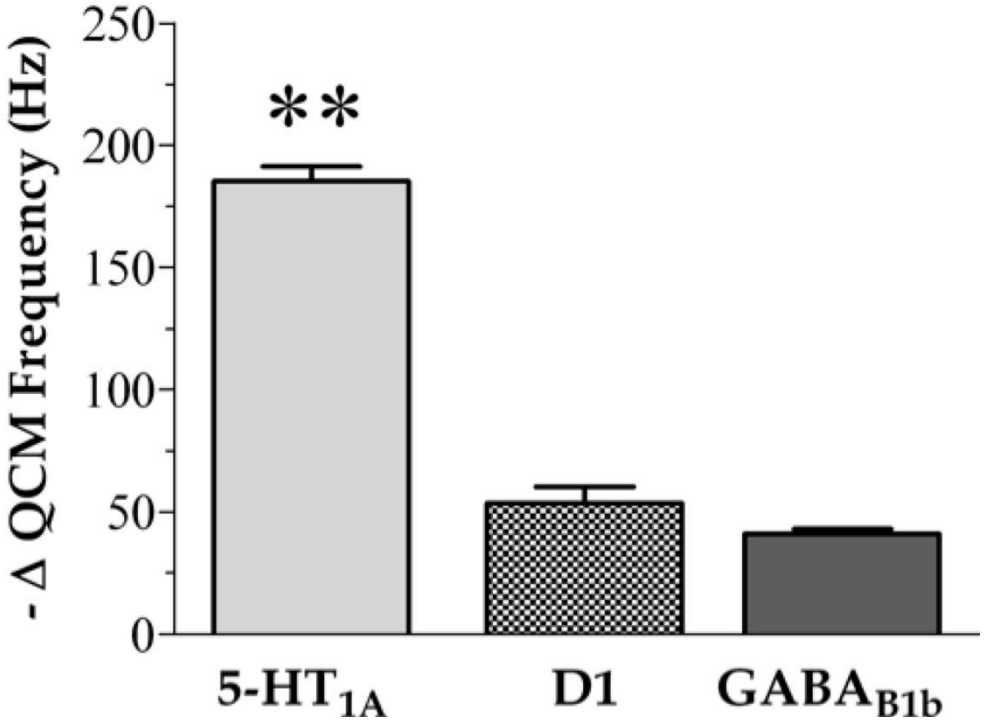

Figure 2-5. **Selective binding of membrane-associated receptors to 5-HTP-functionalized surfaces.** Serotonin 1A receptors ($5\text{-}HT_{1A}$) show 4-5 fold higher binding to 5-HTP-functionalized surfaces compared to dopamine 1(D_1) and gama-aminobutyric acid B1b ($GABA_{B1b}$). This figure is adapted with permission from reference 11.

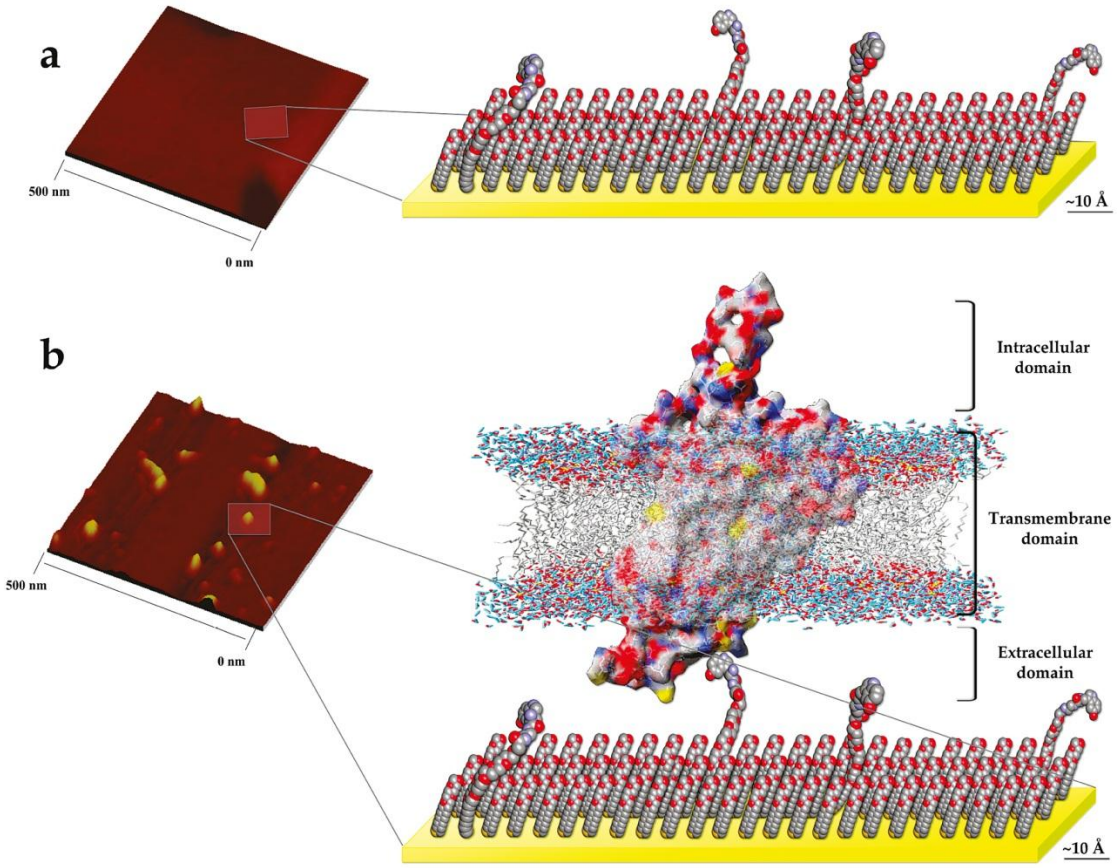

Figure 2-6. **Representative atomic force microscope images of 5-HT$_7$ receptors binding to a 5-HTP-functionalized surfaces.** Substrates (a) before and (b) after 5-HT$_7$ receptor binding. This figure is adapted with permission from reference 11.

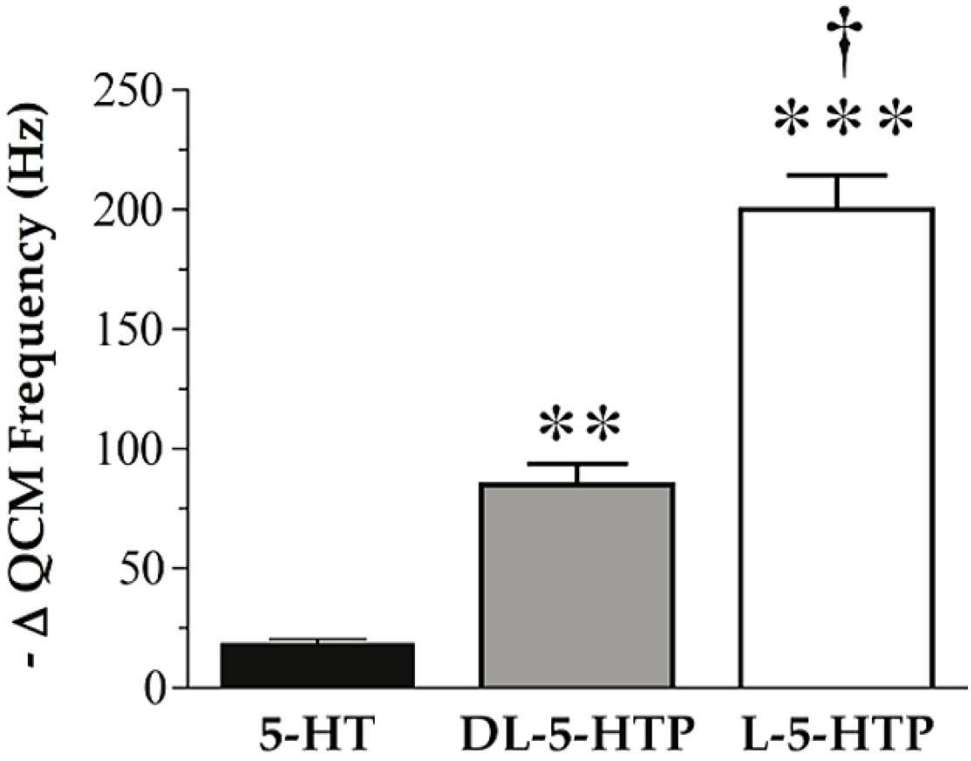

Figure 2-7. **5-HT$_7$ receptor binding to surfaces functionalized with different types of 5-HTP isomers.** L-5-HTP-functionalized surfaces show the highest response to 5-HT$_7$ receptors. This figure is adapted with permission from reference 11.

2.5 References

1. Palomo, V., Perez, D. I., Perez, C., Morales-Garcia, J. A., Soteras, I., Alonso-Gil, S., Encinas, A., Castro, A., Campillo, N. E., Perez-Castillo, A., Gil, C., and Martinez, A. 5-Imino-1,2,4-Thiadiazoles: First Small Molecules as Substrate Competitive Inhibitors of Glycogen Synthase Kinase 3. *J. Med. Chem.* **2012**, *55*, 1645-1661.
2. McCormick, F. Small-Molecule Inhibitors of Cell Signaling. *Curr. Opin. Biotechnol.* **2000**, *11*, 593-597.
3. O'Donnell, J., Zeppenfeld, D., McConnell, E., Pena, S., and Nedergaard, M. Norepinephrine: A Neuromodulator That Boosts the Function of Multiple Cell Types to Optimize CNS Performance. *Neurochem. Res.* **2012**, *37*, 2496-2512.
4. Kawasumi, M., and Nghiem, P. Chemical Genetics: Elucidating Biological Systems with Small-Molecule Compounds. *J. Invest. Dermatol.* **2007**, *127*, 1577-1584.
5. Newman, R. H., and Zhang, J. Small Molecules and Chemical Tools at the Interface. *Nat. Chem. Biol.* **2008**, *4*, 382-386.
6. Thompson, L. A., and Ellman, J. A. Synthesis and Applications of Small Molecule Libraries. *Chem. Rev.* **1996**, *96*, 555-600.
7. Jiang, Y. X., Lee, A., Chen, J. Y., Cadene, M., Chait, B. T., and MacKinnon, R. The Open Pore Conformation of Potassium Channels. *Nature* **2002**, *417*, 523-526.

8. Waldmann, R., Champigny, G., Bassilana, F., Heurteaux, C., and Lazdunski, M. A Proton-Gated Cation Channel Involved in Acid-Sensing. *Nature* **1997**, *386*, 173-177.

9. Daub, H., Weiss, F. U., Wallasch, C., and Ullrich, A. Role of Transactivation of the EGF Receptor in Signalling by G-Protein-Coupled Receptors. *Nature* **1996**, *379*, 557-560.

10. Marinissen, M. J., and Gutkind, J. S. G-Protein-Coupled Receptors and Signaling Networks: Emerging Paradigms. *Trends Pharmacol. Sci.* **2001**, *22*, 368-376.

11. Bloom, F. E. Neurotransmitters: Past, Present, and Future Directions. *FASEB J.* **1988**, *2*, 32-41.

12. Cheido, M., and Idova, G. Neuropeptides in the Immunomodulation: Substance P-Induced Stimulation of Immune Response in Mice. *Int. J. Immunopharmacol.* **1997**, *19*, 529-533.

13. Bridges, T. M., and Lindsley, C. W. G-Protein-Coupled Receptors: From Classical Modes of Modulation to Allosteric Mechanisms. *ACS Chem. Biol.* **2008**, *3*, 530-541.

14. Granier, S., and Kobilka, B. A New Era of GPCR Structural and Chemical Biology. *Nat. Chem. Biol.* **2012**, *8*, 670-673.

15. Rosenbaum, D. M., Rasmussen, S. G., and Kobilka, B. K. The Structure and Function of G-Protein-Coupled Receptors. *Nature* **2009**, *459*, 356-363.

16. Conn, P. J., Christopoulos, A., and Lindsley, C. W. Allosteric Modulators of GPCRs: A Novel Approach for the Treatment of CNS Disorders. *Nat. Rev. Drug Discov.* **2009**, *8*, 41-54.

17. Strader, C. D., Fong, T. M., Tota, M. R., Underwood, D., and Dixon, R. A. F. Structure and Function of G-Protein-Coupled Receptors. *Annu. Rev. Biochem.* **1994**, *63*, 101-132.

18. Strader, C. D., Oprian, D., Lefkowitz, R., and Baldwin, J. 7-Helix Receptors. *FASEB J.* **1994**, *8*, 153-153.

19. Gainetdinov, R. R., Premont, R. T., Bohn, L. M., Lefkowitz, R. J., and Caron, M. G. Desensitization of G Protein-Coupled Receptors and Neuronal Functions. *Annu. Rev. Neurosci.* **2004**, *27*, 107-144.

20. Edwards, S. W., Tan, C. M., and Limbird, L. E. Localization of G-Protein-Coupled Receptors in Health and Disease. *Trends Pharmacol. Sci.* **2000**, *21*, 304-308.

21. Schoneberg, T., Schulz, A., and Gudermann, T. The Structural Basis of G-Protein-Coupled Receptor Function and Dysfunction in Human Diseases. *Rev. Physiol., Biochem. Pharmacol.* **2002**, *144*, 143-227.

22. Berton, O., and Nestler, E. J. New Approaches to Antidepressant Drug Discovery: Beyond Monoamines. *Nat. Rev. Neurosci.* **2006**, *7*, 137-151.

23. Cooper, M. A. Optical Biosensors in Drug Discovery. *Nat. Rev. Drug Discov.* **2002**, *1*, 515-528.

24. Lipinski, C. A., Lombardo, F., Dominy, B. W., and Feeney, P. J. Experimental and Computational Approaches to Estimate Solubility and Permeability in Drug Discovery and Development Settings. *Adv. Drug Del. Rev.* **2001**, *46*, 3-26.

25. Congreve, M., Langmead, C. J., Mason, J. S., and Marshall, F. H. Progress in Structure Based Drug Design for G Protein-Coupled Receptors. *J. Med. Chem.* **2011**, *54*, 4283-4311.

26. Trattnig, S. M., Harpsoe, K., Thygesen, S. B., Rahr, L. M., Ahring, P. K., Balle, T., and Jensen, A. A. Discovery of a Novel Allosteric Modulator of 5-HT3 Receptors: Inhibition and Potentiation of Cys-Loop Receptor Signaling through a Conserved Transmembrane Intersubunit Site. *J. Biol. Chem.* **2012**, *287*, 25241-25254.

27. Taly, A., Corringer, P. J., Guedin, D., Lestage, P., and Changeux, J. P. Nicotinic Receptors: Allosteric Transitions and Therapeutic Targets in the Nervous System. *Nat. Rev. Drug Discov.* **2009**, *8*, 733-750.

28. May, L. T., Leach, K., Sexton, P. M., and Christopoulos, A. Allosteric Modulation of G Protein-Coupled Receptors. *Annu. Rev. Pharmacol. Toxicol.* **2007**, *47*, 1-51.

29. Zhang, Y. Q., Rodriguez, A. L., and Conn, P. J. Allosteric Potentiators of Metabotropic Glutamate Receptor Subtype 5 Have Differential Effects on Different Signaling Pathways in Cortical Astrocytes. *J. Pharmacol. Exp. Ther.* **2005**, *315*, 1212-1219.

30. Conn, P. J., Hemstapat, A., Rodriguez, A. L., Chen, Y., Nong, Y., Jones, C., DePaulis, T., Zhang, Y., and Tamagnan, G. Pharmacological Properties and Therapeutic Potential of Allosteric Potentiators of Metabotropic Glutamate Receptors. *Neuropharmacology* **2005**, *49*, 240-240.

31. Mohler, H., Fritschy, J. M., and Rudolph, U. A New Benzodiazepine Pharmacology. *J. Pharmacol. Exp. Ther.* **2002**, *300*, 2-8.

32. Valant, C., Robert Lane, J., Sexton, P. M., and Christopoulos, A. The Best of Both Worlds? Bitopic Orthosteric/Allosteric Ligands of G-Protein-Coupled Receptors. *Annu. Rev. Pharmacol. Toxicol.* **2012**, *52*, 153-178.

33. Messer, W. S. Bivalent Ligands for G-Protein-Coupled Receptors. *Curr. Pharm. Des.* **2004**, *10*, 2015-2020.

34. Civelli, O. Orphan GPCRs and Neuromodulation. *Neuron* **2012**, *76*, 12-21.

35. Civelli, O., Saito, Y., Wang, Z. W., Nothacker, H. P., and Reinscheid, R. K. Orphan GPCRs and Their Ligands. *Pharmacol. Ther.* **2006**, *110*, 525-532.

36. Zhang, R., and Xie, X. Tools for GPCR Drug Discovery. *Acta Pharmacol. Sin.* **2012**, *33*, 372-384.

37. Vegas, A. J., Fuller, J. H., and Koehler, A. N. Small-Molecule Microarrays as Tools in Ligand Discovery. *Chem. Soc. Rev.* **2008**, *37*, 1385-1394.

38. Bieri, C., Ernst, O. P., Heyse, S., Hofmann, K. P., and Vogel, H. Micropatterned Immobilization of a G Protein-Coupled Receptor and Direct Detection of G Protein Activation. *Nat. Biotechnol.* **1999**, *17*, 1105-1108.

39. Chou, D. H., Bodycombe, N. E., Carrinski, H. A., Lewis, T. A., Clemons, P. A., Schreiber, S. L., and Wagner, B. K. Small-Molecule Suppressors of Cytokine-Induced Beta-Cell Apoptosis. *ACS Chem Biol* **2010**, *5*, 729-734.

40. Nielsen, T. E., and Schreiber, S. L. Diversity-Oriented Synthesis - Towards the Optimal Screening Collection: A Synthesis Strategy. *Angew. Chem. Int. Ed.* **2008**, *47*, 48-56.

41. Drumheller, P. D., Hubbell J. A. (1995) *Surface Immobilization of Adhesion Ligands for Investigations of Cell/Substrate Interactions*, J.D. Bronzino Ed. ed., CRC and IEEE Press 1583-1596.

42. Shuster, M. J., Vaish, A., Szapacs, M. E., Anderson, M. E., Weiss, P. S., and Andrews, A. M. Biospecific Recognition of Tethered Small Molecules Diluted in Self-Assembled Monolayers. *Adv. Mater.* **2008**, *20*, 164-167.

43. Vaish, A., Shuster, M. J., Cheunkar, S., Singh, Y. S., Weiss, P. S., and Andrews, A. M. Native Serotonin Membrane Receptors Recognize 5-Hydroxytryptophan-Functionalized Substrates: Enabling Small-Molecule Recognition. *ACS Chem. Neurosci.* **2010**, *1*, 495-504.

44. Leeson, P. D., and Springthorpe, B. The Influence of Drug-Like Concepts on Decision-Making in Medicinal Chemistry. *Nat. Rev. Drug Discov.* **2007**, *6*, 881-890.

45. Zhu, H., and Snyder, M. Protein Chip Technology. *Curr. Opin. Chem. Biol.* **2003**, *7*, 55-63.

46. Samanta, D., and Sarkar, A. Immobilization of Bio-Macromolecules on Self-Assembled Monolayers: Methods and Sensor Applications. *Chem. Soc. Rev.* **2011**, *40*, 2567-2592.

47. Erickson, H. P. Size and Shape of Protein Molecules at the Nanometer Level Determined by Sedimentation, Gel Filtration, and Electron Microscopy. *Biol. Proced. Online* **2009**, *11*, 32-51.

48. Lahiri, J., Isaacs, L., Grzybowski, B., Carbeck, J. D., and Whitesides, G. M. Biospecific Binding of Carbonic Anhydrase to Mixed SAMs Presenting

Benzenesulfonamide Ligands: A Model System for Studying Lateral Steric Effects. *Langmuir* **1999**, *15*, 7186-7198.

49. Foong, Y. M., Fu, J. Q., Yao, S. Q., and Uttamchandani, M. Current Advances in Peptide and Small Molecule Microarray Technologies. *Curr. Opin. Chem. Biol.* **2012**, *16*, 234-242.

50. Kumar, A. S., Ye, T., Takami, T., Yu, B. C., Flatt, A. K., Tour, J. M., and Weiss, P. S. Reversible Photo-Switching of Single Azobenzene Molecules in Controlled Nanoscale Environments. *Nano Lett.* **2008**, *8*, 1644-1648.

51. Moore, A. M., Dameron, A. A., Mantooth, B. A., Smith, R. K., Fuchs, D. J., Ciszek, J. W., Maya, F., Yao, Y. X., Tour, J. M., and Weiss, P. S. Molecular Engineering and Measurements to Test Hypothesized Mechanisms in Single Molecule Conductance Switching. *J. Am. Chem. Soc.* **2006**, *128*, 1959-1967.

52. Moore, A. M., Mantooth, B. A., Donhauser, Z. J., Maya, F., Price, D. W., Yao, Y. X., Tour, J. M., and Weiss, P. S. Cross-Step Place-Exchange of Oligo(Phenylene-Ethynylene) Molecules. *Nano Lett.* **2005**, *5*, 2292-2297.

53. Moore, A. M., Mantooth, B. A., Donhauser, Z. J., Yao, Y., Tour, J. M., and Weiss, P. S. Real-Time Measurements of Conductance Switching and Motion of Single Oligo(Phenylene Ethynylene) Molecules. *J. Am. Chem. Soc.* **2007**, *129*, 10352-10353.

54. Kim, M., Hohman, J. N., Cao, Y., Houk, K. N., Ma, H., Jen, A. K. Y., and Weiss, P. S. Creating Favorable Geometries for Directing Organic Photoreactions in Alkanethiolate Monolayers. *Science* **2011**, *331*, 1312-1315.

55. Dameron, A. A., Hampton, J. R., Smith, R. K., Mullen, T. J., Gillmor, S. D., and Weiss, P. S. Microdisplacement Printing. *Nano Lett.* **2005**, *5*, 1834-1837.

56. Mullen, T. J., Srinivasan, C., Hohman, J. N., Gillmor, S. D., Shuster, M. J., Horn, M. W., Andrews, A. M., and Weiss, P. S. Microcontact Insertion Printing. *Appl. Phys. Lett.* **2007**, *90*, 063114-063117.

57. Saavedra, H. M., Mullen, T. J., Zhang, P. P., Dewey, D. C., Claridge, S. A., and Weiss, P. S. Hybrid Strategies in Nanolithography. *Rep. Prog. Phys.* **2010**, *73*, 036501.

58. Srinivasan, C., Mullen, T. J., Hohman, J. N., Anderson, M. E., Dameron, A. A., Andrews, A. M., Dickey, E. C., Horn, M. W., and Weiss, P. S. Scanning Electron Microscopy of Nanoscale Chemical Patterns. *ACS Nano* **2007**, *1*, 191-201.

59. Lahiri, J., Isaacs, L., Tien, J., and Whitesides, G. M. A Strategy for the Generation of Surfaces Presenting Ligands for Studies of Binding Based on an Active Ester as a Common Reactive Intermediate: A Surface Plasmon Resonance Study. *Anal. Chem.* **1999**, *71*, 777-790.

60. Nelson, K. E., Gamble, L., Jung, L. S., Boeckl, M. S., Naeemi, E., Golledge, S. L., Sasaki, T., Castner, D. G., Campbell, C. T., and Stayton, P. S. Surface Characterization of Mixed Self-Assembled Monolayers Designed for Streptavidin Immobilization. *Langmuir* **2001**, *17*, 2807-2816.

61. Pathem, B. K., Zheng, Y. B., Payton, J. L., Song, T.-B., Yu, B.-C., Tour, J. M., Yang, Y., Jensen, L., and Weiss, P. S. Effect of Tether Conductivity on the Efficiency of Photoisomerization of Azobenzene-Functionalized Molecules on Au{111}. *J. Phys. Chem. Lett.* **2012**, *3*, 2388-2394.

62. Patolsky, F., Zheng, G., and Lieber, C. M. Nanowire Sensors for Medicine and the Life Sciences. *Nanomedicine* **2006**, *1*, 51-65.

63. Nichols, D. E., and Nichols, C. D. Serotonin Receptors. *Chem. Rev.* **2008**, *108*, 1614-1641.

64. Hoyer, D., Hannon, J. P., and Martin, G. R. Molecular, Pharmacological and Functional Diversity of 5-HT Receptors. *Pharmacol. Biochem. Behav.* **2002**, *71*, 533-554.

65. Murphy, D. L., Andrews, A. M., Wichems, C. H., Li, Q., Tohda, M., and Greenberg, B. Brain Serotonin Neurotransmission: An Overview and Update with an Emphasis on Serotonin Subsystem Heterogeneity, Multiple Receptors, Interactions with Other Neurotransmitter Systems, and Consequent Implications for Understanding the Actions of Serotonergic Drugs. *J. Clin. Psychiatr.* **1998**, *59*, 4-12.

66. Cowen, P. J. Serotonin and Depression: Pathophysiological Mechanism or Marketing Myth? *Trends Pharmacol. Sci.* **2008**, *29*, 433-436.

67. Cowen, P. J. Serotonin Receptor Subtypes in Depression-Evidence from Studies in Neuroendocrine Regulation. *Clin. Neuropharmacol.* **1993**, *16*, S6-S18.

68. Smith, K. A., Williams, C., and Cowen, P. J. Impaired Regulation of Brain Serotonin Function During Dieting in Women Recovered from Depression. *Br. J. Psychiatry* **2000**, *176*, 72-75.

69. Stefani C. Altieri, Y. S., Etienne Sibille, and Anne M. Andrews. (2012) Serotonergic Pathways in Depression, In *Neurobiology of Depression* (Francisco Lopez-Munoz, C. A., Ed.), p 143.

70. Andrews, A. M., and Weiss, P. S. Nano in the Brain: Nano-Neuroscience. *ACS Nano* **2012**, *6*, 8463-8464.

71. Shuster, M. J., Vaish, A., Cao, H. H., Guttentag, A. I., McManigle, J. E., Gibb, A. L., Martinez, M. M., Nezarati, R. M., Hinds, J. M., Liao, W. S., Weiss, P. S., and Andrews, A. M. Patterning Small-Molecule Biocapture Surfaces: Microcontact Insertion Printing vs. Photolithography. *Chem. Commun.* **2011**, *47*, 10641-10643.

72. Mrksich, M. Mass Spectrometry of Self-Assembled Monolayers: A New Tool for Molecular Surface Science. *ACS Nano* **2008**, *2*, 7-18.

73. Vaish, A., Shuster, M. J., Cheunkar, S., Weiss, P. S., and Andrews, A. M. Tuning Stamp Surface Energy for Soft Lithography of Polar Molecules to Fabricate Bioactive Small-Molecule Microarrays. *Small* **2011**, *7*, 1471-1479.

Chapter 3

Kinetic Studies of Ligand-GPCR Molecular Interactions on Label-Free Piezoelectric Transducer Biosensors

3.1 Introduction

Signal transmission through G-protein-coupled receptors delivered by signaling molecules, such as hormones and neurotransmitters, is an indispensable step in cellular communication pathways, which enables cascade reactions that regulate a wide range of physiological responses [*1, 2*]. Because alterations in GPCR bioactivities can lead to diverse neurological disorders, the selective regulation of GPCR functions by small-molecule compounds has become a primary focus in modern drug design and discovery [*3-8*]. Hence, understanding molecular interactions of GPCR with small-molecule ligands will provide essential information for elucidating GPCR signaling mechanisms and developing new drugs for clinical trials.

In classical investigations, interactions of small-molecule ligands to target receptors are quantified *in vitro* in terms of binding parameters such as half-maximal inhibitory (IC_{50}) or equilibrium dissociation constant (K_d) under equilibrium conditions [*9-11*]. These parameters provide insight into the interaction mechanisms and guidelines to optimize the pharmacological efficacy of ligands [*12*]. However, because the *in vivo* ligand-receptor interactions take place under transient, non-equilibrium conditions, the ligand efficacy is kinetically controlled by its interaction duration [*9, 11, 13*]. In theory, the interaction duration or the residence time can be defined by dissociative half-life,

which is reciprocally proportional to the dissociation rate constant (k_{off}) [*9, 13*]. Furthermore, the equilibrium dissociation constant can be derived from k_{off} and the association rate constant (k_{on}) ($K_d = k_{off}/k_{on}$). Thus, ligand-receptor interaction kinetics has been increasingly recognized as a critical aspect of *in vitro* studies for better understanding of *in vivo* binding events [*13*].

Among current biochemical experimental methods, surface-sensitive techniques have been powerful tools in studying kinetics of ligand-receptor interactions [*14-17*]. One working principle relies on changes of substrate properties due to interfacial interactions, thereby detecting ligand-receptor binding events in real time without the need for protein or ligand labeling [*14, 18, 19*]. Thus, raw binding data, from which kinetic and thermodynamic information are extracted, can be obtained under dynamic conditions, comparable to those for *in vivo* binding events [*20*]. Several surface-sensitive techniques have been developed for this purpose, such as surface plasmon resonance [*21, 22*], electrochemical biosensors [*23, 24*], and quartz crystal microbalance [*25*]. Among these techniques, QCM measures the change of resonant frequencies due to the change of the crystal mass resulting from ligand-receptor conjugations, according to the Sauerbrey's equation [*25, 26*]. In practical terms, QCM offers an easy, inexpensive instrumental setup, with real-time and label-free sub-nanogram detection. In addition, its substrate is compatible with various types of chemical modifications, enabling a broad range of investigations [*27, 28*].

To employ a surface-sensitive technique for ligand-GPCR interaction studies, one of the binding partners must be immobilized on a solid substrate, allowing its biomolecular counterparts to interact at the solid-liquid interface [*29, 30*]. Previous

studies demonstrated that GPCRs can be immobilized on surfaces through several attachment strategies such as non-covalent interactions [*29, 31, 32*], lipid bilayer cushions [*33*], and permanent covalent linkages [*21, 34*]. However, attaching GPCRs to surfaces involves membrane solubilization and fragmentation, which may compromise structural and functional integrity of receptors due to their complex nature in biological environments [*10*]. In addition to their complexity, GPCR-functionalized substrates often encounter detection limit problems when monitoring small-molecule or low-mass analyte binding [*35*].

Alternatively, the small-molecule ligands can be attached to the surface through covalent immobilization with bovine serum albumin (BSA) [*36*], biotin-streptavidin linkages [*37*], or other functionalization strategies [*16, 17, 38, 39*]. For instance, Wang and coworkers have demonstrated that γ-aminobutyric acid (GABA), an inhibitory neurotransmitter, covalently attached to the carboxyl-containing polymer on a QCM sensor substrate, was able to capture GABA antibodies from solution [*40*]. In biological conditions, membrane-associated proteins may require their ligands to present all epitopes for biorecognition [*6*]. However, surface functionalization strategies may utilize one of the available epitopes for tethering ligands to surfaces, causing that epitope to be unavailable for subsequent protein recognition [*16, 17*]. To address these concerns, we and Funder et al. have reported an alternative surface immobilization protocol to conjugate small-molecule neurotransmitters to solid supports [*17, 41*]. With this protocol, the original molecular structures were not significantly altered, which lead to the retention of biorecognition towards their aptamer binding partners [*41*]. We have demonstrated a synthesis protocol in which 5-hydroxytryptophan (5-HTP) molecules, the

biological precursors of serotonin (5-HT), were conjugated onto solid surfaces. The surface-bound 5-HTP molecules are therefore able to mimic the bioaffinity of free 5-HT molecules in solution [*17, 42, 43*]. The 5-HTP-functionalized substrates, fabricated by this strategy, have demonstrated bioselectivity for both anti-5-HTP antibodies and 5-HT membrane proteins [*17*].

Here, 5-HTP-functionalized surfaces were utilized to investigate the kinetics and thermodynamics of ligand-GPCR interactions in a label-free fashion. The serotonin 1A receptor (5-HT_{1A}) was selected as a representative example of GPCRs because not only is it a well-characterized receptor, but it also plays key roles in modulating mood and major anxiety disorders [*44*]. Employing well-defined self-assembled monolayers of oligo(ethylene glycol)alkanethiolates on noble metal substrates is a common strategy for functionalizing small-molecule ligands and minimizing nonspecific interaction [*45-47*]. Here, the fabrication of 5-HTP-unctionalized sensor surfaces involved using mixed SAMs of hydrazide-terminated hexa(ethylene glycol)undecanethiols (HHEG) and hydroxyl-terminated tri(ethylene glycol)undecanethiols (TEG). The presence of an amine moiety in HHEG enables the immobilization of ligands with carboxylic functional groups such as 5-HTP through activated ester reactions [*48, 49*]. A systematic study was first carried out to characterize the formation of mixed SAMs of HHEG and TEG. Chemical functionalization was examined using ellipsometry and polarization-modulation infrared reflection absorption spectroscopy. The selectivities of sensor surfaces were tested by challenging substrates with antibodies specifically raised against the surface-bound 5-HTP molecules. Finally, the thermodynamics and kinetics of 5-HT_{1A} receptor recognition on the sensor surfaces were monitored in real time using a liquid-flow QCM setup.

3.2 Experimental Section

3.2.1 Materials

Hydrazide-terminated hexa(ethylene glycol)undecanethiol and hydroxy-terminated tri(ethylene glycol)undecanethiol were purchased from Nanoscience Instruments, Inc. (Phoenix, AZ, USA) and Toronto Research Candna (Toronto, ON, Canada), respectively. 9-Fluorenylmethoxycarbonyl-5-hydroxy-L-tryptophan (FMOC-L-5-HTP) was obtained from Anaspec (San Jose, CA, USA). *N*-ethyl-*N*-(dimethylaminopropyl)-carbodiimide (EDC), *N*-hydroxysuccinimide (NHS), *N*,*N*-dimethylformamide (DMF), 4-methylpiperidine, phosphate-buffered saline (PBS, 10 mM pH 7.4), and Trizma buffer (TBS, 50 mM pH 7.4) were obtained from Sigma-Aldrich (St. Louis, MO, USA). Ethanol (200-proof grade) was obtained from Gold Shield Chemical Co. (Hayward, CA, USA). Sulfuric acid (H_2SO_4, 98%) was obtained from EMD Chemical Inc. (Gibbstown, NJ, USA). Hydrogen peroxide (H_2O_2, 30%) was obtained from Fisher Chemical (Fairlawn, NJ, USA). Deionized (DI) water (18 MΩ) was obtained from built-in Millipore water purifier (Billerica, MA, USA). L-5-Hydroxytrytophan (L-5-HTP) and 5-hydroxytrytamine (5-HT) polyclonal antibody were purchased from Abcam Plc. (San Francisco, CA, USA). Human recombinant serotonin 1A receptor (5-HT_{1A}) was purchased from PerkinElmer (Waltham, MA, USA).

3.2.2 Surface Preparation and Functionalization of Mixed SAMs

Substrates for this study were all coated with a 1000-Å Au film upon a 100-Å Cr adhesive layer. Before each experiment, the Au-coated substrates were cleaned in piranha

solution, 3:1 (v/v) of H_2SO_4 and H_2O_2, at room temperature for 3 min. *(Caution: the piranha solution reacts violently with most organic materials and must be handled with extreme care.)* Then, the substrates were washed thoroughly with DI water for approximately 10 min. Procedures for surface modification of self-assembled monolayers (SAMs) were modified from our previous publications [*16, 17, 42*]. Briefly, an ethanolic mixture of HHEG and TEG were co-deposited on the substrates with a total thiol concentration of 1 mM at a given mole fraction, depending on each experiment, for 12 h. Next, the substrates were rinsed with ethanol and blown dry under a stream of nitrogen. For surface modification, the mixed-SAM-coated substrates were incubated in a mixture of 15 mM FMOC-L-5-HTP, 15 mM NHS, and 15 mM EDC in 60:40 (v/v) of DMF and DI water for at least 2 hr. Any unreacted chemicals were then sonicated off in DMF and washed away with ethanol and DI water. The surfaces were then blown dry with a stream of nitrogen. In the final step, the FMOC protecting groups were removed from FMOC-L-5-HTP by immersing the substrates in 20% (v/v) 4-methylpiperidine in DMF for 20 min. The detached FMOC groups were sonicated off in DMF and rinsed away with ethanol and the surfaces were then blown dry with a stream of nitrogen. As a result, the L-5-HTP molecules were bound to the hydrazide moiety of HHEG via a robust amide linker (Figure 3-1), mimicking free serotonin (5-HT) in solution.

3.2.3 Ellipsometry

The mixed-SAM thickness was measured using a commercial strokes ellipsometer, LSE (Gaertner Scientific Corporation, Skokie, IL, USA). The data were taken at a fixed 70˚ incidence angle of the 632.8-nm HeNe laser beam. The Au-coated

silicon substrates were cut into squares, approximately 1 cm by 1 cm. The refractive index and the extinction coefficient of piranha-cleaned substrates were measured before and after SAM formation to determine the film thickness at different molar ratios of thiol solutions.

3.2.4 Polarization-Modulation Infrared Reflection Absorption Spectroscopy

The IR spectra were recorded using a Thermo Nicolet 8700 FT-IR spectrometer (Thermo Electron Corp., Madison, WI, USA) with the polarization modulator at an operating frequency of 50 kHz. The spectra were taken in reflectance mode using infrared light incident at 81˚ relative to the surface normal. The spectra are the result of 1024 scans with a resolution of 6 cm^{-1}. The Au-coated silicon substrates for IR measurements were cut into rectangular pieces, approximately 2.5 cm x 4.5 cm, to maximize the total signal intensity. Before collecting IR spectra, the sample chamber was purged with nitrogen to minimize the interference from environmental water and carbon dioxide.

3.2.5 Quartz Crystal Microbalance

3.2.5.1 Instrumentation

Figure 3-2 describes the QCM instrumental setup. The 10-MHz lever oscillator (International Crystal Manufacturing, Oklahoma City, OK, USA) was used for all QCM studies. The 10-MHz QCM substrates were coated with a 1000-Å Au film upon a 100-Å Cr adhesive layer with the electrode area of 0.2 cm^2 (International Crystal Manufacturing). A modified substrate was mounted to an HC-48/U base, providing both physical and electrical connectivity to the lever oscillator. The substrates were then

integrated into the liquid flow cell (International Crystal Manufacturing) with a rubber O-ring sealing on both sides. One side of the substrate was exposed to liquid and the other was exposed to air. The entire liquid flow cell setup was housed in a styrofoam box to maintain the whole system in the dark and at room temperature. The analyte solution was injected into the liquid flow cell via a Rheodyne switching valve and an 8-roller Ismatec peristaltic pump (IDEX Health & Science, Oak Harbor, WA, USA). The oscillator output signal was read by Agilent 53131A Universal Counter (Agilent, Palo Alto, CA, USA) and recorded as a function of time using IntuiLink Excel Connectivity Software (Agilent). Note that all QCM substrates can be reused by cleaning with piranha solution.

3.2.5.2 Protein Binding Studies

For all QCM experiments, the flow rate was maintained at 100 µL/min. The functionalized QCM substrates were washed with the incubation buffer until a stable baseline was obtained (about 30 min). In the direct affinity binding experiments, the target antibodies and receptors with a given concentration were injected into the liquid-flow cell for 10 min, followed by washing with PBS buffer until a plateau was obtained. The receptor binding data were analyzed by nonlinear regression fitting using Graphpad Prism (GraphPad Software, La Jolla, CA, USA).

3.2.5.3 Kinetic Analysis of Ligand-Receptor Complex

Comprehensive kinetic analyses of ligand-receptor complexation at the solid-liquid interface have been performed for many systems [*38, 50*]. Based on a one-site

binding assumption, the surface-bound 5-HTP (L^s) interacts with 5-HT_{1A} (R) in solution with the association rate constant (k_{on}, $M^{-1}s^{-1}$) and the dissociation rate constant (k_{off}, s^{-1}), as described in the following reaction scheme:

$$R + L \underset{k_{off}}{\overset{k_{on}}{\rightleftharpoons}} R\text{-}L \tag{3-1}$$

In a QCM experiment, the change in the resonant frequency (Δf) due to the binding events monitored as a function of time (t) can be described as:

$$\Delta f = \Delta f_e[1 - \exp(-k_s t)], \tag{3-2}$$

where Δf_e is the change in the resonant frequency at equilibrium and k_s is the observed binding rate, which is linearly dependent on the receptor concentrations as described by:

$$k_s = k_{on}[R] + k_{off}. \tag{3-3}$$

Measuring k_s as a function of receptor concentrations ([R]) yields k_{on} as a slope and k_{off} as a y-intercept, thus the equilibrium dissociation constant (K_d) is

$$K_d = \frac{k_{off}}{k_{on}}. \tag{3-4}$$

Finally, the dissociative half-life (τ), which is directly related to the residence time of a receptor-ligand complex, is defined as $0.693/k_{off}$ [9]. The detail derivations of these equations are provided in appendix A in chapter 6.

3.3 Results and Discussion

3.3.1 Characterization of Mixed SAMs

In our previous study, codeposition of carboxyl-terminated hexa(ethylene glycol)undecanethiols (HEG) as surface tethers and TEG with specific nominal molar ratios was carried out to optimize biorecognition on mixed SAM-modified Au substrates [*16, 17, 51*]. In this work, mixed SAMs of HHEG and TEG were employed for surface conjugation chemistry instead of HEG/TEG SAMs. The chemical structure of HHEG is almost identical to HEG, except that the hydroxyl of the carboxylic group is replaced by a reactive hydrazine ($-NH_2$-NH_2) moiety (Figure 3-3). As a result, the tail group of HHEG is available for chemical conjugation with a wide range of functional groups, such as aldehyde, acyl halide, activated ester, and oxidized RNA [*48*].

Here, we utilize the long molecular backbone of HHEG to determine the surface composition of HHEG as a function of the mole fraction of HHEG in solution (χ_{HHEG}) by monitoring the SAM thickness with ellipsometry. The piranha-cleaned Au-coated substrates were submersed in solutions of HHEG/TEG at different nominal molar ratios to form mixed SAMs. As shown in Figure 3-4, the ellipsometric thickness of HHEG/TEG mixed SAMs increases proportionally as a function of χ_{HHEG}, which is contrary to the codeposition behavior of HEG/TEG [*38*]. This can be attributed to the different terminal groups leading to the different intermolecular forces, thus affecting solubility and mobility of the adsorbate molecules [*52, 53*]. In many biological applications, a dilute surface concentration of tethers in mixed SAMs is used, depending on proteins of interest, so that better access for recognition will be available to relatively large proteins

[*17, 39, 53*]. For subsequent protein binding studies, we therefore used χ_{HHEG} of 0.1 to obtain the surface composition at approximately 10%.

Previously, we showed that by tethering 5-HTP, the biological precursor of 5-HT, to HEG/TEG mixed SAMs, the surface-bound 5-HTP can mimic free 5-HT in biological conditions, and exhibited selective binding toward 5-HT receptors [*17*]. Here, we conjugated 5-HTP molecules to HHEG/TEG mixed SAMs by incubating substrates with a solution of 15 mM NHS/EDC/FMOC-5-HTP in 60/40 DMF/DI water. The FMOC group in FMOC-5-HTP protects the reactive amine moiety from cross reacting with another amine on a different 5-HTP molecule. The protection group can be removed after conjugating FMOC-5-HTP to the SAM-modified Au substrates [*54*]. This surface conjugation chemistry allows the NHS-activated carboxyl groups on 5-HTP molecules to react with the hydrazide groups from HHEG through stable amide bonds [*16, 17, 55*].

To monitor 5-HTP functionalization on HHEG/TEG SAMs, polarization modulation infrared reflection absorption spectroscopy (PM-IRRAS) was used to identify vibrational fingerprints of chemical bond formation in each surface conjugation step [*51*]. This technique allows the collection of differential reflectance spectra by subtracting the atmospheric background, thus resulting in increases in sensitivity and reliability [*56*]. To achieve high signal intensity of diagnostic peaks, the Au substrates were passivated with pure HHEG SAMs. The 1400 to 1800 cm^{-1} region was scanned carefully to identify the spectral peaks of amine, amide, and carboxyl groups as vibrational characteristics of the immobilized 5-HTP molecules. As shown in Figure 3-5a, the formation of HHEG SAMs is indicated by the absorption peak at 1463 cm^{-1}, which is attributed to the CH_2-scissor mode of the crystalline phase of HHEG backbone [*57*]. The hydrazide groups of HHEG

SAMs are identified by the NH out-of-plane bending mode at 1540 cm^{-1}, NH_2 deformation at 1633 cm^{-1}, and carbonyl stretching mode at 1680 cm^{-1} [*58*].

Immobilization of 5-HTP on HHEG tethers includes the covalent conjugation of FMOC-5-HTP and the deprotection of FMOC groups [*17*, *42*, *51*]. As illustrated in Figure 3-5b, FMOC-5-HTP conjugation is indicated by the IR peaks at 1450, 1540, 1690, and 1720 cm^{-1}. In detail, the appearance of the shoulder band at 1450 cm^{-1} and the intensity increase of NH out-of-plane bending mode at 1540 cm^{-1} represent the indole ring vibration and the FMOC-protected amine group of 5-HTP molecules, respectively [*54*]. The significant increase in intensity of the carbonyl stretching mode at 1690 cm^{-1} indicates the amide bond formation between 5-HTP and HHEG SAMs. In addition, the appearance of the band at 1720 cm^{-1} is assigned to the ester carbonyl stretch of the FMOC group that disappears after the deprotection step (Figure 3-5c) [*54*]. Altogether, these PM-IRRAS data indicate that 5-HTP molecules were immobilized on the hydrazide terminal groups of HHEG/TEG SAMs.

3.3.2 Biofunctionality of 5-HTP-Functionalized Surfaces

The biofunctionality of 5-HTP-functionalized surfaces was first tested with polyclonal antibodies (pAb) raised against 5-HTP and 5-HT molecules. Antibody binding was measured by a QCM setup, as shown in Figure 3-2. Before antibody exposure, the substrates were incubated with PBS buffer to stabilize the background frequency response. Each antibody solution was injected to the sensor substrates for 10 min and PBS buffer was then injected to wash away nonspecific adsorbates. Figure 3-6 shows that 5-HTP-functionalized surfaces are selective toward 5-HTP pAbs with approximately

25% non-specific adsorption. Similar results were also obtained in monoclonal antibodies tests (Figure 3-7). During buffer rinse on the sensor surfaces, we observed slightly increased QCM frequencies, possibly resulting from the dissociation of antibodies and non-specific adsorption. This behavior has been observed in other systems when the dissociation constant of antibody and antigen ranges from 10^{-6} to 10^{-8} M [*59-61*].

3.3.3 Kinetic Studies of 5-HT_{1A} Recognition by 5-HTP-Functionalized Substrates

To investigate the binding kinetics of ligand-GPCR interactions, 5-HTP-functionalized surfaces were challenged with serotonin $5HT_{1A}$ receptors. The frequency drop, as shown in Figure 3-8, results from the binding of 5-HT_{1A} receptors toward 5-HTP-functionalized surfaces. Surprisingly, no significant dissociation of 5-HT_{1A} receptors was observed upon the buffer rinse. Similar results were also found in competitive displacement experiments by 5-HT solution (Figure 3-9). This is in a good agreement with previous studies when K_d for receptor binding is low ($K_d \sim 10^{-11}$ M) and also implies that the receptors bind tightly onto the surface-immobilized 5-HTP molecules. [*36, 37, 62*].

Concentrations of 5-HT_{1A} receptors exposed to the sensor substrates were varied to evaluate the kinetics of dynamic binding interactions. Figure 3-10a shows the QCM binding results for different 5-HT_{1A} concentrations. By assuming that the interactions between receptors and immobilized ligands are due to single-site binding (as widely understood) [*37*], fitting an individual binding event with equation 2 gives the observed binding rate constant (k_s) with excellent fit to the experiment data. It should be noted that k_s is the frequency decay rate at each receptor concentration, which does not directly

reflect the rate constant of receptor binding. Hence, by using equation 3 to plot k_s versus 5-HT_{1A} receptor concentrations (Figure 3-10b), we can estimate the association rate constant (k_{on}) and the dissociation rate constant (k_{off}) from the slope and the y-intercept in equation 3, respectively. The plot shows a linear correlation with a coefficient of 0.93. The value of k_{on} and k_{off} are $1.5 \pm 0.3 \times 10^{7}$ $M^{-1}s^{-1}$ and $2.0 \pm 0.2 \times 10^{-3}$ s^{-1}, respectively. From these values, the calculated K_d is 0.15 ± 0.02 nM and the dissociative half-life (τ) is 330 ± 10 s (~5 min). The affinity values obtained by our strategy are in the range that has been reported previously from other GPCR studies through labeling techniques. For instance, in a system that tests the binding of antipsychotic drugs with the dopamine subtype-2 GPCR, the value of K_d ranges from 0.025 to 155 nM and the value of k_{off} ranges from 0.03 to 50 ($\times 10^{-3}$) s^{-1} [*63*]. A previous study of the muscarinic GPCR binding to allosteric modulators showed a monophasic dissociation with reported half-lives from 6 to 12 min [*64*]. Our sensitive-surface strategy provides a potential alternative approach for studying ligand-GPCR interactions in a label-free manner.

3.4 Conclusions and Prospects

We present a surface-based strategy to study the interactions of ligands mimicking endogenous 5-HT neurotransmitters and their 5-HT_{1A} receptors in a real-time, label-free manner. Mixed SAMs on Au substrates were characterized with ellipsometry to determine the optimal solution concentration of surface tethers. The sensor substrates were modified with the small-molecule 5-HTP ligands on mixed SAMs to express 5-HT pharmacophore. Displays of unique vibrational features during surface conjugation chemistry and the selective recognition of specific antibodies to 5-HTP molecules confirm the presence of surface-bound 5-HTP on the substrates. The interactions of 5-HT_{1A} receptors with 5-HTP-functionalized surfaces were examined with QCM to extract key binding parameters, including K_d, k_{on}, and k_{off}. These values are comparable to previous literature values for other GPCR systems. This binding information demonstrates that this platform is a suitable alternative for receptor binding studies, which are conventionally carried out by labeling methodologies. Moreover, this strategy can be extended to other neurotransmitters or related molecules containing an auxiliary carboxylic moiety for anchoring reactions for better understanding of cell signaling mechanisms and discovering new drugs for clinical trials.

The content of this chapter is in preparation for submission to *ACS Chem. Neuro.* Cheunkar, S., Cao, H. H., Liao, W. -S., Weiss, P. S., and Andrews, A. M. Kinetic Studies of Ligand-GPCR Molecular Interactions on Label-Free Piezoelectric Transducer Biosensors.

3.5 Figures

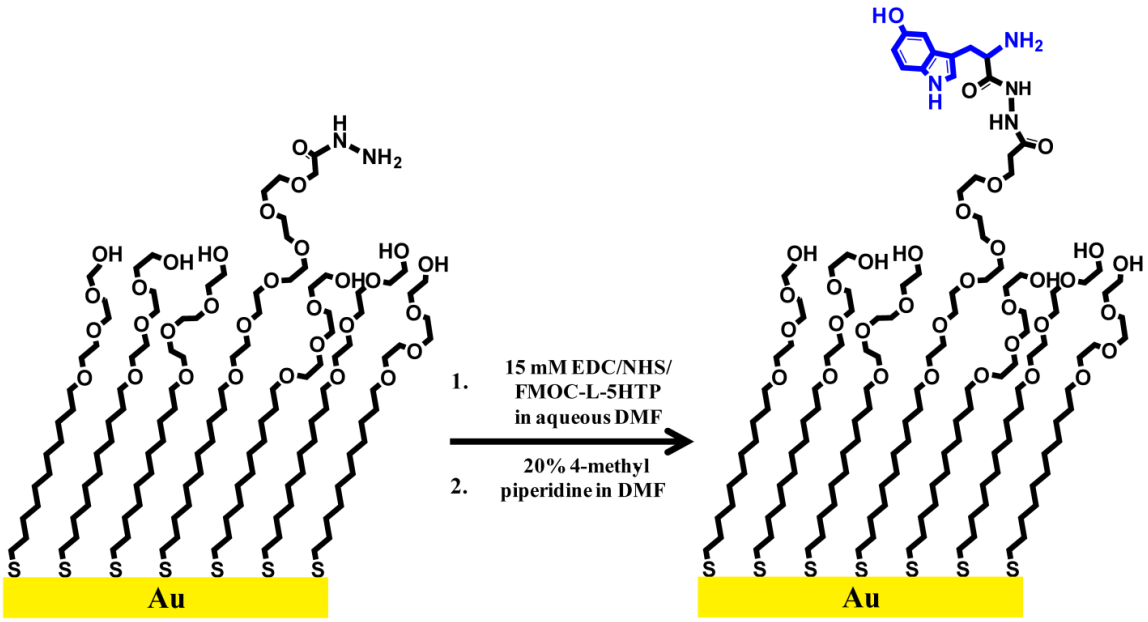

Figure 3-1. **Schematic representation of the 5-HTP-functionalized surfaces.** The Au-coated substrates are passivated with HHEG/TEG mixed SAMs. Then, the 5-HTP molecules are immobilized on HHEG as surface tethers via the solutions of 15 mM NHS/EDC/FMOC-L-5-HTP in 60:40 (v/v) DMF/DI water. The FMOC protecting groups are then removed using 20% v/v 4-methyl-piperidine in DMF, resulting in surfaces capable of capturing biomacromolecular targets.

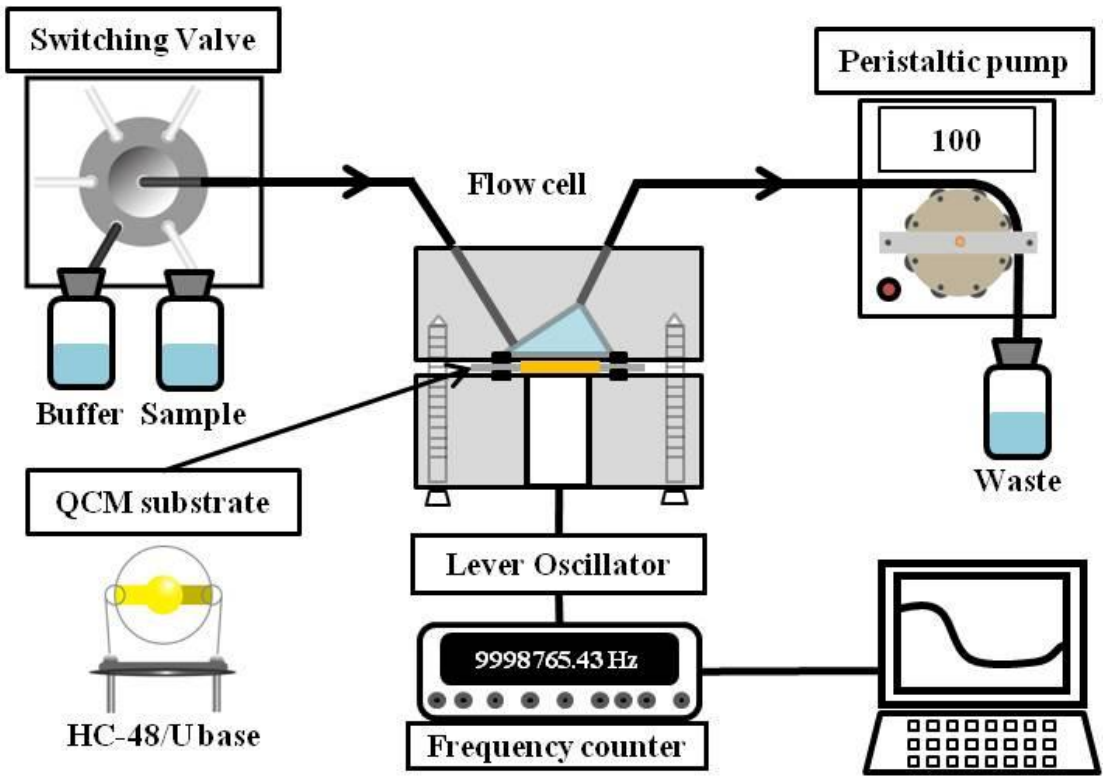

Figure 3-2. **Illustration of the QCM setup**. Quartz crystals used in this study are coated with 10-nm Cr and 100-nm Au. After chemical modifications of the Au surfaces, the crystals are mounted on the HC-48/U base and are integrated into the liquid flow cell. Analyte solution is injected into the cell using a switching valve and peristaltic pump from the withdrawing direction (from left to right in the above diagram).

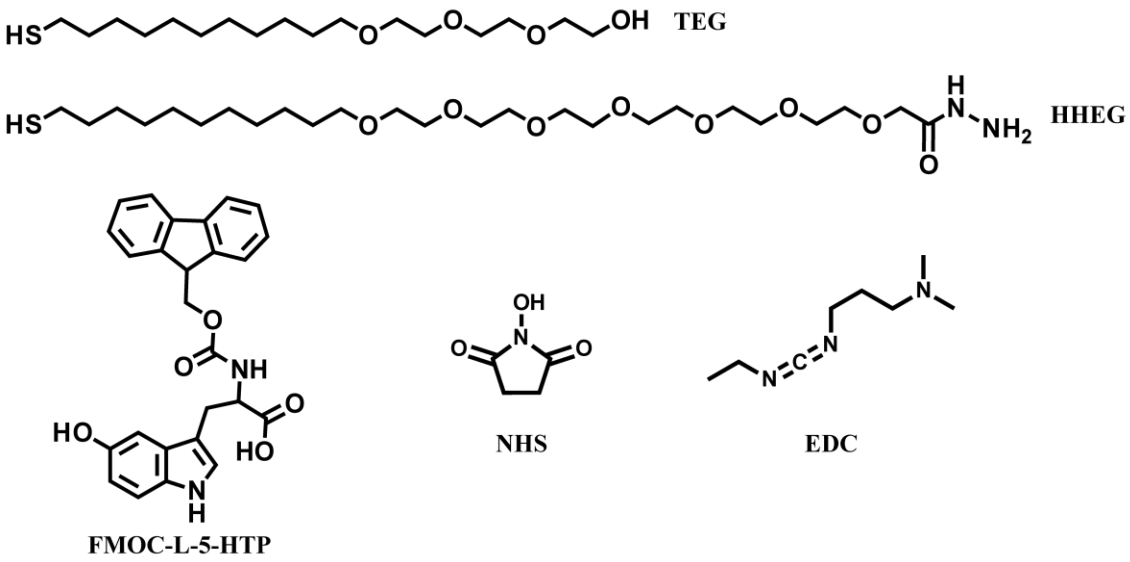

Figure 3-3. **Molecular structures of chemicals that are utilized to fabricate 5-HTP-functionalized surfaces**. The commercially available hydroxyl-terminated tri(ethylene glycol)alkanethiols (TEG) and hydrazide-terminated hexa(ethylene glycol)alkanethiols (HHEG) were used to form mixed self-assembled monolayers. The HHEG molecules in the mixed SAMs were modified with 5-HTP molecules using FMOC-L-5-HTP, *N*-hydroxysuccinimide (NHS), and *N*,*N*′-diisopropylcarbodiimide (EDC).

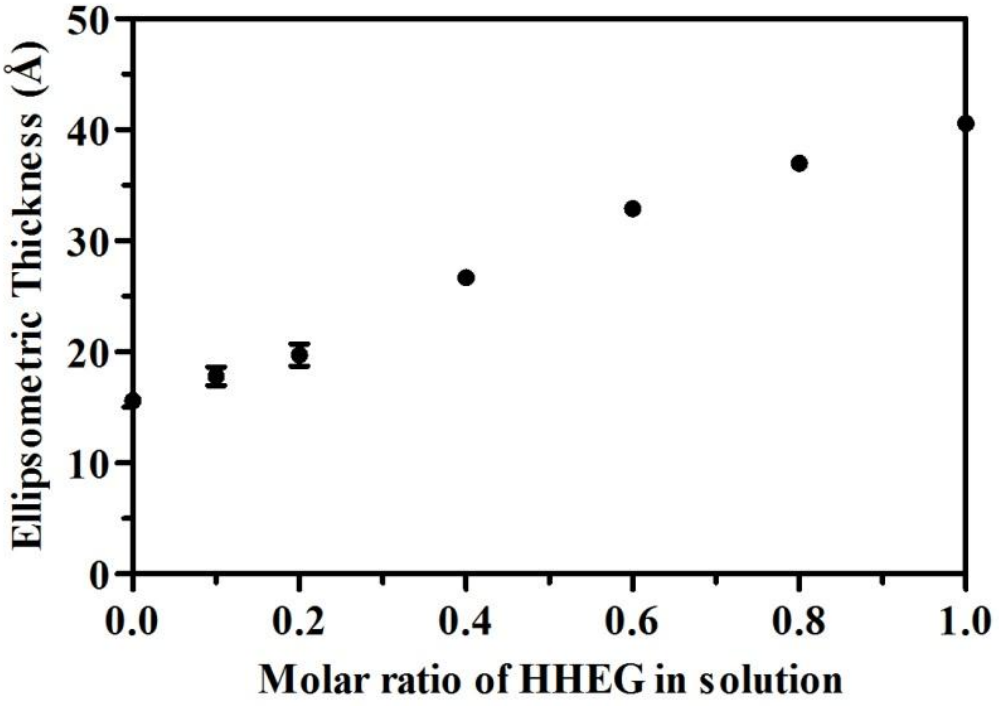

Figure 3-4. **Ellipsometric thickness of the HHEG/TEG mixed SAMs as a function of molar ratio of HHEG (χ_{HHEG}) in solution.** An increase in total SAM thickness with increasing χ_{HHEG} indicates the codeposition of HHEG/TEG on the sensor surfaces.

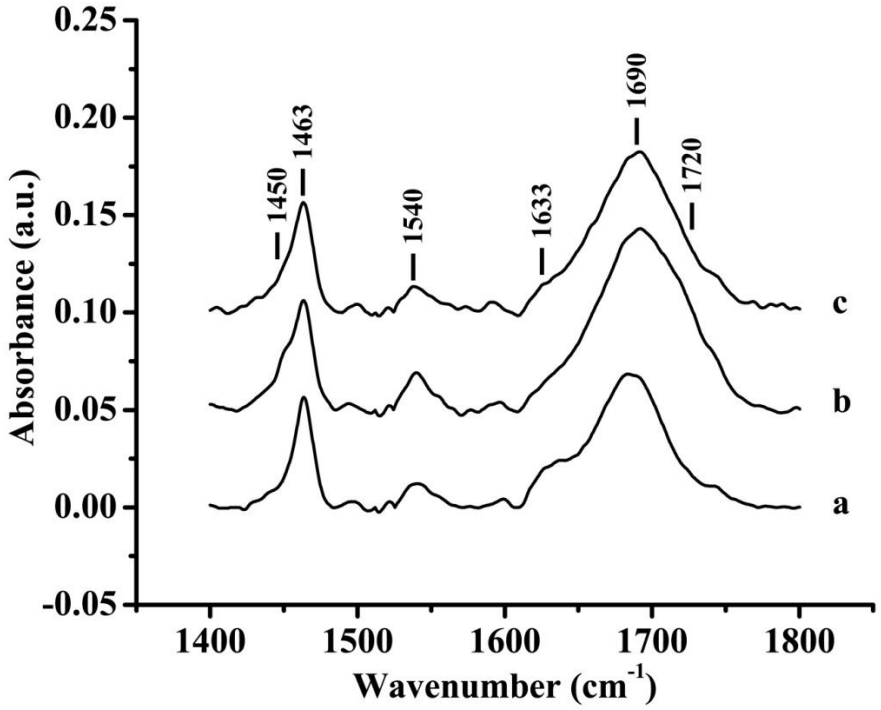

Figure 3-5. **Vibrational spectra obtained by polarization modulation infrared reflection absorption spectroscopy (PM-IRRAS)** showed that 5-hydroxytryptophan (5-HTP) molecules are bound to the hydrazide moiety of HHEG/TEG SAMs. To monitor the surface functionalization, detailed scans are focused in the range from 1400 to 1800 cm^{-1}, which are the positions of carbonyl and amine vibrations. (a) The spectrum of 100% HHEG SAMs shows the absorption peaks of crystalline oligo(ethylene glycol) backbones at 1463 cm^{-1} and the hydrazide terminal groups at 1540, 1633, and 1680 cm^{-1}. Then, HHEG-SAM-modified substrates were treated with a solution of NHS, EDC, and FMOC-L-5-HTP. (b) The spectra of FMOC-L-5-HTP-functionalized HHEG SAMs show intensity increases at 1450, 1540, 1690, and 1720 cm^{-1}, indicating that FMOC-L-5-HTP molecules are bound to the hydrazide moiety. (c) The intensity decrease of the peaks at 1450, 1540, and 1720 cm^{-1} indicates the FMOC deprotection, resulting in 5-HTP-functionalized substrates.

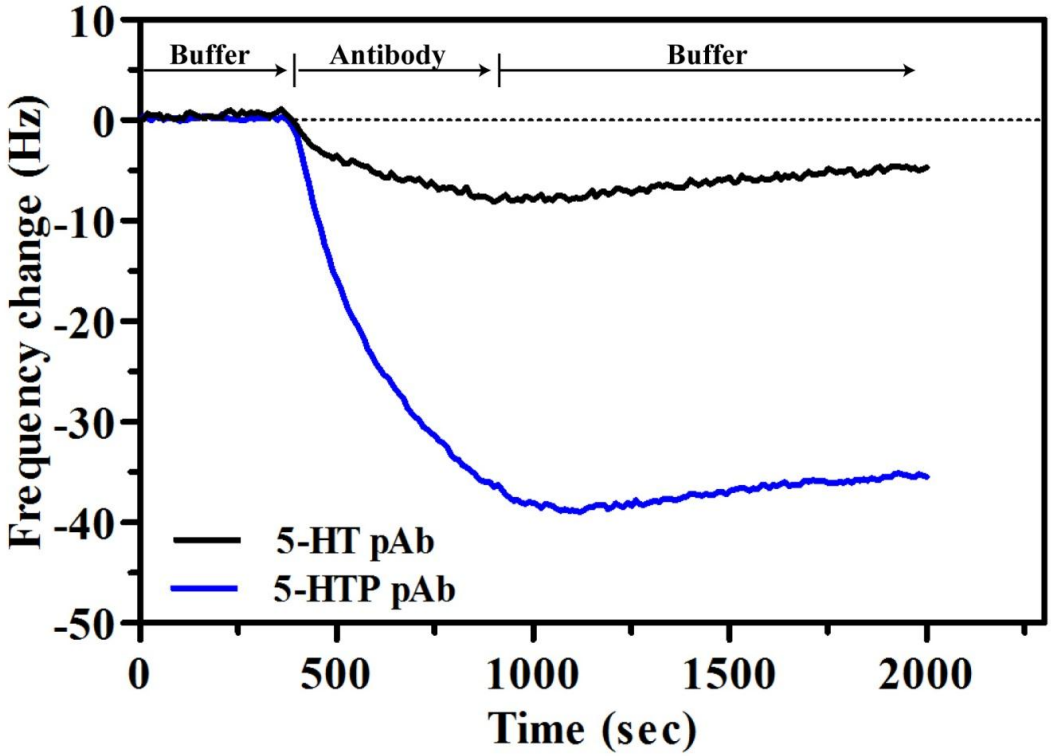

Figure 3-6. **The biofunctionality and bioselectivity of the 5-HTP-functionalized surfaces are tested using polyclonal antibodies (pAbs).** The frequency responses of the quartz crystal microbalance (QCM) indicate that 5-HTP functionalized surfaces recognize 5-HTP pAbs (blue line) as target antibodies while having approximately 25% nonspecific adsorption from 5-HT pAb (black line).

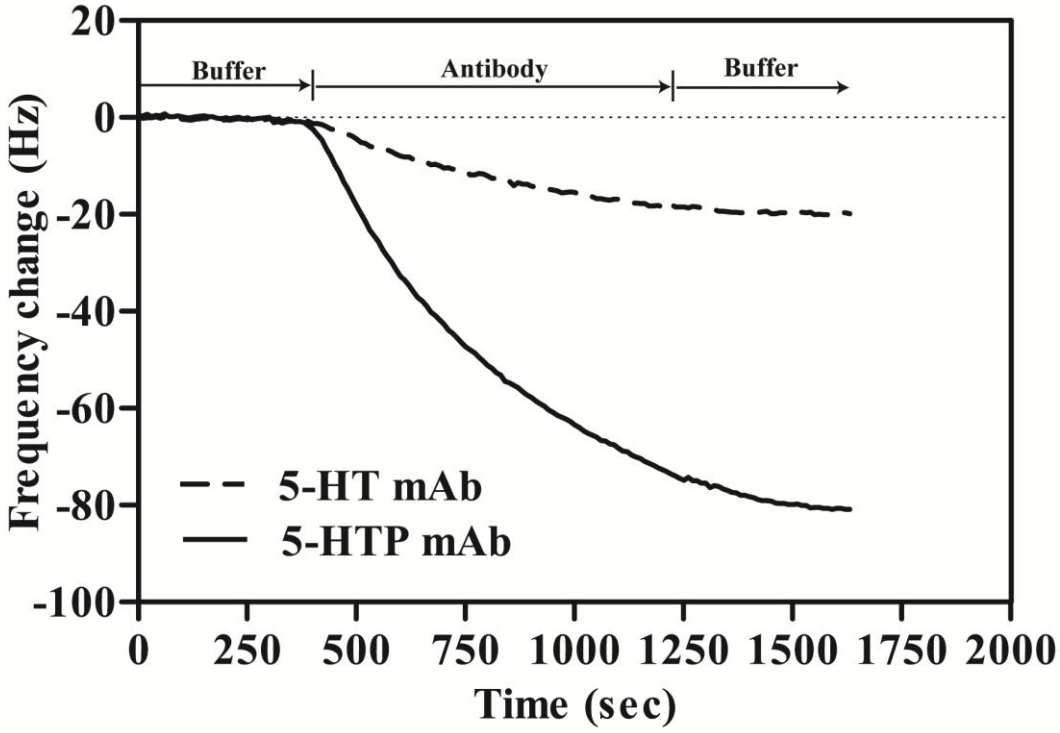

Figure 3-7. **The biofunctionality and bioselectivity of the 5-HTP-functionalized surfaces** are also tested using monoclonal antibodies (mAbs) for 5-HT and 5-HTP, in addition to pAbs. In this experiment, the surfaces were exposed to 5-HT and 5-HTP mAbs for 15 min. Similar to the results from pAbs, QCM frequency responses indicate that 5-HTP functionalized surfaces recognize 5-HTP mAbs (solid line) as target antibodies while showing about 25% nonspecific adsorption from 5-HT mAb (dashed line).

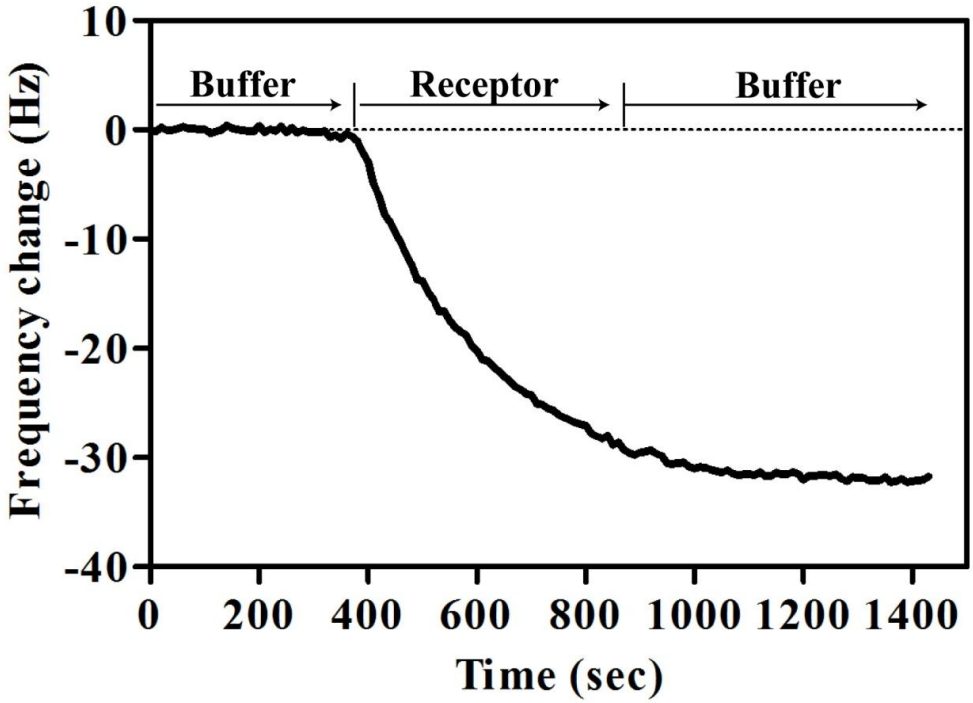

Figure 3-8. **A representative QCM response of 5-HT$_{1A}$ receptors binding to 5-HTP-functionalized surfaces.** After obtaining a stable baseline, the 5-HT$_{1A}$ receptors are injected at a given concentration for 10 min. Upon washing with buffer, no significant dissociation of receptors was observed.

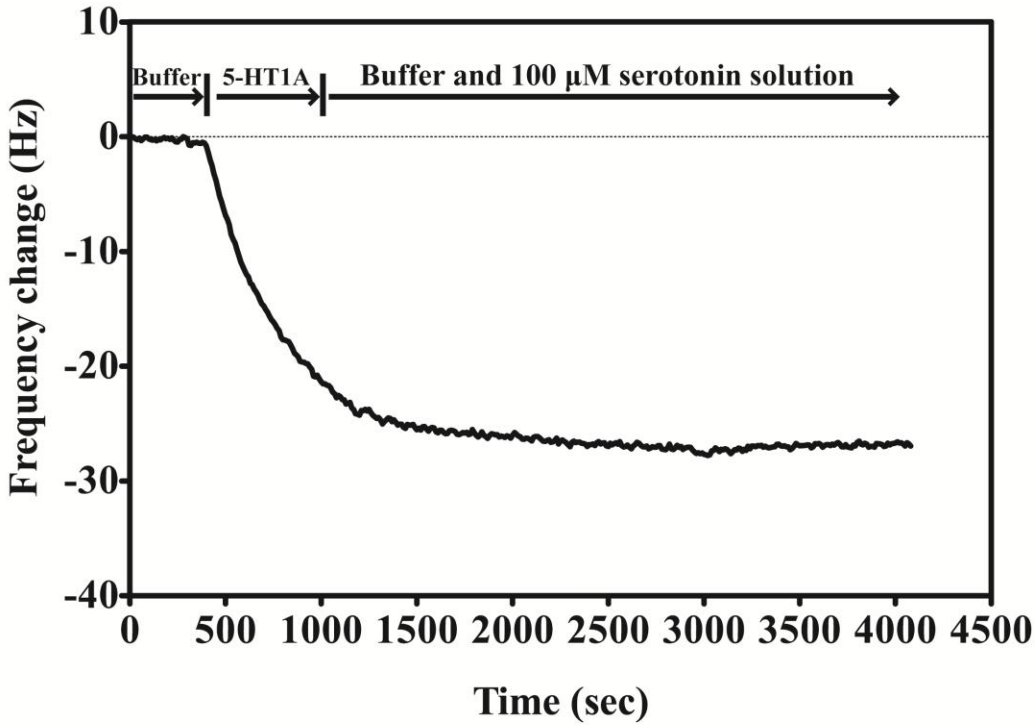

Figure 3-9. **A representative QCM response of 5-HT_{1A} receptors binding to 5-HTP-functionalized surfaces with serotonin solution wash.** The response of QCM frequency displaying 5-HTP-functionalized surfaces exposed to 5-HT_{1A} receptors for 10 min and then with buffer solutions containing 100 µM of serotonin. The serotonin solution was used as an agonist (a ligand that activates receptor functions) to compete with the surface-bound 5-HTP on the surfaces. After serotonin incubation, no dissociation of 5-HT_{1A} was observed (frequency was not increased). This result is similar to the previous studies of receptors with very low K_d (~ 10^{-11} M) (*21*).

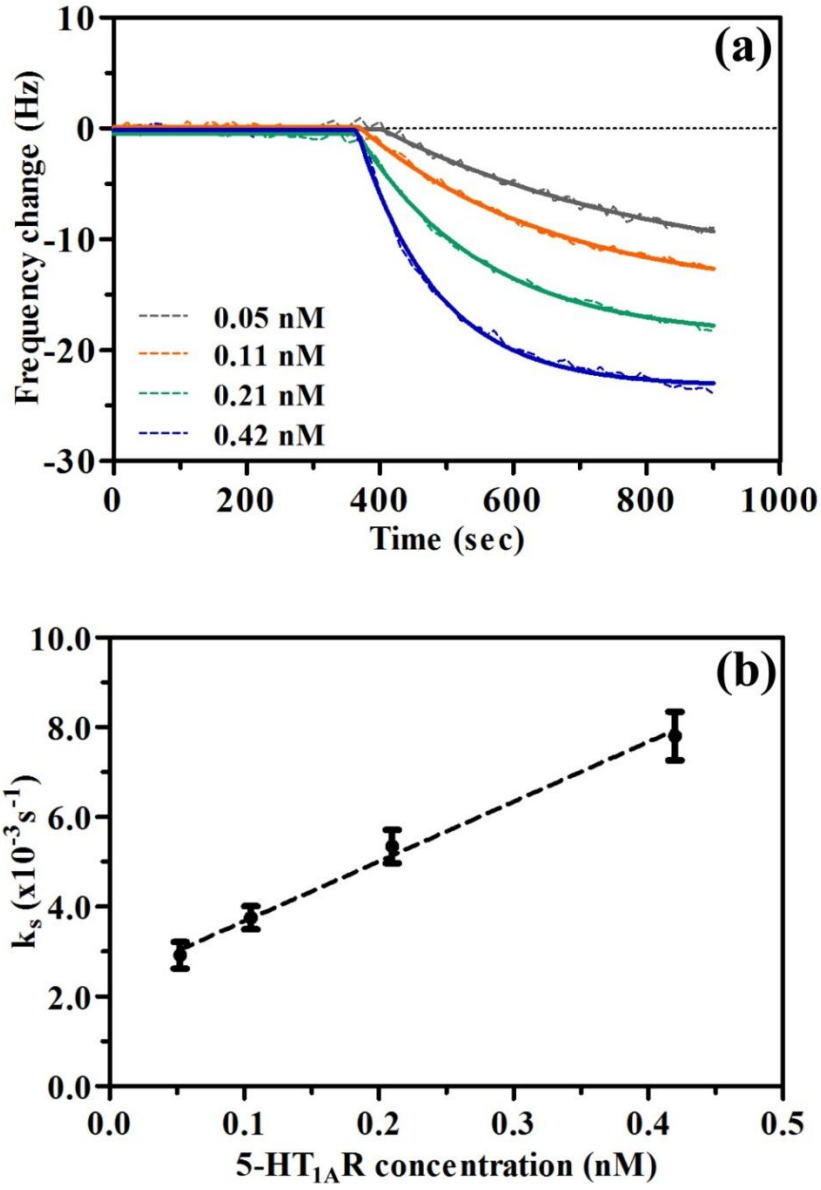

Figure 3-10. **Responses of QCM frequencies at different 5-HT_{1A} concentrations.** (a) QCM responses of 5-HT_{1A} receptors at different concentrations binding to 5-HTP-functionalized surfaces. Each binding curve is fit with a one-phase association equation, giving the observed binding rate (k_s). (b) Linear correlation between k_s and the 5-HT_{1A} concentration, in which the slope is k_{on} and the y-intercept is $k_{off.}$.

3.6 References

1. Rosenbaum, D. M., Rasmussen, S. G., and Kobilka, B. K. The Structure and Function of G-Protein-Coupled Receptors. *Nature* **2009**, *459*, 356-363.
2. Granier, S., and Kobilka, B. A New Era of GPCR Structural and Chemical Biology. *Nat. Chem. Biol.* **2012**, *8*, 670-673.
3. Berton, O., and Nestler, E. J. New Approaches to Antidepressant Drug Discovery: Beyond Monoamines. *Nat. Rev. Neurosci.* **2006**, *7*, 137-151.
4. Taly, A., Corringer, P. J., Guedin, D., Lestage, P., and Changeux, J. P. Nicotinic Receptors: Allosteric Transitions and Therapeutic Targets in the Nervous System. *Nat. Rev. Drug Discov.* **2009**, *8*, 733-750.
5. Lagerstrom, M. C., and Schioth, H. B. Structural Diversity of G Protein-Coupled Receptors and Significance for Drug Discovery. *Nat. Rev. Drug Discov.* **2008**, *7*, 339-357.
6. Congreve, M., Langmead, C. J., Mason, J. S., and Marshall, F. H. Progress in Structure Based Drug Design for G Protein-Coupled Receptors. *J. Med. Chem.* **2011**, *54*, 4283-4311.
7. Bikker, J. A., Trumpp-Kallmeyer, S., and Humblet, C. G-Protein Coupled Receptors: Models, Mutagenesis, and Drug Design. *J. Med. Chem.* **1998**, *41*, 2911-2927.
8. Cooper, M. A. Optical Biosensors in Drug Discovery. *Nat. Rev. Drug Discov.* **2002**, *1*, 515-528.

9. Copeland, R. A., Pompliano, D. L., and Meek, T. D. Opinion: Drug-Target Residence Time and Its Implications for Lead Optimization. *Nat. Rev. Drug Discov.* **2006**, *5*, 730-739.

10. de Jong, L. A., Uges, D. R., Franke, J. P., and Bischoff, R. Receptor-Ligand Binding Assays: Technologies and Applications. *J. Chromatogr. B* **2005**, *829*, 1-25.

11. Kenakin, T. Quantifying Biological Activity in Chemical Terms: A Pharmacology Primer to Describe Drug Effect. *ACS Chem Biol* **2009**, *4*, 249-260.

12. Hulme, E. C., and Trevethick, M. A. Ligand Binding Assays at Equilibrium: Validation and Interpretation. *Br. J. Pharmacol.* **2010**, *161*, 1219-1237.

13. Gunnarsson, A., Dexlin, L., Wallin, P., Svedhem, S., Jonsson, P., Wingren, C., and Hook, F. Kinetics of Ligand Binding to Membrane Receptors from Equilibrium Fluctuation Analysis of Single Binding Events. *J. Am. Chem. Soc.* **2011**, *133*, 14852-14855.

14. Lee, P. H. Label-Free Optical Biosensor: A Tool for G Protein-Coupled Receptors Pharmacology Profiling and Inverse Agonists Identification. *J. Recept. Signal Transduct.* **2009**, *29*, 146-153.

15. Becker, B., and Cooper, M. A. A Survey of the 2006-2009 Quartz Crystal Microbalance Biosensor Literature. *J. Mol. Recognit.* **2011**, *24*, 754-787.

16. Shuster, M. J., Vaish, A., Szapacs, M. E., Anderson, M. E., Weiss, P. S., and Andrews, A. M. Biospecific Recognition of Tethered Small Molecules Diluted in Self-Assembled Monolayers. *Adv. Mater.* **2008**, *20*, 164-167.

17. Vaish, A., Shuster, M. J., Cheunkar, S., Singh, Y. S., Weiss, P. S., and Andrews, A. M. Native Serotonin Membrane Receptors Recognize 5-Hydroxytryptophan-Functionalized Substrates: Enabling Small-Molecule Recognition. *ACS Chem. Neurosci.* **2010**, *1*, 495-504.

18. Stern, E., Klemic, J. F., Routenberg, D. A., Wyrembak, P. N., Turner-Evans, D. B., Hamilton, A. D., LaVan, D. A., Fahmy, T. M., and Reed, M. A. Label-Free Immunodetection with CMOS-Compatible Semiconducting Nanowires. *Nature* **2007**, *445*, 519-522.

19. Liao, W. S., Chen, X., Yang, T., Castellana, E. T., Chen, J., and Cremer, P. S. Benchtop Chemistry for the Rapid Prototyping of Label-Free Biosensors: Transmission Localized Surface Plasmon Resonance Platforms. *Biointerphases* **2009**, *4*, 80-85.

20. Cooper, M. A. Label-Free Screening of Bio-Molecular Interactions. *Anal. Bioanal. Chem.* **2003**, *377*, 834-842.

21. Schmid, E. L., Tairi, A. P., Hovius, R., and Vogel, H. Screening Ligands for Membrane Protein Receptors by Total Internal Reflection Fluorescence: The 5-HT_3 Serotonin Receptor. *Anal. Chem.* **1998**, *70*, 1331-1338.

22. Leatherbarrow, R. J., and Edwards, P. R. Analysis of Molecular Recognition Using Optical Biosensors. *Curr. Opin. Chem. Biol.* **1999**, *3*, 544-547.

23. Ronkainen, N. J., Halsall, H. B., and Heineman, W. R. Electrochemical Biosensors. *Chem. Soc. Rev.* **2010**, *39*, 1747-1763.

24. Cheng, A. K., Sen, D., and Yu, H. Z. Design and Testing of Aptamer-Based Electrochemical Biosensors for Proteins and Small Molecules. *Bioelectrochemistry* **2009**, *77*, 1-12.

25. Cheng, C. I., Chang, Y. P., and Chu, Y. H. Biomolecular Interactions and Tools for Their Recognition: Focus on the Quartz Crystal Microbalance and Its Diverse Surface Chemistries and Applications. *Chem. Soc. Rev.* **2012**, *41*, 1947-1971.

26. Edvardsson, M., Rodahl, M., Kasemo, B., and Hook, F. A Dual-Frequency QCM-D Setup Operating at Elevated Oscillation Amplitudes. *Anal. Chem.* **2005**, *77*, 4918-4926.

27. Ariga, K., Lvov, Y., and Kunitake, T. Assembling Alternate Dye-Polyion Molecular Films by Electrostatic Layer-by-Layer Adsorption. *J. Am. Chem. Soc.* **1997**, *119*, 2224-2231.

28. Hook, F., Voros, J., Rodahl, M., Kurrat, R., Boni, P., Ramsden, J. J., Textor, M., Spencer, N. D., Tengvall, P., Gold, J., and Kasemo, B. A Comparative Study of Protein Adsorption on Titanium Oxide Surfaces Using in Situ Ellipsometry, Optical Waveguide Lightmode Spectroscopy, and Quartz Crystal Microbalance/Dissipation. *Colloid Surface B* **2002**, *24*, 155-170.

29. Mori, T., Toyoda, M., Ohtsuka, T., and Okahata, Y. Kinetic Analyses for Bindings of Concanavalin a to Dispersed and Condensed Mannose Surfaces on a Quartz Crystal Microbalance. *Anal. Biochem.* **2009**, *395*, 211-216.

30. Frasconi, M., Mazzei, F., and Ferri, T. Protein Immobilization at Gold-Thiol Surfaces and Potential for Biosensing. *Anal. Bioanal. Chem.* **2010**, *398*, 1545-1564.

31. Neumann, L., Wohland, T., Whelan, R. J., Zare, R. N., and Kobilka, B. K. Functional Immobilization of a Ligand-Activated G-Protein-Coupled Receptor. *ChemBioChem* **2002**, *3*, 993-998.

32. Hodneland, C. D., Lee, Y. S., Min, D. H., and Mrksich, M. Selective Immobilization of Proteins to Self-Assembled Monolayers Presenting Active Site-Directed Capture Ligands. *Proc. Natl. Acad. Sci. USA* **2002**, *99*, 5048-5052.

33. Sevin-Landais, A., Rigler, P., Tzartos, S., Hucho, F., Hovius, R., and Vogel, H. Functional Immobilisation of the Nicotinic Acetylcholine Receptor in Tethered Lipid Membranes. *Biophys. Chem.* **2000**, *85*, 141-152.

34. Samanta, D., and Sarkar, A. Immobilization of Bio-Macromolecules on Self-Assembled Monolayers: Methods and Sensor Applications. *Chem. Soc. Rev.* **2011**, *40*, 2567-2592.

35. Gestwicki, J. E., Hsieh, H. V., and Pitner, J. B. Using Receptor Conformational Change to Detect Low Molecular Weight Analytes by Surface Plasmon Resonance. *Anal. Chem.* **2001**, *73*, 5732-5737.

36. Kumbhat, S., Shankaran, D. R., Kim, S. J., Gobi, K. V., Joshi, V., and Miura, N. Surface Plasmon Resonance Biosensor for Dopamine Using D3 Dopamine Receptor as a Biorecognition Molecule. *Biosensors Bioelectron.* **2007**, *23*, 421-427.

37. Kroger, D., Hucho, F., and Vogel, H. Ligand Binding to Nicotinic Acetylcholine Receptor Investigated by Surface Plasmon Resonance. *Anal. Chem.* **1999**, *71*, 3157-3165.

38. Lahiri, J., Isaacs, L., Tien, J., and Whitesides, G. M. A Strategy for the Generation of Surfaces Presenting Ligands for Studies of Binding Based on an Active Ester as a Common Reactive Intermediate: A Surface Plasmon Resonance Study. *Anal. Chem.* **1999**, *71*, 777-790.

39. Claridge, S. A., Liao, W. S., Thomas, J. C., Zhao, Y., Cao, H. H., Cheunkar, S., Serino, A. C., Andrews, A., and Weiss, P. S. From the Bottom Up: Dimensional Control and Characterization in Molecular Monolayers. *Chem. Soc. Rev.* **2013**, *in press*,

40. Wang, T. T., and Muthuswamy, J. Immunosensor for Detection of Inhibitory Neurotransmitter Gamma-Aminobutyric Acid Using Quartz Crystal Microbalance. *Anal. Chem.* **2008**, *80*, 8576-8582.

41. Funder, E. D., Jensen, A. B., Torring, T., Kodal, A. L. B., Azcargorta, A. R., and Gothelf, K. V. Synthesis of Dopamine and Serotonin Derivatives for Immobilization on a Solid Support. *J. Org. Chem.* **2012**, *77*, 3134-3142.

42. Vaish, A., Shuster, M. J., Cheunkar, S., Weiss, P. S., and Andrews, A. M. Tuning Stamp Surface Energy for Soft Lithography of Polar Molecules to Fabricate Bioactive Small-Molecule Microarrays. *Small* **2011**, *7*, 1471-1479.

43. Shuster, M. J., Vaish, A., Cao, H. H., Guttentag, A. I., McManigle, J. E., Gibb, A. L., Martinez, M. M., Nezarati, R. M., Hinds, J. M., Liao, W. S., Weiss, P. S., and Andrews, A. M. Patterning Small-Molecule Biocapture Surfaces: Microcontact Insertion Printing vs. Photolithography. *Chem. Commun.* **2011**, *47*, 10641-10643.

44. Stefani C. Altieri, Y. S., Etienne Sibille, and Anne M. Andrews. (2012) Serotonergic Pathways in Depression, In *Neurobiology of Depression* (Francisco Lopez-Munoz, C. A., Ed.), p 143.

45. Harder, P., Grunze, M., Dahint, R., Whitesides, G. M., and Laibinis, P. E. Molecular Conformation in Oligo(Ethylene Glycol)-Terminated Self-Assembled Monolayers on Gold and Silver Surfaces Determines Their Ability to Resist Protein Adsorption. *J. Phys. Chem. B* **1998**, *102*, 426-436.

46. Prime, K. L., and Whitesides, G. M. Self-Assembled Organic Monolayers - Model Systems for Studying Adsorption of Proteins at Surfaces. *Science* **1991**, *252*, 1164-1167.

47. Palegrosdemange, C., Simon, E. S., Prime, K. L., and Whitesides, G. M. Formation of Self-Assembled Monolayers by Chemisorption of Derivatives of Oligo(Ethylene Glycol) of Structure $HS(CH_2)_{11}(OCH_2CH_2)_mOH$ on Gold. *J. Am. Chem. Soc.* **1991**, *113*, 12-20.

48. Raddatz, S., Mueller-Ibeler, J., Kluge, J., Wass, L., Burdinski, G., Havens, J. R., Onofrey, T. J., Wang, D., and Schweitzer, M. Hydrazide Oligonucleotides: New Chemical Modification for Chip Array Attachment and Conjugation. *Nucleic Acids Res.* **2002**, *30*, 4793-4802.

49. Yewle, J. N., Wei, Y. N., Puleo, D. A., Daunert, S., and Bachas, L. G. Oriented Immobilization of Proteins on Hydroxyapatite Surface Using Bifunctional Bisphosphonates as Linkers. *Biomacromolecules* **2012**, *13*, 1742-1749.

50. Green, R. J., Frazier, R. A., Shakesheff, K. M., Davies, M. C., Roberts, C. J., and Tendler, S. J. B. Surface Plasmon Resonance Analysis of Dynamic Biological Interactions with Biomaterials. *Biomaterials* **2000**, *21*, 1823-1835.

51. Shuster, M. J., Vaish, A., Gilbert, M. L., Martinez-Rivera, M., Nezarati, R. M., Weiss, P. S., and Andrews, A. M. Comparison of Oligo(Ethylene Glycol)Alkanethiols Versus *N*-Alkanethiols: Self-Assembly, Insertion, and Functionalization. *J. Phys. Chem. C* **2011**, *115*, 24778-24787.

52. Lewis, P. A., Smith, R. K., Kelly, K. F., Bumm, L. A., Reed, S. M., Clegg, R. S., Gunderson, J. D., Hutchison, J. E., and Weiss, P. S. The Role of Buried Hydrogen Bonds in Self-Assembled Mixed Composition Thiols on Au{111}. *J. Phys. Chem. B* **2001**, *105*, 10630-10636.

53. Love, J. C., Estroff, L. A., Kriebel, J. K., Nuzzo, R. G., and Whitesides, G. M. Self-Assembled Monolayers of Thiolates on Metals as a Form of Nanotechnology. *Chem. Rev.* **2005**, *105*, 1103-1169.

54. Frutos, A. G., Brockman, J. M., and Corn, R. M. Reversible Protection and Reactive Patterning of Amine- and Hydroxyl-Terminated Self-Assembled Monolayers on Gold Surfaces for the Fabrication of Biopolymer Arrays. *Langmuir* **2000**, *16*, 2192-2197.

55. Valeur, E., and Bradley, M. Amide Bond Formation: Beyond the Myth of Coupling Reagents. *Chem. Soc. Rev.* **2009**, *38*, 606-631.

56. Brian L. Frey, R. M. C., and Stephen C. Weibel. (2002) Polarization-Modulation Approaches to Reflection-Absorption Spectroscopy In *Handbook of Vibrational Spectroscopy* (Griffiths, C. J. M. a. P., Ed.), p 1042, John Wiley & Sons, Inc.

57. Zorn, S., Martin, N., Gerlach, A., and Schreiber, F. Real-Time Pmirras Studies of in Situ Growth of $C_{11}(EG_6)OMe$ on Gold and Immersion Effects. *PCCP* **2010**, *12*, 8986-8991.

58. Yang, M., Teeuwen, R. L. M., Giesbers, M., Baggerman, J., Arafat, A., de Wolf, F. A., van Hest, J. C. M., and Zuilhof, H. One-Step Photochemical Attachment of NHS-Terminated Monolayers onto Silicon Surfaces and Subsequent Functionalization. *Langmuir* **2008**, *24*, 7931-7938.

59. Englebienne, P. Use of Colloidal Gold Surface Plasmon Resonance Peak Shift to Infer Affinity Constants from the Interactions between Protein Antigens and Antibodies Specific for Single or Multiple Epitopes. *The Analyst* **1998**, *123*, 1599-1603.

60. MacKenzie, C. R., Hirama, T., Deng, S. J., Bundle, D. R., Narang, S. A., and Young, N. M. Analysis by Surface Plasmon Resonance of the Influence of Valence on the Ligand Binding Affinity and Kinetics of an Anti-Carbohydrate Antibody. *J. Biol. Chem.* **1996**, *271*, 1527-1533.

61. Nieba, L., Krebber, A., and Pluckthun, A. Competition Biacore for Measuring True Affinities: Large Differences from Values Determined from Binding Kinetics. *Anal. Biochem.* **1996**, *234*, 155-165.

62. Bailey, K., Bally, M., Leifert, W., Voros, J., and McMurchie, T. G-Protein Coupled Receptor Array Technologies: Site Directed Immobilisation of Liposomes Containing the H1-Histamine or M2-Muscarinic Receptors. *Proteomics* **2009**, *9*, 2052-2063.

63. Kapur, S., and Seeman, P. Antipsychotic Agents Differ in How Fast They Come Off the Dopamine D-2 Receptors. Implications for Atypical Antipsychotic Action. *J. Psychiatry Neurosci.* **2000**, *25*, 161-166.

64. Pfaffendorf, M., Batink, H. D., Trankle, C., Mohr, K., and van Zwieten, P. A. Probing the Selectivity of Allosteric Modulators of Muscarinic Receptors at Other G-Protein-Coupled Receptors. *J. Auton. Pharmacol.* **2000**, *20*, 55-62.

Chapter 4

Patterning of Polar Molecules to Fabricate Small-Molecule Microarrays

4.1 Introduction

Many biological mechanisms and pathways, such as chemical signaling, are regulated by interactions of small molecules with cell surface receptors, nucleotides, and other large biomolecules [*1, 2*]. The ability to characterize, visualize, and screen biological activities in a high-throughput manner is necessary to address the fast-growing needs in biological investigations. Among currently available techniques, small-molecule microarrays have been used for identifying and investigating endogenous binding partners and screening combinatorial libraries for drug applications [*3*]. Furthermore, small-molecule microarrays have been produced for biologically active substrates for cell growth and connectivity for tissue engineering [*4, 5*].

Progress in microarray fabrication has been made by patterning large biomolecules including proteins, oligonucleotides, and peptides using lithographic strategies such as photolithography [*6*], electron beam lithography [*7*], nanografting [*8, 9*], dip-pen nanolithography [*10, 11*], and soft lithography [*12, 13*]. In contrast, comparatively less work has been done to create small-molecule microarrays using microarray spotting [*14*] or photolithography [*15*]. However, these patterning techniques cannot produce the sufficient interspace between small-molecule probes to facilitate large biomolecular recognition. It

has been suggested that biorecognition of immobilized small molecules on solid supports depends on dilute placement to preserve functional affinity [*13, 16-19*].

Microcontact printing, a hybrid soft lithography, is widely used for chemical patterning over large areas at the micro- and nanoscales [*20*]. In this method, an elastic PDMS stamp is coated with molecular inks, such as organic molecules, proteins, or nanoparticles, and is brought into conformal contact with noble-metal substrates, resulting in SAM formation in the contact regions. However, as previously reported, the success of microcontact printing is limited by lateral diffusion and gas phase deposition of ink molecules such that pattern fidelity is reduced [*21, 22*]. Besides, the proper spacing between probe molecules required for large-biomolecule binding cannot be overcome. To produce small-molecule microarrays with the capability of recognizing large biomolecules, issues surrounding high densities of small-molecule probes in the patterned regions must also be addressed. In fact, closely packed small molecules *reduce* the bioaccessiblity and bioavailability of microarrays due to steric hindrance and nonspecific adsorption [*16*]. Our group developed a chemical patterning method, microcontact insertion printing, whereby molecules are patterned at low coverages, while preserving pattern fidelity. This occurs by inserting molecular inks into defect sites on preformed SAMs [*22-25*].

Commonly, in microcontact printing [*26*] and microcontact insertion printing [*23*], hydrophobic PDMS stamps are inked with hydrophobic alkanethiols for substrate patterning. However, creating biologically active surfaces, either with small-molecule or large-biomolecule immobilization, often requires tether molecules having polar head groups (*e.g.*, carboxyl, amine) and hydrophilic OEG backbones. The polar and

hydrophilic inks result in inadequate ink transfer to substrates due to poor adsorption of molecular inks onto hydrophobic PDMS stamps [*21, 27*]. One solution to counter this problem is to treat a PDMS stamp with oxygen plasma prior to inking [*28-30*]. Here, we find that oxygen plasma treatment not only increases the interactions between stamps and polar inks but it also facilitates ink transfer to hydrophilic host SAMs. The experimental control by carefully tuning the treatment time can extend the scope of microcontact insertion printing.

By using tuned PDMS stamps, hydrophilic amine-terminated alkanethiols (AEG) tethers were successfully transferred to pre-existing OEG SAMs, creating favorable environment for biorecognition. We describe direct coupling of 5-hydroxytryptophan (5-HTP) to AEG molecules, which shorten the synthetic steps from our previous complex coupling chemistry [*18*]. Finally, the 5-HTP-functionalized miroarrays exhibit selective recognition of native membrane-associated receptors.

4.2 Materials and Methods

4.2.1 Chemicals

Hydroxyl-terminated tri(ethylene glycol) alkanethiol was purchased from Toronto Research Canada (Toronto, ON, Canada). Amine-terminated hexa(ethylene glycol)alkanethiol was purchased from Prochimia (Sopot, Poland). Ethanol (200-proof grade) was obtained from Gold Shield Chemical Co. (Hayward, CA, USA). Deionized water (18 MΩ) was obtained from built-in Millipore water purifier (Billerica, MA, USA). Streptavidin was purchased from Invitrogen Inc. (Carlsbad, CA, USA). Human recombinant 5-HT_{1A}, 5-HT_{2C}, and 5-HT_7 were purchased from PerkinElmer (Waltham, MA, USA). *N*,*N*-dimethylformamide, *N*-(ethyl)-*N´*-(dimethylaminopropyl)-carbodiimide, *N*-hydroxysuccinimide, and diisopropylcarbodiimide were obtained from Sigma-Aldrich (St. Louis, MO, USA). 9-Fluorenylmethoxycarbonyl-5-hydroxy-L-tryptophan was obtained from Anaspec-Eurogentec (San Jose, CA, USA).

4.2.2 Preparation of Polydimethylsiloxane Stamps

Patterned silicon wafers prepared by standard photolithographic procedures were used as master wafers for patterned stamp fabrication [*22, 31*]. Patterned and unpatterned Si wafers were silanized by vacuum evaporation of heptadecafluoro-1,1,2,2-tetra-hydrodecyl trichlorosilane (Gelest, Morrisville, PA, USA) in a vacuum desiccator. They were then rinsed with EtOH, water, and EtOH, followed by drying under a steam of nitrogen. To create PDMS stamps, polydimethylsiloxane and curing agent (Sylgard 184 Cure; Dow Corning, Midland, MI, USA) were mixed thoroughly in a 10:1 ratio by

weight. The mixture was degassed under vacuum to remove bubbles and then poured into a petri dish lined with aluminum foil with the master wafer sitting on the foil. The entire setup was degassed under vacuum. Flat stamps (unpatterned) were fabricated in the same fashion except an unpatterned Si wafer was used.

In all cases (patterned and flat stamps), the uncured PDMS was cured at 75 °C for 24 h. The cured PDMS was carefully removed from the wafer and cut into appropriately sized stamps using a razor blade. Stamps were soaked in hexane for 1.5 h, then incubated into fresh solutions of hexane two additional times for about 4.5 h to remove uncrosslinked and low molecular weight PDMS. Then, stamps were baked at 75 °C for 24 h. Prior to inking, stamps were sonicated in a 50/50 v/v mixture of deionized H_2O and EtOH for 30 min to remove surface contaminants. Stamps were then blotted onto an unpatterned silicon wafer that was cleaned by exposure to UV ozone for 10 min, followed by rinsing with deionized H_2O and EtOH. Sonication and blotting were repeated three times to minimize transfer of residual contaminants to experimental substrates.

4.2.3 Preparation and Functionalization of Self-Assembled Monolayer

Self-assembled monolayers were formed on Au substrates using EtOH as the solvent. Au substrates were prepared by depositing 100 Å Cr followed by 1000 Å Au on Si substrates (Silicon Quest, Santa Clara, CA, USA) using an electron-beam evaporator (Kurt J. Lesker Co., Clairton, PA, USA). For microcontact insertion printing, host SAMs were prepared by immersing flame-annealed Au substrates in 1 mM solution of TEG for 12 h. In some cases, mixed SAMs were prepared by immersing Au surfaces in 1 mM

solution containing TEG and AEG (molar ratio; 95:5) for 12 h. Following SAM formation, substrates were cleaned with EtOH and dried under a stream of nitrogen.

Surfaces were functionalized with 5-HTP as shown in Figure 4-3. Surfaces prepared by either microcontact insertion printing or co-deposition were treated with 15 mM FMOC-5-HTP in the presence of 10 mM NHS, 1 mM DIC, and 30 mM EDC in DMF. The FMOC-protecting groups were removed by immersing substrates in 20% piperidine in DMF for 20 min, resulting in 5-HTP-functionalized surfaces. Samples were rinsed with DMF, followed by 50:50 EtOH:DI H_2O, then DI H_2O, and finally EtOH, and dried under a stream of nitrogen. Samples prepared via co-deposition of SAMs were used for XPS and QCM measurements.

4.2.4 Microcontact Insertion Prining

Patterned stamps with 5-µm square posts and 5-µm pitch were used. Polydimethylsiloxane stamps were treated with oxygen plasma using a Harrick Plasma Cleaner (Harrick Plasma, Ithaca, NY, USA), which was operated under low radio frequency (RF) power at 6.8 W. Oxygen was used as the process gas at 5 psi. In preliminary experiments, we found that higher RF powers (>7 W) leads to complete (uncontrolled) oxidation of PDMS. Stamps were treated with oxygen plasma for varying lengths of time at low RF power to investigate the effects on insertion printing.

For printing, PDMS stamps were inked with 200 µL of either 2 mM AEG in EtOH. Inked stamps were dried after 1 min under a stream of nitrogen. Stamps were then placed in contact with substrates having pre-assembled TEG SAMs for 30 min. Printed surfaces were rinsed 4-5 times with EtOH to remove residual non-inserted ink molecules.

In a test experiment, we found that after carrying out microcontact insertion printing, we could use the same stamp without re-inking to produce a pattern on a bare Au substrate using microcontact printing. This suggests that the majority of ink molecules that are not inserted during the microcontact insertion printing process remain on the stamps.

4.2.5 Characterization Methods

4.2.5.1 X-Ray Photoelectron Spectroscopy

X-ray photoelectron spectroscopy measurements were made using a Kratos Axis Ultra XPS system (Kratos Analytical, Chestnut Ridge, NY, USA), a monochromatic Al kα X-ray source (20 mA, 14 kV) with a 200 μm circular spot size and ultrahigh vacuum (10^{-9} Torr). High-resolution spectra of the C 1s, N 1s, O 1s, S 2p, and Au 4f regions were acquired at a pass energy of 80 eV. All binding energies were referenced to the Au $4f_{7/2}$ peak at 84 eV. Each acquired spectra was an average of scans taken at five different spots on each sample.

4.2.5.2 Contact Angle

Contact angle measurements were carried out using an FTA 100 series instrument (First Ten Angstroms, Portsmouth, VA, USA) at room temperature with water and hexadecane as the experimental liquids. Static contact angles were measured immediately after adding a ~5 μl sessile drop onto PDMS surfaces from a microsyringe. Measurements were taken at least six times with three different samples for each surface.

Surface energies were determined by the method of Owens and Wendt [*32, 33*] using a generalized form of the Young-Dupré equation:

$$\gamma_l(1 + cos\theta) = 2\sqrt{\gamma_l^d \gamma_s^d} + 2\sqrt{\gamma_l^p \gamma_s^p}. \quad (4\text{-}1)$$

For polar systems, surface energies are composed of two components: the dispersive component (γ^d) and the polar component (γ^p), such that $\gamma_s = \gamma_s^d + \gamma_s^p$ and $\gamma_l = \gamma_l^d + \gamma_l^p$ for the solid and liquid surface energies, respectively. By measuring the contact angles (θ) of two different liquids with known surface energy parameters (*i.e.*,γ_l^d, γ_l^p) on a solid, Eq. 4-1 yields two equations that can be solved simultaneously for γ_s^d and γ_s^p.

4.2.5.3 Atomic Force Microscopy

Atomic force microscopy images were acquired using a commercial Dimension 5000 AFM (Bruker Instruments, Santa Barbara, CA, USA) in tapping mode for both topography and phase-contrast imaging. All images were obtained at a scan rate of 0.5 Hz using silicon cantilevers (Bruker Instruments) and a scan size of 20 μm with a resonant frequency of 280 kHz.

4.2.5.4 Quartz crystal Microbalance

Quartz crystal microgravimetry was used to examine protein binding on functionalized surfaces. Measurements were made using a 10 MHz lever oscillator (International Crystal Manufacturing, Oklahoma City, OK, USA) and an Agilent digital multimeter and frequency counter (Agilent, Palo Alto, CA, USA). Binding interactions were carried out on Au-coated QCM crystals (International Crystal Manufacturing) prepared by microcontact insertion printing using AEG-inked stamps on TEG host SAM matrices or co-deposition of mixed monolayers and in some cases, functionalization with

5-HTP, as described above. Crystals had a base resonant frequency of 10 MHz and electrode areas of 0.2 cm^2. Derivatized QCM crystals were placed in an acrylic liquid-flow cell (International Crystal Manufacturing) with a 70-µL volume. The flow cell was sealed with an O-ring and each QCM crystal was allowed to reach a stable baseline frequency. After stabilization, 10 cell volumes of phosphate buffer (PB) (11 mM NaH_2PO_4, 39 mM Na_2HPO_4, pH 7.4) were flowed through the cell and resonant frequencies were recorded.

For binding studies, solutions of 10 µg/mL of each receptor in Tris-HCl buffer (50 mM, pH 7.4) were injected into the flow cell and allowed to equilibrate with 5-HTP-functionalized QCM crystals, respectively, for 10 min. Subsequently, 10 cell volumes of PB buffer were injected and changes in resonant frequencies were recorded. Frequency changes were calculated as the difference between the stable frequencies obtained before and after injection of proteins followed by washing. Each functionalized QCM crystal was challenged only once with one type of protein and crystals were not reused.

4.2.5.5 Statistical Analysis

All analyses were performed using GrapPad Prism (GrapPad Software Inc., San Diego, CA, USA). Two group comparisons were analyzed by unpaired one-tailed *t*-tests as per a *priori* hypotheses. Multiple group comparisons were evaluated for overall significant differences by on-way analysis of variance (ANOVA). Statistics for ANOVA are reported in the figure legends as F statistics with respect to the degrees of freedom. Data were further analyzed by Tukey's post hoc comparisons to evaluate differences

between individual group means. Data are reported as mean ± standard errors of the means with probabilities (P) < 0.05 considered statistically significant.

4.3 Results and Discussion

4.3.1 Wettability of Oxygen-Plasma-Treated Stamps

We systematically explored the effects of tuning the surface energy of PDMS stamps (γ_{PDMS}) by varying oxygen plasma treatment times. Stamps were then inked with AEG tethers, which were inserted via microcontact insertion printing into a background matrix of TEG. As shown in Figure (4-1), the polar component of the surface energy of PDMS stamps (γ_{PDMS}^{p}) changes measurably with increasing plasma treatment times, whereas the dispersive component (γ_{PDMS}^{d}) changes little over the same treatment times. Surface energies were calculated from contact angle measurements. Initially, γ_{PDMS}^{p} increased marginally as a function of plasma treatment time (region I in Figure 4-1). A sharp increase in γ_{PDMS}^{p} was observed between 11-14 s of oxygen plasma treatment corresponding to water contact angles (θ_{water}) $40^{o} \leq \theta_{water} \leq 60^{o}$ (region II). Further plasma treatment for longer times had little further effect on γ_{PDMS}^{p}(region III).

4.3.2 Microcontact Insertion Printing Using Oxygen Plasma Treated PDMS Stamps

We carried out microcontact insertion printing using AEG-inked stamps having different surface energies corresponding to regions I, II, or III of Figure 4-1 (Figure 4-2). Phase-contrast AFM images of the patterns generated by these stamps were obtained. As shown in Figure 4-2B (ii), we observed patterns only on substrates prepared using stamps with intermediate surface energies (γ_{PDMS}^{p} region II). By contrast, patterns were not observed for stamps with γ_{PDMS}^{p} corresponding to region I (hydrophobic stamp; Figure 4-2B (i)) or region III (hydrophilic stamp; Figure 4-2B (iii)). These results suggest that

the inking and transport of polar AEG molecules from oxygen plasma-treated stamps to hydrophilic host TEG SAM matrices during microcontact insertion printing depends on the polar component of the PDMS surface energy. We hypothesize that in region I of Figure 4-1, low γ_{PDMS}^{p} is associated with minimal loading of polar ink on stamps, resulting in poor pattern transfer to host SAMs. In region II, where γ_{PDMS}^{p} is higher but still less than γ_{SAM}^{p} (41.6 mJ/m^2), inking and subsequent transfer of adsorbed ink to the host matrix is favorable and insertion of ink molecules into SAM defect sites results in chemical patterns (Figure 4-2B (ii)). In region III, where $\gamma_{PDMS}^{p} > \gamma_{SAM}^{p}$, ink molecules are likely to remain on the stamp due to strong polar interactions with the stamp surface resulting in poor patterning. Although the time interval to obtain favorable stamp conditions is narrow using an oxygen plasma cleaner, preliminary work indicates that stamp modification can also be accomplished over a broader range of plasma treatment times by finely controlling the oxygen plasma conditions using an oxygen plasma etching system, such as reactive ion etching (RIE), for PDMS oxidation (data not shown).

4.3.3 Characterization of 5-HTP Functionalization

We also investigated representative interactions involving small-molecule capture of membrane-associated receptors, which are difficult to isolate and are an important class of proteins involved in intercellular signaling. We used microcontact insertion printing to pattern AEG tethers and functionalized them with 5-HTP molecules, serotonin precursors [*18*], as a first key step towards the fabrication of bioactive small-molecule microarrays. As mention in earlier chapters, serotonin is a small-molecule neurotransmitter that modulates important brain functions and is a primary molecular and

genetic target in the treatment of mood and anxiety disorders and in diseases of aging [*34-38*].

To follow the functionalization steps, XPS was used to quantify changes in the nitrogen content of SAMs after steps i and iii (Figure 4-3) during the fabrication of 5-HTP-functionalized surfaces. Figure 4-4A shows the N 1s region from representative high-resolution XPS spectra. To quantify the nitrogen content, the normalized area under the peak in the N 1s region was obtained for each sample by dividing individual sample peak areas by the average peak area of mixed SAMs (N=3). Figure 4-4B depicts the normalized mean N 1s peak areas for three separate samples at each functionalization step. Nitrogen was detected on the initial SAM surfaces prepared by solution co-deposition of a 95:5 molar ratio of TEG/AEG in the XPS spectra. Primary and secondary amines have N 1s binding energies in the range of 399 to 402 eV. Formation of amide bonds (step ii, Figure 4-3) with FMOC-5-HTP followed by deprotection (step iii, Figure 4-3) resulted in an approximate tripling of the amount of nitrogen detected by XPS, as illustrated by the significant increase in the mean normalized N 1s peak area (Figure 4-4B). Together with Fourier transform infrared spectroscopy absorption data (not shown), these findings indicate that the coupling of 5-HTP, which contains two nitrogen atoms per molecule, to AEG tethers having one nitrogen atom per molecule, occurs stoichiometrically.

4.3.4 5-HTP-Functionalized Microarrays for Capturing Membrane-Associated Receptors

As shown in Figure 4-5, we studied biorecognition of substrates patterned with inserted AEG tethers using microcontact insertion printing and functionalized with 5-HTP. Previously, we determined that surfaces functionalized with serotonin itself fail to be recognized by native membrane-associated serotonin receptors [*18*]. In contrast, surfaces functionalized with 5-HTP selectively capture serotonin $5HT_{1A}$ and $5HT_7$ receptors. 5-Hydroxytryptophan is the proximal amino acid precursor of serotonin and its additional carboxyl moiety is used for tethering, leaving all functional groups associated with the serotonin core structure available for recognition and binding. Here, we created 5-HTP-patterned substrates using a three-step process involving self-assembly, microcontact insertion printing, and chemical functionalization (Figure 4-5A). First, TEG host SAM matrices were prepared on gold substrates via solution deposition. Next, AEG was inserted via microcontact insertion printing into TEG matrices as described above using stamps with γ_{PDMS}^{p}corresponding to region II of Figure 4-1. Finally, amide bonds were formed between the carboxyl moieties of FMOC-5-HTP and the terminal amine groups of the inserted AEG tethers, followed by removal of the FMOC protecting groups. This streamlined strategy to conjugate 5-HTP directly to amine-terminated tether molecules obviates the need for the diethylamine linkers used with carboxyl-terminated tethers in our previous work [*18*]. The surfaces produced bear microarrays of tethered 5-HTP patterned according to the geometries of the stamps.

To investigate biorecognition of these microarrays, 5-HTP-patterned surfaces were incubated with membrane-associated 5-HT_7 receptors. Because SAMs composed of TEG have been shown to resist nonspecific binding, we hypothesized that capture of 5-HT_7 receptor-containing nanovesicles would occur only in the patterned regions. The AFM topographic images of 5-HTP-patterned surfaces before (Figure 4-5B) and after (Figure 4-5C) 5-HT_7 immobilization shows that capture of receptor-containing vesicles occurs in patterns that replicate the stamp topography. For 5-HTP-patterned substrates before receptor incubation, we were unable to detect patterns. This is because the patterned and inserted regions contain only dilute concentrations of AEG molecules resulting in no discernible height differences between the patterned areas and the surrounding unpatterned regions when imaged using tapping mode AFM topographic imaging. In contrast to topographic imaging, phase-mode imaging detects the presence of the AEG pattern on substrates prior to functionalization and receptor capture (Figure 4-2B (ii)).

We further tested the selectivity of patterned substrates by challenging them with receptors for a different neurotransmitter, GABA, using $GABA_{B1b}$ receptors. We observed that $GABA_{B1b}$ receptor immobilization on 5-HTP-patterned surfaces failed to result in detectable AFM topographic image patterns but instead appeared similar to 5-HTP-patterned surfaces prior to receptor immobilization (images not shown). This is consistent with findings using QCM on unpatterned surfaces bearing dilute AEG tethers co-deposited with TEG and functionalized with 5-HTP, which capture 5-HT_7, 5-HT_{1A}, and 5-HT_{2C} receptors with 4-5 fold selectivity over receptors for other small-molecule neurotransmitters (Figure 4-6).

4.4 Conclusions and Prospects

Tuning the wettability of PDMS stamp surface energies by precisely controlling oxygen plasma treatment times enables the use of microcontact insertion printing with polar ink molecules inserted into hydrophilic host SAMs. We employed microcontact insertion printing to create 5-HTP-functionalized surfaces as a small-molecule microarray prototype and observed selective and patterned capture of serotonin-specific receptors imaged by AFM. Together, these results illustrate that on-chip functionalization produces low-density bioactive small-molecule patterned surfaces by microcontact insertion printing. At present, patterning small-molecule probes in a necessarily dilute fashion cannot be achieved by other patterning methods.

Nonetheless, the current findings suggest that printing, whether by microcontact printing, microcontact insertion printing, or other techniques, using inks and substrates having a wide range of different chemistries will benefit from careful control of PDMS surface properties to optimize ink transfer. Moreover, knowledge of PDMS contact angles associated with optimal stamp surface properties for individual applications enables stamps to be plasma-treated reproducibly. We envision that this system will be extended to small-microarrays functionalized with multiple probes having precisely patterned geometries, including feature shapes, sizes, and spacing to enable capture and identification of small-molecule binding partners from a range of complex milieus.

The content of this chapter was adapted with permission from Vaish, A., Shuster, M. J., Cheunkar, S., Weiss, P. S., and Andrews, A. M. Tuning Stamp Surface Energy for Soft

Lithography of Polar Molecules to Fabricate Bioactive Small-Molecule Microarrays. *Small* **2011**, 7, 1471-1479.

4.5 Figures

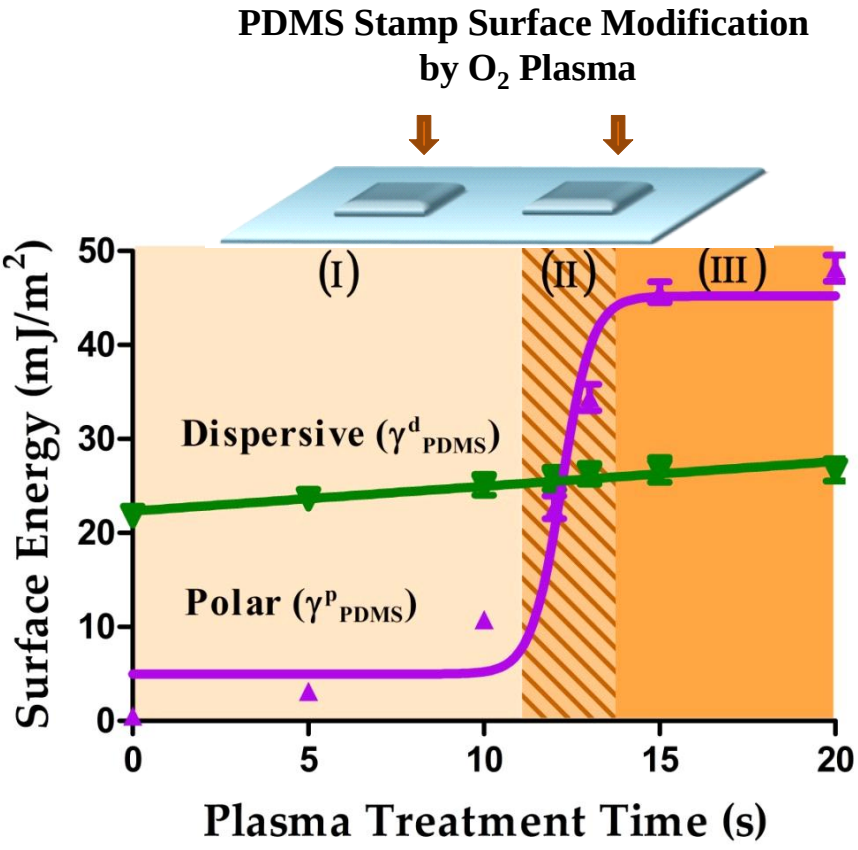

Figure 4-1. **Changes in surface energy components of PDMS stamps treated with oxygen plasma for different times.** The polar component of the surface energy (purple curve; γ_{PDMS}^{p}) is highly dependent on plasma treatment time while the dispersive component (green curve; γ_{PDMS}^{d}) remains relatively stable. Plasma treatment was under relatively mild conditions (O_2 at 5 psi, radio frequency power at 6.8 W). This figure is adapted with permission from reference 12.

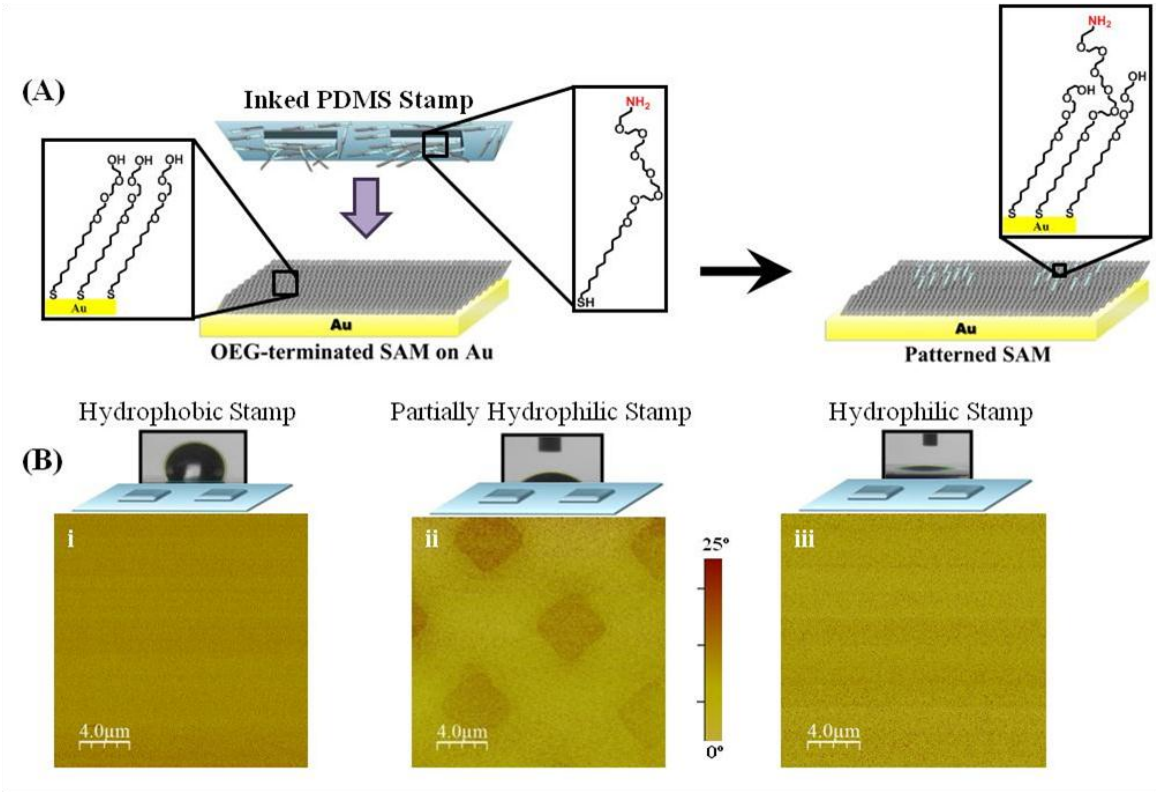

Figure 4-2. **Microcontact insertion printing of amine-terminated hexa(ethylene-glycol)alkanethiols (AEG) by oxygen-plasma-treated stamps.** (A) Schematic of microcontact insertion printing to pattern self-assembled monolayers (SAMs). The surface of a polydimethylsiloxane (PDMS) stamp is modified using oxygen-plasma treatment, followed by inking with AEG. A hydroxyl-terminated tri(ethylene glycol)alkanethiol (TEG) SAM is fabricated on a gold substrate and an AEG-coated stamp is brought into contact with the substrate. The resulting surface contains AEG molecules inserted into the TEG matrix only in the areas where the stamp was in contact with the substrate. (B) Representative atomic force microscope (AFM) tapping mode phase-contrast images of patterned substrates prepared by microcontact insertion printing using PDMS stamps with γ_{PDMS}^{p}corresponding to (i) region I (hydrophobic stamp), (ii)

region II (partially hydrophilic stamp), and (iii) region III (hydrophilic stamp) (Figure 4-1) with 5-µm square posts and 5-µm pitch. Images from substrates inked with stamps with (i) hydrophobic (low PDMS polar surface energy) or (iii) hydrophilic (high PDMS polar surface energy) do not show detectable patterns. However, the contrast differences between the patterned and unpatterned regions of the TEG SAM in (ii) prepared by partially hydrophilic stamps (intermediate PDMS polar surface energy) indicate that insertion of AEG molecules takes place in the patterned regions. This figure is adapted with permission from reference 12.

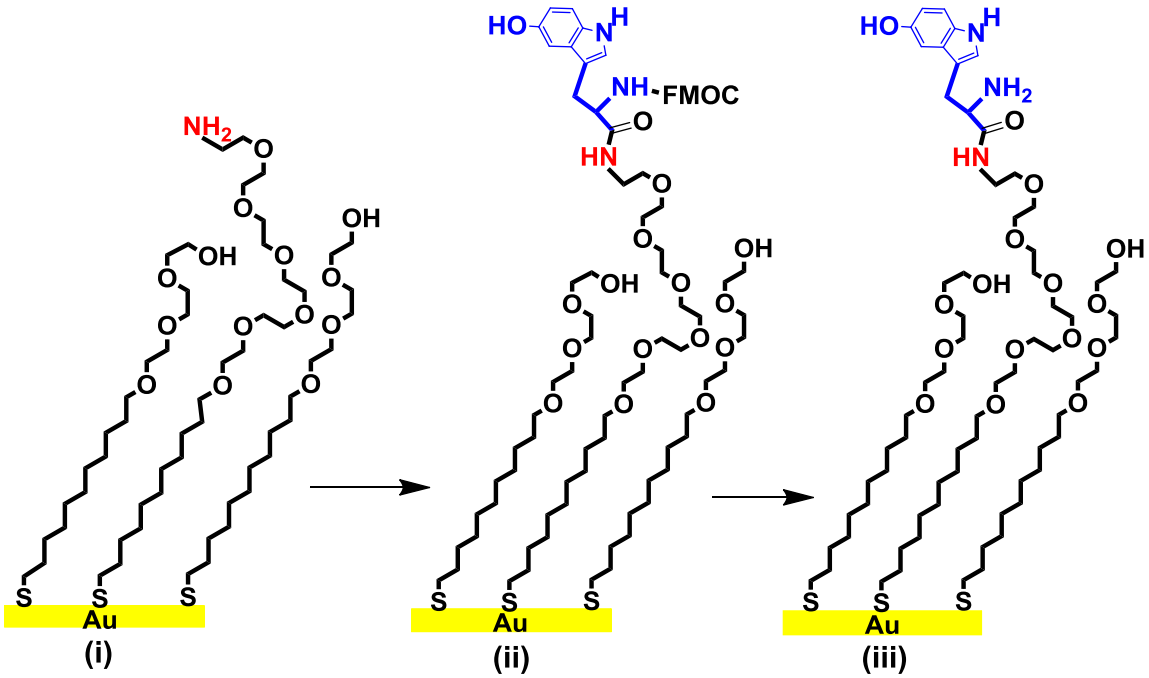

Figure 4-3. Stepwise illustration of the covalent immobilization of 5-hydroxytryptophan on mixed SAMs. (i) Fabrication of mixed SAMs on gold surfaces by microcontact insertion printing or solution deposition of TEG/AEG at a 95:5 molar ratio. (ii) Covalent attachment of FMOC-5-HTP was followed by (iii) FMOC deprotection to produce surface-tethered 5-HTP. This figure is adapted with permission from reference 12.

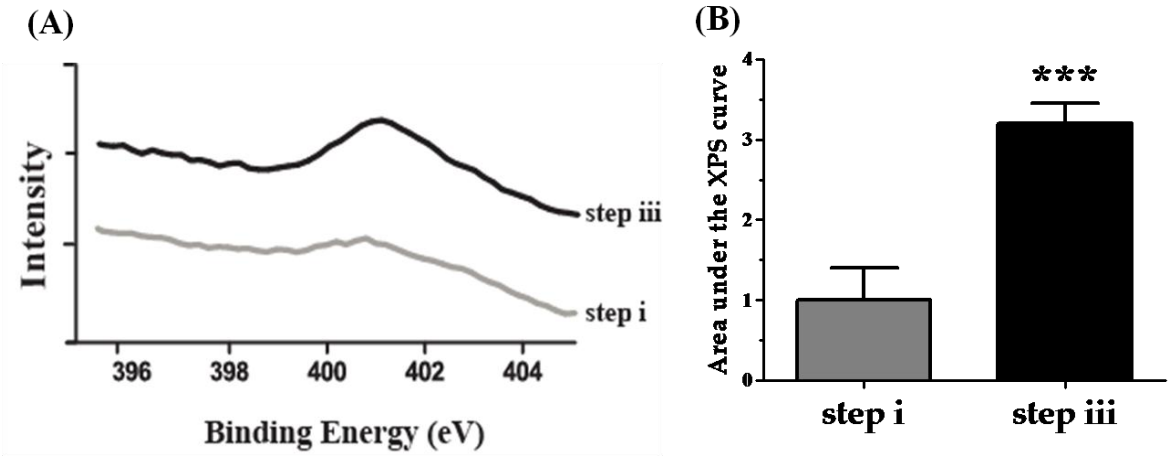

Figure 4-4. **Characterization of surface functionalization by X-ray photoelectron spectroscopy (XPS).** (A) Representative XPS spectra of the N 1s region from mixed self-assembled monolayers co-deposited from a 95:5 molar ratio of TEG/AEG (step i, Figure 4-3) and conjugated with 5-HTP (step iii, Figure 4-3). (B) Peak areas indicate that approximately three times the amount of nitrogen is present after step iii compared to step i, consistent with the stoichiometry of the surface chemistry. Mixed monolayers were prepared using solution co-deposition of TEG/AEG to achieve detectable N 1s peaks while maintaining dilute coverage. Student *t*-test indicated a significant difference between groups ($t(4)=8.1$); ***$P<0.001$ vs. step i. This figure is adapted with permission from reference 12.

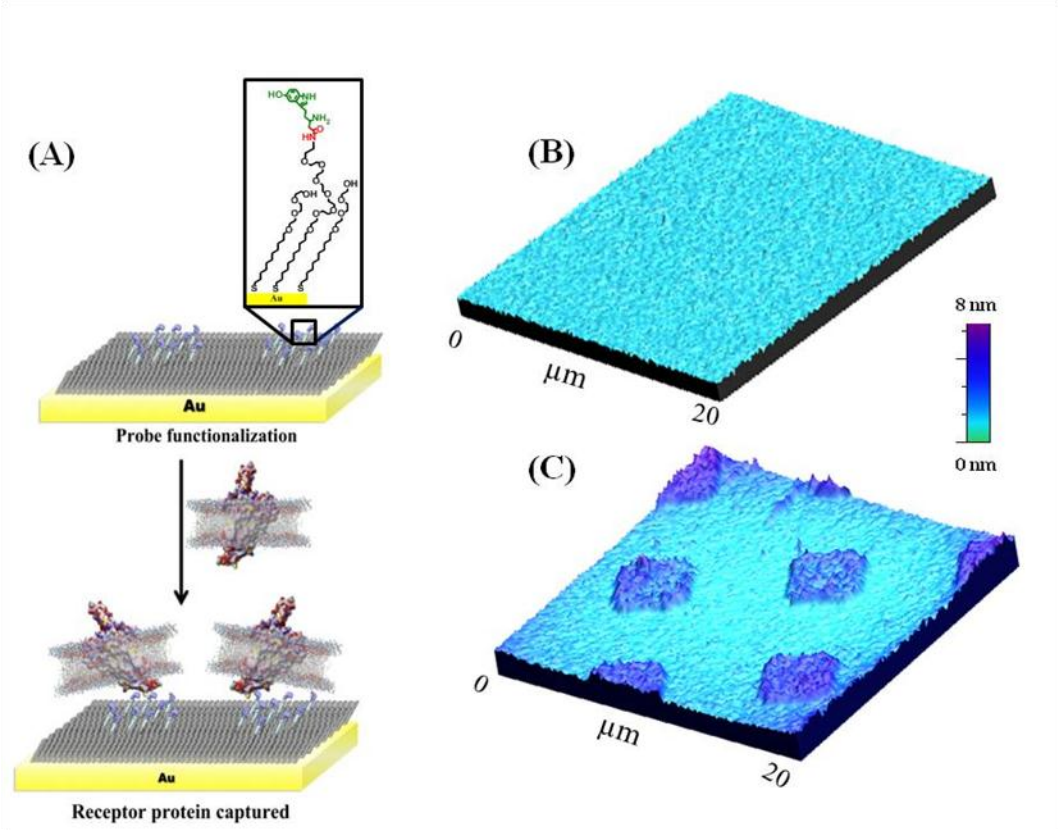

Figure 4-5. **Schematic illustration of membrane-associated 5-HT$_7$ receptor-containing vesicles binding to 5-hydroxytryptophan (5-HTP)-patterned substrates**. (A) Surfaces were prepared via microcontact insertion printing using a PDMS stamp with precisely controlled intermediate hydrophilicity (5 μm square posts/5 μm pitch). Representative AFM topographic images (tapping mode) of a 5-HTP-patterned surface are shown (B) before and (C) after 5-HT$_7$ receptor immobilization. This figure is adapted with permission from reference 12.

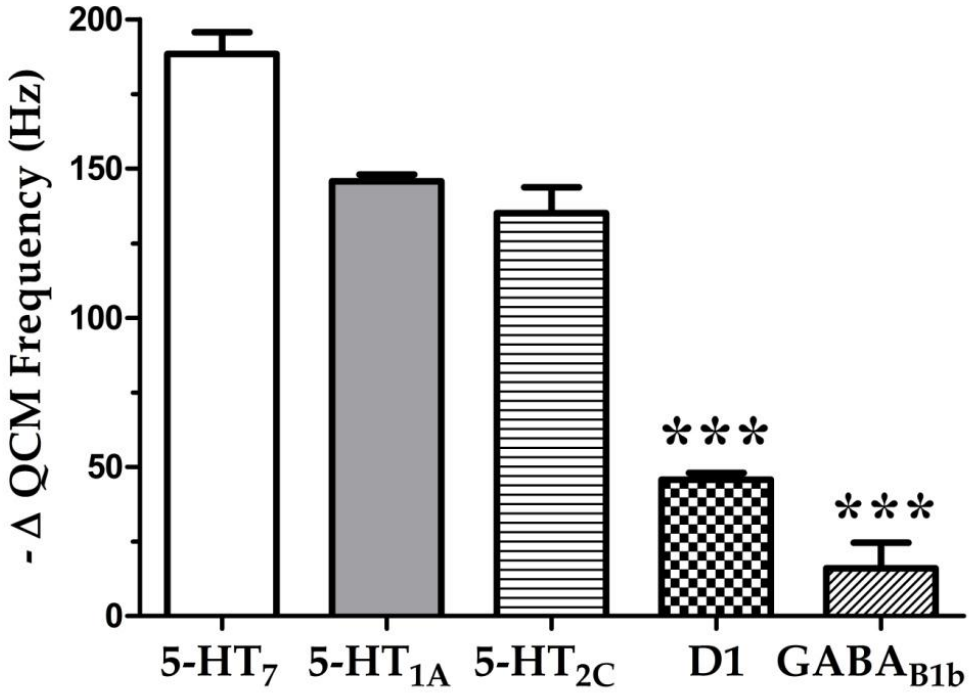

Figure 4-6. **Detection of binding of membrane-associated receptors by QCM.** Mixed monolayers of TEG and AEG (95:5) were formed by co-deposition from solution and dilute AEG tethers were functionalized with 5-hydroxytryptophan (5-HTP). Serotonin receptor subtypes 5-HT_7, 5-HT_{1A}, and 5-HT_{2C} specifically recognize serotonin-mimicking 5-HTP-functionalized surfaces. By contrast, receptors for the structurally similar small-molecule neurotransmitters dopamine and GABA show significantly lower affinity for these surfaces. Error bars represent SEMs for N=3 samples per group. Analysis of variance indicated significant differences between means [$F(4,10)=122.8;P<0.001$]. ***$P<0.001$ vs. 5-HT_7, 5-HT_{1A}, and $5HT_{2C}$ receptors. This figure is adapted with permission from reference 12.

4.6 References

1. Marinissen, M. J., and Gutkind, J. S. G-Protein-Coupled Receptors and Signaling Networks: Emerging Paradigms. *Trends Pharmacol. Sci.* **2001**, *22*, 368-376.
2. Duester, G. Retinoic Acid Synthesis and Signaling During Early Organogenesis. *Cell* **2008**, *134*, 921-931.
3. Hong, Y. L., Webb, B. L., Su, H., Mozdy, E. J., Fang, Y., Wu, Q., Liu, L., Beck, J., Ferrie, A. M., Raghavan, S., Mauro, J., Carre, A., Mueller, D., Lai, F., Rasnow, B., Johnson, M., Min, H. S., Salon, J., and Lahiri, J. Functional GPCR Microarrays. *J. Am. Chem. Soc.* **2005**, *127*, 15350-15351.
4. Sanchez-Cortes, J., Bahr, K., and Mrksich, M. Cell Adhesion to Unnatural Ligands Mediated by a Bifunctional Protein. *J. Am. Chem. Soc.* **2010**, *132*, 9733-9737.
5. Mrksich, M., Chen, C. S., Xia, Y., Dike, L. E., Ingber, D. E., and Whitesides, G. M. Controlling Cell Attachment on Contoured Surfaces with Self-Assembled Monolayers of Alkanethiolates on Gold. *Proc. Natl. Acad. Sci. USA* **1996**, *93*, 10775-10778.
6. Wegner, G. J., Lee, H. J., and Corn, R. M. Characterization and Optimization of Peptide Arrays for the Study of Epitope-Antibody Interactions Using Surface Plasmon Resonance Imaging. *Anal. Chem.* **2002**, *74*, 5161-5168.
7. Christman, K. L., Enriquez-Rios, V. D., and Maynard, H. D. Nanopatterning Proteins and Peptides. *Soft Matter* **2006**, *2*, 928-939.

8. Liu, M., Amro, N. A., and Liu, G.-y. Nanografting for Surface Physical Chemistry. *Annu. Rev. Phys. Chem.* **2008**, *59*, 367-386.

9. Castronovo, M., Radovic, S., Grunwald, C., Casalis, L., Morgante, M., and Scoles, G. Control of Steric Hindrance on Restriction Enzyme Reactions with Surface-Bound DNA Nanostructures. *Nano Lett.* **2008**, *8*, 4140-4145.

10. Lee, K. B., Park, S. J., Mirkin, C. A., Smith, J. C., and Mrksich, M. Protein Nanoarrays Generated by Dip-Pen Nanolithography. *Science* **2002**, *295*, 1702-1705.

11. Demers, L. M., Ginger, D. S., Park, S. J., Li, Z., Chung, S. W., and Mirkin, C. A. Direct Patterning of Modified Oligonucleotides on Metals and Insulators by Dip-Pen Nanolithography. *Science* **2002**, *296*, 1836-1838.

12. Ruiz, S. A., and Chen, C. S. Microcontact Printing: A Tool to Pattern. *Soft Matter* **2007**, *3*, 168-177.

13. Mrksich, M., Grunwell, J. R., and Whitesides, G. M. Biospecific Adsorption of Carbonic Anhydrase to Self-Assembled Monolayers of Alkanethiolates That Present Benzenesulfonamide Groups on Gold. *J. Am. Chem. Soc.* **1995**, *117*, 12009-12010.

14. MacBeath, G., Koehler, A. N., and Schreiber, S. L. Printing Small Molecules as Microarrays and Detecting Protein-Ligand Interactions En Masse. *J. Am. Chem. Soc.* **1999**, *121*, 7967-7968.

15. He, X. Z. G., Gerona-Navarro, G., and Jaffrey, S. R. Ligand Discovery Using Small Molecule Microarrays. *J. Pharmacol. Exp. Ther.* **2005**, *313*, 1-7.

16. Nelson, K. E., Gamble, L., Jung, L. S., Boeckl, M. S., Naeemi, E., Golledge, S. L., Sasaki, T., Castner, D. G., Campbell, C. T., and Stayton, P. S. Surface Characterization of Mixed Self-Assembled Monolayers Designed for Streptavidin Immobilization. *Langmuir* **2001**, *17*, 2807-2816.

17. Shuster, M. J., Vaish, A., Szapacs, M. E., Anderson, M. E., Weiss, P. S., and Andrews, A. M. Biospecific Recognition of Tethered Small Molecules Diluted in Self-Assembled Monolayers. *Adv. Mater.* **2008**, *20*, 164-167.

18. Vaish, A., Shuster, M. J., Cheunkar, S., Singh, Y. S., Weiss, P. S., and Andrews, A. M. Native Serotonin Membrane Receptors Recognize 5-Hydroxytryptophan-Functionalized Substrates: Enabling Small-Molecule Recognition. *ACS Chem. Neurosci.* **2010**, *1*, 495-504.

19. Yu, F., Yao, D. F., and Knoll, W. Surface Plasmon Field-Enhanced Fluorescence Spectroscopy Studies of the Interaction between an Antibody and Its Surface-Coupled Antigen. *Anal. Chem.* **2003**, *75*, 2610-2617.

20. Saavedra, H. M., Mullen, T. J., Zhang, P. P., Dewey, D. C., Claridge, S. A., and Weiss, P. S. Hybrid Strategies in Nanolithography. *Rep. Prog. Phys.* **2010**, *73*, 036501.

21. Vidic, J., Pla-Roca, M., Grosclaude, J., Persuy, M.-A., Monnerie, R., Caballero, D., Errachid, A., Hou, Y., Jaffrezic-Renault, N., Salesse, R., Pajot-Augy, E., and Samitier, J. Gold Surface Functionalization and Patterning for Specific Immobilization of Olfactory Receptors Carried by Nanosomes. *Anal. Chem.* **2007**, *79*, 3280-3290.

22. Srinivasan, C., Mullen, T. J., Hohman, J. N., Anderson, M. E., Dameron, A. A., Andrews, A. M., Dickey, E. C., Horn, M. W., and Weiss, P. S. Scanning Electron Microscopy of Nanoscale Chemical Patterns. *ACS Nano* **2007**, *1*, 191-201.

23. Mullen, T. J., Srinivasan, C., Hohman, J. N., Gillmor, S. D., Shuster, M. J., Horn, M. W., Andrews, A. M., and Weiss, P. S. Microcontact Insertion Printing. *Appl. Phys. Lett.* **2007**, *90*, 063114-063117.

24. Mullen, T. J., Dameron, A. A., Andrews, A. M., and Weiss, P. S. Selecting and Driving Monolayer Structures through Tailored Intermolecular Interactions. *Aldrichimica Acta* **2007**, *40*, 21-31.

25. Mullen, T. J., Srinivasan, C., Shuster, M. J., Horn, M. W., Andrews, A. M., and Weiss, P. S. Hybrid Approaches to Nanometer-Scale Patterning: Exploiting Tailored Intermolecular Interactions. *J. Nanopart. Res.* **2008**, *10*, 1231-1240.

26. Love, J. C., Estroff, L. A., Kriebel, J. K., Nuzzo, R. G., and Whitesides, G. M. Self-Assembled Monolayers of Thiolates on Metals as a Form of Nanotechnology. *Chem. Rev.* **2005**, *105*, 1103-1169.

27. Burdinski, D., Saalmink, M., Van den Berg, J., and Van der Marel, C. Universal Ink for Microcontact Printing. *Angew. Chem. Int. Ed.* **2006**, *45*, 4355-4358.

28. Delamarche, E., Geissler, M., Bernard, A., Wolf, H., Michel, B., Hilborn, J., and Donzel, C. Hydrophilic Poly (Dimethylsloxane) Stamps for Microcontact Printing. *Adv. Mater.* **2001**, *13*, 1164-1167.

29. Kaufmann, T., and Ravoo, B. J. Stamps, Inks and Substrates: Polymers in Microcontact Printing. *Polym. Chem.* **2010**, *1*, 371-387.

30. Lahiri, J., Ostuni, E., and Whitesides, G. M. Patterning Ligands on Reactive SAMs by Microcontact Printing. *Langmuir* **1999**, *15*, 2055-2060.

31. Dameron, A. A., Hampton, J. R., Smith, R. K., Mullen, T. J., Gillmor, S. D., and Weiss, P. S. Microdisplacement Printing. *Nano Lett.* **2005**, *5*, 1834-1837.

32. Owens, D. K., and Wendt, R. C. Estimation of Surface Free Energy of Polymers. *J. Appl. Polym. Sci.* **1969**, *13*, 1741-1747.

33. Chaudhury, M. K. Surface Free-Energies of Alkylsiloxane Monolayers Supported on Elastomeric Polydimethylsiloxanes. *J. Adhes. Sci. Technol.* **1993**, *7*, 669-675.

34. Singh, Y. S., Sawarynski, L. E., Michael, H. M., Ferrell, R. E., Murphey-Corb, M. A., Swain, G. M., Patel, B. A., and Andrews, A. M. Boron-Doped Diamond Microelectrodes Reveal Reduced Serotonin Uptake Rates in Lymphocytes from Adult Rhesus Monkeys Carrying the Short Allele of the 5-HTTLPR. *ACS Chem. Neurosci.* **2010**, *1*, 49-64.

35. Murphy, D. L., Fox, M. A., Timpano, K. R., Moya, P. R., Ren-Patterson, R., Andrews, A. M., Holmes, A., Lesch, K.-P., and Wendland, J. R. How the Serotonin Story is Being Rewritten by New Gene-Based Discoveries Principally Related to SLC6A4, the Serotonin Transporter Gene, Which Functions to Influence All Cellular Serotonin Systems. *Neuropharmacology* **2008**, *55*, 932-960.

36. Fox, M. A., Andrews, A. M., Wendland, J. R., Lesch, K.-P., Holmes, A., and Murphy, D. L. A Pharmacological Analysis of Mice with a Targeted Disruption of the Serotonin Transporter. *Psychopharmacology* **2007**, *195*, 147-166.

37. Luellen, B. A., Bianco, L. E., Schneider, L. M., and Andrews, A. M. Reduced Brain-Derived Neurotrophic Factor is Associated with a Loss of Serotonergic Innervation in the Hippocampus of Aging Mice. *Genes Brain Behav.* **2007**, *6*, 482-490.

38. Szapacs, M. E., Numis, A. L., and Andrews, A. M. Late Onset Loss of Hippocampal 5-HT and NE is Accompanied by Increases in BDNF Protein Expression in Mice Co-Expressing Mutant APP and PS1. *Neurobiol. Dis.* **2004**, *16*, 572-580.

Chapter 5

Subtractive Patterning of Self-Assembled Monolayers via Chemical Lift-Off Lithography

5.1 Introduction

High-throughput molecular printing strategies with high feature resolution are central goals for lithography. Yet, large-area fabrication *vs.* precision, and convenience *vs.* cost are typically conflicting aims [*1-4*]. For instance, although photolithography enables patterning over large areas (centimeters), the prototyping process is time consuming and resolution is restricted by light diffraction [*1-3*]. Patterning by electron-beam lithography (EBL) or scanning probe lithography (SPL) techniques, such as dip-pen nanolithography, nanoshaving, and nanografting [*5-7*], produce high-resolution features (<10 nm and <100 nm for EBL and SPL, respectively) [*1-3*] but throughput is limited by serial processing speeds.

Soft-lithography strategies produce patterns over large areas at the micro- and nanoscales [*1, 3, 4, 8-10*]. Commercial polymers (such as PDMS) are used as molds for pattern transfer via contact printing. The bas-relief pattern on a master mold is fabricated by photolithography for large-area patterning or EBL for high-resolution patterning [*1, 3*]. Once the master is generated, patterned features are negatively transferred to PDMS stamps, which are then “inked” with organic molecules, proteins, nanoparticles, or DNA [*1, 10-16*].

Among the materials transferred, organic molecules, such as alkanethiols and other related molecules, which form SAMs on Au substrates, can be readily subjected to chemical modification at the exposed terminal groups for capturing biomolecules [*1, 16-18*]. Moreover, SAMs serve as "molecular resists" against different wet etchants enabling patterns to be transferred reproducibly to underlying substrates [*19*]. However, the success of contact printing and related soft lithography techniques is also limited by the chemistries and compatibility of the inks, stamps, and substrates [*1, 3, 4*]. For example, lateral diffusion and gas-phase deposition of ink molecules tend to reduce pattern fidelity [*20, 21*] creating a typical resolution limit of ~100 nm for alkanethiols on Au.

To overcome the limitations of stamp feature replication in soft lithography, the general principles of contact printing need to be modified to achieve sharp, stable, and reproducible chemical features on substrates [*7, 19, 22, 23*]. We transformed the conventional contact printing process such that the polymer stamp is activated, and then used to lift-off a pre-formed SAM resist. Strong contact-induced interactions at the stamp-SAM interface enable the transfer of sharp stamp features by mechanical desorption of resist only in the areas of stamp-substrate contact. The subtractive nature of this process precisely replicates features from the master mold [*9, 24*]. This approach, CLL, also enables the intact areas to act as an etch resist for the transfer of features to the underlying substrate. Moreover, stamps used for CLL can be cleaned and reused many times without deterioration.

Here, alkanethiols with different terminal groups (Table 5-1) were used to form SAMs on Au-coated Si substrates. Soft-lithography stamps were created from PDMS to

transfer features of different geometries from standard photolithography/electron-beam lithography-fabricated master molds to the molecular-resist layers [*1, 8, 10*]. The CLL process is outlined schematically in Figure 5-1. A PDMS stamp was first activated by exposure to oxygen plasma, yielding a fully hydrophilic and reactive surface [*17, 25-27*]. The stamp and SAM-modified substrate were then brought into conformal contact. The stamp was peeled away from the substrate, which removed resist molecules selectively in the areas contacted by the stamp, transferring stamp features with high resolution to the substrate. This approach also facilitates the addition of different molecules into the lift-off areas to produce multi-component patterned SAMs.

5.2 Experimental Method

5.2.1 Chemicals

Hydroxyl-terminated tri(ethylene glycol)undecanethiol was purchased from Toronto Research Chemicals Inc., (Toronto, ON, Canada). Biotin-terminated hexa(ethylene glycol)undecanethiol (BEG) was purchased from Nanoscience Instruments Inc. (Phoeniz, AZ, USA). Methoxy-terminated tri(ethylene glycol)undecanthiol was purchased from Prochimia (Sopot, Poland). Hydroxyl-terminated undecanethiol, methyl-terminated undecanethiol, iron nitrate, thiourea, and BSA were purchased from Sigma-Aldrich (St. Louis, MO, USA). Streptavidin was purchased from Invitrogen Inc. (Carlsbad, CA, USA). Anti-streptavidin antibody conjugated to fluorescein isothiocyanate (FITC) was purchased from Abcam Inc. (Cambridge, MA, USA). SYLGARD® 184 silicone elastomer base and curing agent were purchased from Ellsworth Adhesives (Germantown, WI). Ethanol (200-proof grade) was obtained from Gold Shield Chemical Co. (Hayward, CA, USA).

5.2.2 Chemical Lift-Off Process

5.2.2.1 Stamp Preparation

Polydimethylsiloxane stamps of different geometries were formed using standard photolithography-fabricated masters. A 10:1 mass ratio of SYLGARD® 184 silicone elastomer base and curing agent was mixed thoroughly, degassed under vacuum, and cured at 60 $^{\circ}$C overnight.

5.2.2.2 Preparation of Self-Assembled Monolayers

Substrates consisted of 30-nm-thick Au evaporated on Si with a 5-nm Ti/Cr adhesion layer (Platypus, Madison, WI, USA). Before SAM formation, Au Substrates were cleaned with hydrogen flame annealing for a few minutes. Alkanethiols with different terminal groups were used to form SAMs on flame-annealed Au surfaces via incubation in 1 mM ethanolic solutions at room temperature for 18 h, except where noted.

5.2.2.3 Lift-Off Process

Stamps were activated by 30-s exposure to oxygen plasma (Harrick Plasma, Ithaca, NY, USA) at a power of 18 W and an oxygen pressure of 10 psi to yield a fully hydrophilic reactive surface. Thereafter, stamps and SAM-modified substrates were brought into conformal contact for 5 min. Stamps were then carefully peeled away from substrates with stamp features transferred to the substrates. After lift-off, stamps were cleaned by wiping with lab tissues soaked in ethanol, additional rinsing with ethanol, and drying under N_2 gas. Cleaned stamps were sealed against clean glass slides for storage before additional patterning.

5.2.3 Wet-Chemical Gold Etching

An aqueous solution of 20 mM iron nitrate and 30 mM thiourea was applied to post-lift-off substrates for 20 min to carry out selective wet etching of the exposed substrate areas after chemical lift-off lithography. Substrates were cleaned with deionized water and dried with N_2 prior to imaging.

5.2.4 Fabrication of Biotin-Streptavidin Recognition Arrays

Biotinylated patterns were created by lifting off areas of initial TEG SAMs to expose the Au substrates underneath (Figure 5-1). Substrates were then exposed to a 90:10 molar ratio of TEG and BEG in ethanol for 18 h. Before streptavidin incubation, patterned substrates were exposed to 10 mg/mL BSA for 5 min to reduce nonspecific protein adsorption on BEG/TEG SAMs. Patterned surfaces were incubated with 50 μg/mL streptavidin for 20 min followed by 10 μg/mL FITC-conjugated anti-streptavidin antibody for 20 min. Substrates were rinsed with deionized water between steps.

For double lift-off processing, areas of pre-existing TEG SAMs, which were in conformal contact with a PDMS stamp having 90±5-nm-diameter holes, were lifted off to expose the Au substrate underneath (Figure 5-2A and 2B). The patterned substrates were then backfilled with 100% BEG for 1 h (Figure 5-2C). In this case, the PDMS stamp was brought into conformal contact a second time but was shifted relative to its original contact position in the initial lift-off step (Figure 5-2D and 2E). The patterned surfaces were then backfilled with 100% BEG and incubated with 50 μg/mL streptavidin for 30 min, rinsed with deionized water, and dried under N_2 before AFM imaging. (Figure 5-2F)

5.2.5 Surface Characterization

5.2.5.1 Atomic Force Microscopy

Self-assembled monolayers and Au topographic features were characterized by tapping mode AFM (Dimension 5000, Bruker AXS, Santa Barbara, CA, USA). Topographic and phase-contrast AFM images were collected using Si cantilevers with a spring constant of 280 kHz (Bruker Instruments).

5.2.5.2 Fluorescent Microscopy

Bright-field optical images were obtained with an upright digital Nikon LV150 microscope (Nikon Instruments Inc., Melville, NY, USA). Visualization of bound fluorophores was carried out using an inverted fluorescence microscope (Carl Zeiss MicroImaging, Inc., Thornwood, NY, USA) with a fluorescence filter set (38 HE/high efficiency) having excitation and emission wavelengths at 470 ± 20 nm and 525 ± 25 nm, respectively.

5.2.5.3 X-Ray Photoelectron Spectroscopy

All XPS data were collected using an AXIS Ultra DLD instrument (Kratos Analytical Inc., Chestnut Ridge, NY, USA). A monochromatic Al K_α X-ray source (20 mA, 14 kV) with a 200 μm circular spot size and ultrahigh vacuum (10^{-9} torr) were used in all XPS experiments. Spectra were acquired at a pass energy of 80 mV for survey spectra and 20 mV for high resolution spectra of C 1s, S 2p, O 1s, and Au 4f regions using a 200 ms dwell time. Different numbers of scans were carried out depending on the

difficulty of identifying each peak from background, ranging from 20 scans for C 1s to 100 for Au 4f.

Polydimethylsiloxane is an insulator; thus, a charge neutralizer (flood gun) was used to obtain signals. This has the effect of shifting peaks slightly from their expected regions (for C 1s this is 4-5 eV lower than the reference). Due to the small number of peaks and their separation, peak shifting did not affect identification. Peaks of interest had strong signals post-optimization. No corrections were carried out during data collection to shift peaks back to particular regions or to scale peaks based on reference locations.

5.2.5.4 Infrared Reflection Absorption Spectroscopy

Both Fourier-transform infrared reflection-absorption spectroscopy (FT-IRRAS) and PM-IRRAS were carried out using a Thermo Nicolet 8700 FT-IR spectrometer (Thermo Electron Corp., Madison, WI, USA) in reflectance mode using infrared light incident at 82° relative to the surface normal. For PM-IRRAS, the infrared-light beam is controlled by the polarization modulator at operating frequency of 50 kHz. Spectra with 1024 scans were collected in all cases. Before collecting FT-IRRAS spectra, the sample chamber was purged with N_2 to reduce the interferences from atmospheric water and CO_2. Additionally, D12 SAM-modified Au substrates were used as reference samples for FT-IRRAS to subtract water and CO_2 contributions from experimental sample spectra.

5.3 Results and Discussion

5.3.1 The Role of the Terminal Groups in the Chemical Lift-Off Process

To investigate the role of the molecular resist tail groups in the CLL process, two different hydroxyl-terminated alkanethiol molecules, with and without oligo(ethylene glycol), were each assembled as molecular resist monolayers (Table 1). Both provided good transfer of stamp features to SAM-coated Au substrates (Figure 5-3A). In contrast, when methoxy- or methyl-terminated alkanethiol molecules (as highlighted in Table 1) were tested under the same assembly and lift-off conditions, no detectable transfer of stamp features was found on SAM-coated Au surfaces (Figure 5-3B and 5-3C, respectively). Stamp features were not transferred when a hydrophilic PDMS stamp was used directly with a bare Au substrate (Figure 5-3D). Thus, tail group reactivity dictates whether lift-off occurs via hydrophilic PDMS stamps.

5.3.2 Surface Morphology of Lift-Off SAM-Modified Substrates

Chemical patterns of TEG were characterized by AFM and bright-field optical microscopy, as shown in Figure 5-4 and 5-7. Stamps with depressed well-like motifs or protruding posts were used to create different surface relief patterns. Notably, the stamp negative was produced in the resist, as molecules were removed (instead of added) by patterning. For example, islands of SAM resist remained when a stamp with a depressed relief was used; the areas surrounding the relief on the stamp contact the SAM surface and the molecular resist was removed in these areas during the lift-off step. The AFM topographic image in Figure 5-4A illustrates the protruding SAM islands after patterning.

By contrast, well-shaped features were observed on the substrate when a stamp with a protruding relief was used for patterning (Figure 5-4B). In Figure 5-4, AFM topography profiles indicate 2.0 ± 0.3 nm differences between lift-off and non-lift-off areas. The thickness of TEG SAMs is 1.6 ± 0.1 nm by ellipsometry. The difference can be accounted for by a single atomic layer of Au removed during the lift-off process.

5.3.3 The Efficiency of Chemical Lift-Off Process

The reaction yield of lift-off was investigated using FT-IRRAS on hydroxyl-terminated SAM-coated Au substrates before and after the lift-off process. An unpatterned, flat PDMS stamp was oxygen plasma-treated and used to produce the lift-off area for interrogation by FT-IRRAS. Spectra were collected in the range of 2500–3650 cm^{-1} to monitor relative changes in peaks arising from O-H tail groups of hydroxyl-terminated SAMs. Before lift-off, a broad band centered around 3350 cm^{-1} representing the O-H stretching modes and strong bands at 2800–3000 cm^{-1} indicative of C-H stretching modes were observed as shown in representative spectra in Figure 5-5. After lift-off, a decrease of 75-80% in the relative peak area was observed for the broad O-H stretching band. Weaker peak intensity decreases were observed for the C-H stretching bands. Pan and coworkers have shown that the IR intensity of the O-H stretching modes depends only on the surface coverage of hydroxy-terminated alkanethiols, while that of the C-H stretching modes depends on both the surface coverage and the C-H dipole orientation [*28*]. Thus, a 75-80% decrease in the peak area of the O-H stretching band reflects the actual decrease in the surface coverage of alkanethiols due to the lift-off process. Because the IR peak areas of the C-H stretching

modes depend on both the surface coverage and the dipole orientation, it is possible that the remaining alkanethiol molecules that were not lifted off after the stamp-SAM contact reaction undergo rearrangement of the C-H dipoles to enhance the IR intensity/peak area. This would cancel out the reduction in C-H IR peak area due to the removal of alkanethiols via the lift-off process. Thus, only a weak IR peak area decrease of the C-H stretching bands was observed in Figure 5-5. The decrease in the peak area of the O-H stretching band enables a better estimation of the contact reaction lift-off yield for hydroxyl-terminated alkanethiols.

Polarization-modulation infrared reflection-absorption spectroscopy was used to investigate the role of orientational changes in modulating the intensity of the C-H stretching peaks. In PM-IRRAS, both *p*-polarized and *s*-polarized radiation are modulated by a photoelastic modulator to reduce contributions to the spectra from water in the vapor phase above the substrates. As before, a featureless PDMS stamp was used to lift-off molecules from hydroxyl-terminated alkanethiol SAMs on Au substrates. After lift-off, the same hydroxyl-terminated alkanethiol molecules were backfilled into the exposed Au regions. Representative spectra are shown in Figure 5-6. Similar to findings in FT-IRRAS experiments, only the broad O-H stretching peak area was reduced after lift-off; the C-H stretching peak was essentially unchanged. After the backfilling step, the O-H stretching peak returned to its pre-lift-off intensity. Again, the C-H stretch peak did not change, within experimental error. These results support the conclusion that the O-H intensity depends on surface coverage. By contrast, the C-H streching intensity, which depends on both surface coverage and dipole orientation, does not appear to be a good indicator of coverage. While similar conclusions are drawn from both the FT-IRRAS and PM-IRRAS

data, conventional FT-IRRAS measurements are more quantitative, and are used to estimate the fractions of the monolayers removed here.

Previous reactive patterning of hydrogen-bonding SAMs showed that this level of damage makes the SAM labile to complete displacement and the hydrogen bonding in the intact areas prevents diffusion and thus pattern dissolution [*29*]. The terminal functionality of the initial SAM influences lift-off via the extent of the contact-induced reaction at the SAM-stamp interface. Lift-off from SAMs of TEG was sufficient to enable patterning of underlying substrates by wet etching and to produce patterned multi-component SAMs capable of biorecognition.

5.3.4 Lift-Off of Molecular Resist for Wet Etching

We explored using the intact SAM areas as an unconventional resist to transfer patterns to the underlying material, Au, through selective wet chemical etching [*19, 30*]. Exposed areas of the Au surface were contacted by the etchant solution, while the intact SAM molecular resist protected the remaining regions of Au. Etchant solutions removed exposed Au via oxidation by Fe^{3+}, followed by complexation and dissolution of oxidized metal by thiourea [*31*]. A variety of patterns (inverse replicas of the PDMS stamp features) with features of different sizes were transferred, including lines, holes, and pillars (Figure 5-7). The advantages of large patterning areas and high-fidelity features are apparent in the bright-field images (Figure 5-7A to 7C) and AFM topography images (Figure 5-7D to 7F), respectively. Differences in AFM heights indicate that features have been transferred to the level of the underlying substrate at depth of 30 nm; the thickness of the original Au layer.

5.3.5 The Breakage of Au-Au Substrate Bonds

Based on earlier work, we hypothesized that the Au-Au bonds in the substrate metal lattice, rather than the Au-S bonds between the substrate and alkanethiol, are preferentially broken during lift-off. Notably, breaking Au-Au bonds during SAM desorption has been the subject of controversy [*6, 32-36*]. The mobility of Au-thiolates within SAMs [*33, 37, 38*] indicates that weak Au-Au bonds are present at the substrate surface. Furthermore, recent studies show the presence of Au adatoms beneath SAMs, which leads to facile Au-Au bond breakage because of reduced coordination of the adatoms [*39-42*]. We made a featureless PDMS stamp that was oxygen-plasma-treated and brought it into contact with a hydroxyl-terminated SAM-coated Au surface. After lift-off, a peak indicating the presence of Au was observed on the PDMS stamp surface using X-ray photoelectron spectroscopy as seen in Figure 5-8. In contrast, when a PDMS stamp was not treated with oxygen plasma prior to the contact reaction and lift-off process, no Au peaks were observed in the XPS spectrum (Figure 5-9). This finding is consistent with Au being removed from the underlying substrate *(39)*.

The presence of Au on oxygen-plasma-treated PDMS surfaces after chemical lift-off led us to propose that a contact-induced chemical reaction between the hydrophilic stamp surface and the molecular-resist layer results in Au-Au bond rupture during stamp removal. Studies have shown that oxygen plasma treatment yields siloxyl groups on PDMS stamp surfaces, as illustrated in Figure 5-10, facilitating condensation reactions between Si-OH and hydroxyl groups on different oxides, such as Au, Ti, and Si to form the Si-O-Au, Si-O-Ti, and Si-O-Si linkages, respectively [*9, 24, 43-45*]. We anticipated

that the same type of linkage (Si-O-SAM) would be established between Si-OH groups on oxygen plasma-treated PDMS stamp surfaces and hydroxyl terminal groups on SAMs.

5.3.6 Biotin-Streptavidin Patterning Substrates

In addition to transferring patterns to SAMs and underlying Au substrates, CLL enables a SAM of a different composition to be assembled on the lift-off areas. Figure 5-11A shows a large-area, high-fidelity pattern of streptavidin binding to a biotinylated pattern created by lifting off areas of an initial TEG SAM to expose fresh Au substrate underneath. The substrate was then exposed to 90:10 TEG/biotin-terminated hexa(ethylene glycol)alkanethiol (Table 1) to produce a low-density biotinylated patterned SAM [*17, 18*]. Streptavidin was captured from solution by surface-tethered biotin. Bound streptavidin was visualized with fluorescein isothiocyanate (FITC)-conjugated antibodies against streptavidin using fluorescence microscopy.

The bright fluorescent regions in Figure 5-11A and its inset display the lift-off areas where biotin-terminated alkanethiols were backfilled and used to capture streptavidin from solution. The dark regions display minimal fluorescence because of the absence of biotin-terminated alkanethiol and the resistance to nonspecific protein adsorption by TEG [*17, 46*]. The fabrication of biotin-streptavidin patterns demonstrates that CLL not only transfers large-area, high-fidelity patterns to SAMs, but the post-lift-off exposed Au areas are advantageous for producing multiplexed bioselective patterned surfaces.

To carry out nanometer-scale chemical patterning, we implemented the lift-off process for biotin-streptavidin described above using a PDMS stamp with 90-nm well-

like features (Figure 5-11B). Areas surrounding the wells were lifted off and backfilled with biotin-terminated alkanethiol to capture streptavidin, whereas the areas inside the wells were not removed, producing TEG islands. In addition, sharp 40±2 nm features were fabricated directly using a stamp with 40-nm channels, indicating that we have not yet reached the resolution limit of the CLL method (Figure 5-11C). Exploring the effects of Au grain size will also be important for future mechanistic studies and possibly further improving nanoscale feature resolution.

5.3.7 Nanometer-Scale Patterning by Double Lift-Off Process

Alternatively, to achieve sub-90-nm features, a double lift-off strategy was used in which the PDMS stamp was twice brought into conformal contact with the substrate (Figure 5-2). The initial lift-off step removed the molecules in the areas surrounding the stamp wells leaving the TEG SAM inside the wells intact. During the second lift-off step, the stamp was offset with respect to the first pattern. (This result was initially a serendipitous consequence of being unable to maintain exact registry between multiple stamping steps.) Additional areas of the TEG SAM were removed, depending on the amount of registration. The exposed Au surfaces resulting from both TEG removal steps were backfilled with biotin-terminated alkanethiol. Figure 5-11D illustrates decreasing registration associated with smaller feature sizes. The resulting intact TEG regions form increasingly narrow marquise-shaped features with decreased spacing between biotin-streptavidin molecular recognition areas. Note that if conventional contact printing were used in this case, lateral diffusion of ink molecules would blur nanospaced features beyond detection by AFM [*47*].

5.3.8 Lateral Diffusion of Molecular Resist After Lift-Off Process

Lateral diffusion of ink molecules, which occurs during increasing stamp contact times and/or molecular ink concentrations for additive printing methods on bare Au substrates, is avoided in CLL. Preformed well-ordered SAMs, strong intermolecular interactions between hydrophilic SAM molecules, and a diffusion barrier created by the Au step-edges [*48*] formed during lift-off prevent pattern dissolution. Patterned TEG SAMs produced by CLL showed no discernable dissolution after 2 days under ambient storage conditions (Figure 5-12). Furthermore, the backfilled multi-component SAMs shown in Figure 5-11 were produced by solution deposition of the second SAM component over 12 h. Nonetheless, sharp pattern features are produced arguing against diffusion/dissolution of the original lift-off pattern.

5.3.9 The Effect of Contact Duration on Interfacial Chemical Reactions

We investigated the time needed for the contact-induced chemical reaction at the stamp-substrate interface by examining 1-min *vs.* 5-min contact times between oxygen-plasma-treated PDMS stamps and hydroxyl-terminated alkanethiol-coated Au surfaces. Features were transferred even with 1-min contact times; however, shorter contact times resulted in poor features produced after wet etching. Additionally, pattern transfer was maintained with short SAM deposition times. Hydroxyl-terminated alkanethiol SAMs formed by 1-h deposition were found to provide good transfer of stamp features to Au substrates, comparable to transfer obtained from SAMs formed overnight. These findings demonstrate advantages associated with short contact and SAM formation times for facilitating robust, expeditious, and high-throughput patterning by CLL. Ultimately,

limits for SAM deposition and stamp contacts times will depend on the specific molecules used for SAM formation.

5.4 Conclusions and Prospects

Conventional nanolithographic patterning techniques, such as photolithography and electron-beam lithography, which are expensive, time-consuming, and require specialized equipment/instrumentation, only need to be used for the fabrication of stamp master molds. Once individual masters are produced, CLL can be implemented as a strategy for high-resolution, high-throughput, low-cost pattern fabrication. Since CLL enables patterns to be transferred to underlying substrates and a multiple-stamping strategy can be used to produce patterns that are smaller than the actual stamp features, CLL can be used to produce high-fidelity nanometer-scale patterns on Au substrates, with the possibility also for patterning different materials such as Si, Ge, Pd, Pt, and graphene.

The content of this chapter was adapted with permission from Liao, W. –S., Cheunkar, S., Cao, H. H., Bednar, H. R., Weiss, P. S., and Andrews, A. M. Subtractive Patterning via Chemical Lift-Off Lithography. *Science* **2012**, 337, 1517-1521.

5.5 Figures

Hydroxyl-terminated tri(ethylene glycol)undecanethiol (TEG)	*$HS\text{-}(CH_2)_{11}\text{-}(C_2H_4O)_3\text{-}OH$*
Biotin-terminated hexa(ethylene glycol)undecanethiol (BEG)	**$HS\text{-}(CH_2)_{11}\text{-}(C_2H_4O)_6\text{-}NH\text{-}C_{10}H_{15}O_2N_2S$**
Hydroxyl-terminated undecanethiol	**$HS\text{-}(CH_2)_{11}\text{-}OH$**
Methyl-terminated undecanethiol	**$HS\text{-}(CH_2)_{11}\text{-}CH_3$**
Methoxy-terminated tri(ethylene glycol)undecanethiol	**$HS\text{-}(CH_2)_{11}\text{-}(C_2H_4O)_3\text{-}O\text{-}CH_3$**

Table 5-1. Alkanethiol molecules and terminal groups used in chemical lift-off lithography. This table is adapted with permission from reference 132.

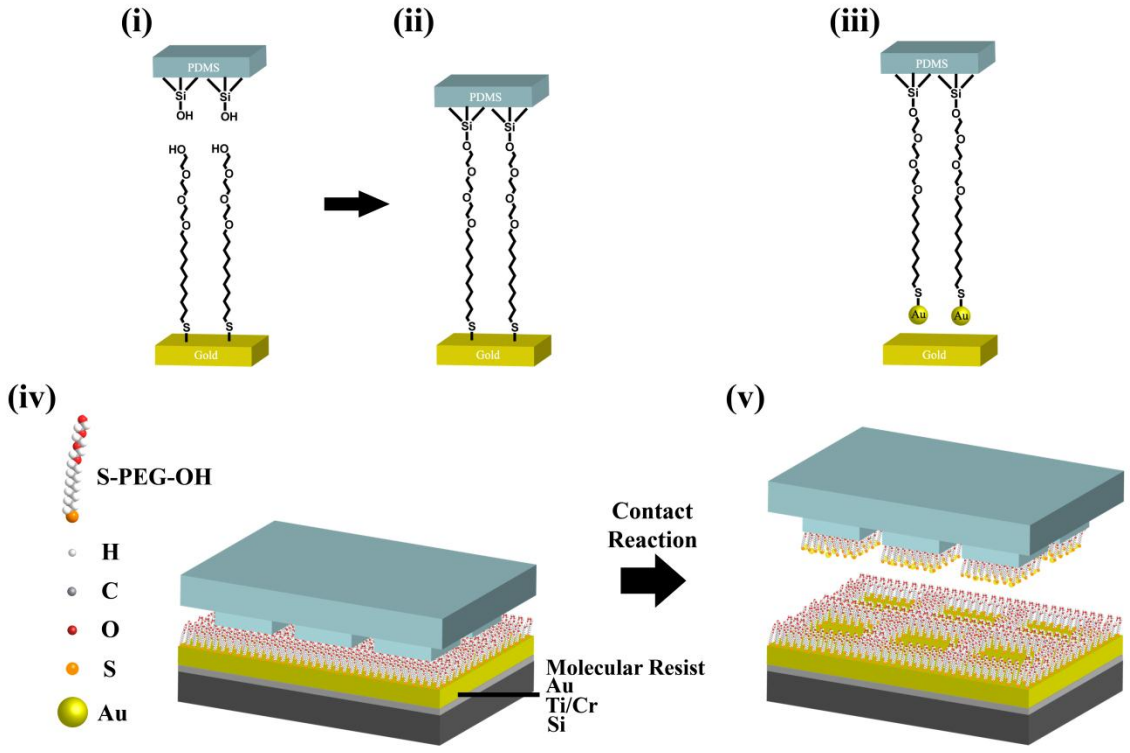

Figure 5-1. Schematic illustration of the molecular-resist lift-off process. (i) A polydimethylsiloxane (PDMS) stamp is first activated by oxygen plasma treatment producing hydrophilic siloxyl groups. (ii) A surface-induced contact reaction is implemented via close contact between the stamp and hydroxyl-terminated molecules self-assembled on a Au substrate. (iii) Stamp removal lifts-off resist molecules and underlying Au. (iv) In chemical lift-off lithography, a patterned PDMS stamp is brought into conformal contact with a self-assembled molecular resist. (v) Lift-off is limited to the stamp-contact regions. This figure is adapted with permission from reference 132.

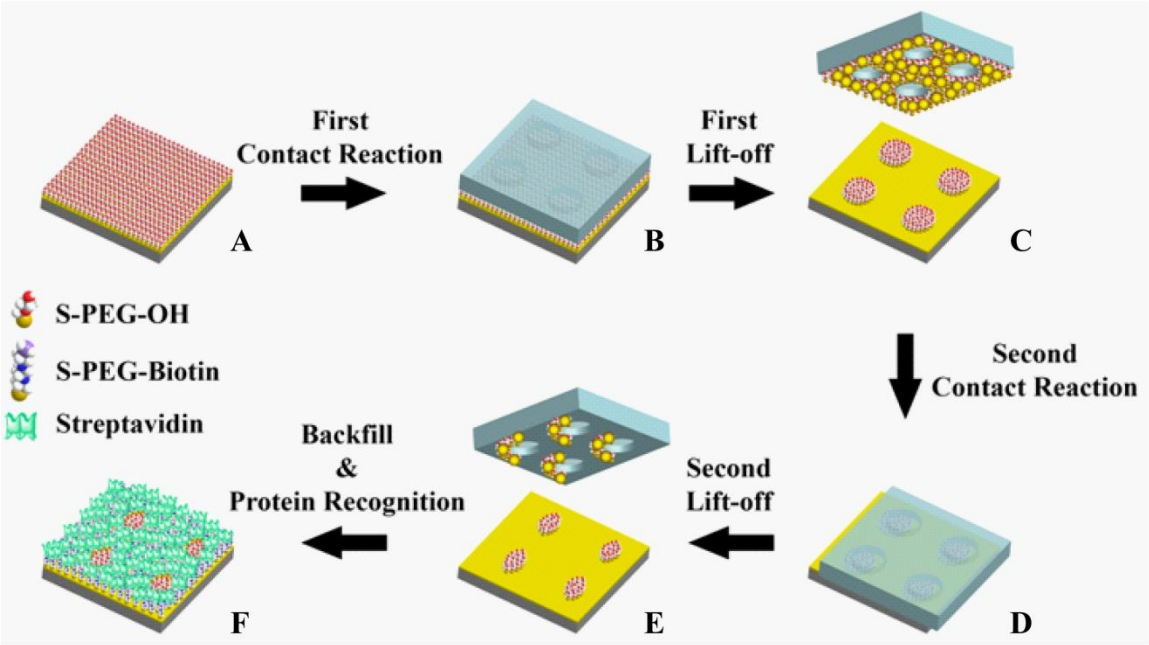

Figure 5-2. Schematic illustration of the double molecular-resist lift-off process. (A) A TEG SAM was formed on Au substrates. (B) A PDMS stamp with 90-nm-diameter holes was brought into conformal contact once with a TEG SAM. (C) Lifting-off of a TEG SAM produce about 90-nm-diameter pillar features. (D-E) Substrates were stamped twice and lifted off with decreasing registry. (F) Patterned substrates were backfilled with biotin-terminated alkanethiol for streptavidin binding. This figure is adapted with permission from reference 132.

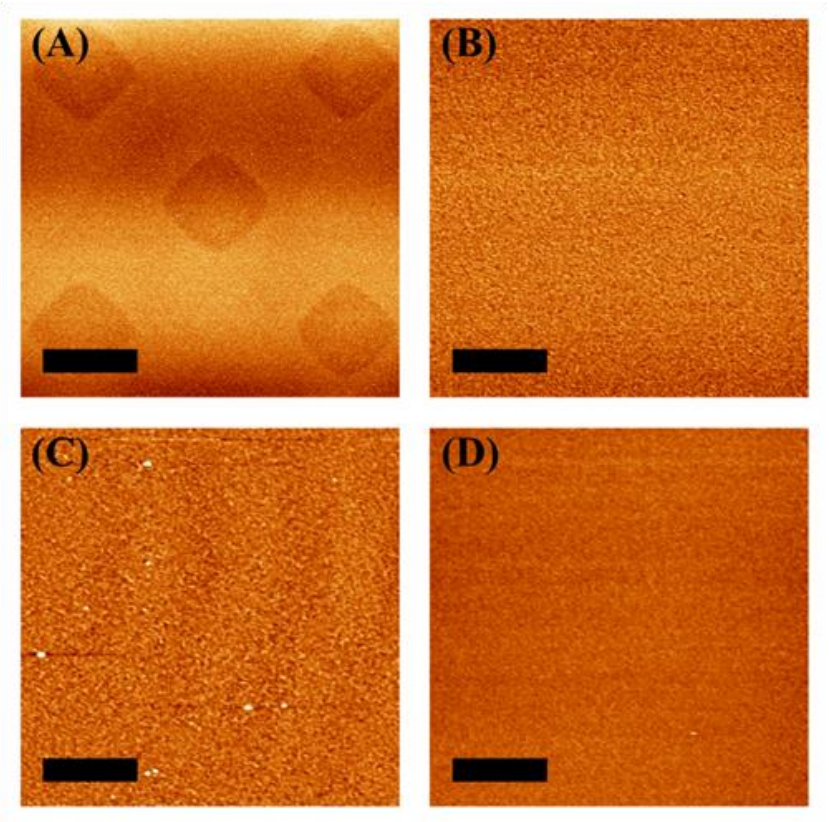

Figure 5-3. Atomic force microscope topographic images of chemical lift-off lithography on different types of SAMs. Self-assembled monolayers of alkanethiols with different tail groups on Au substrates were investigated using chemical lift-off lithography and PDMS stamps with 10-μm × 10-μm protruding posts. (A) Similar to TEG SAMs, monolayers of hydroxyl-terminated undecanethiol are patterned when contacted by oxygen plasma-treated PDMS stamps. By contrast, (B) a methoxy-terminated tri(ethylene glycol)un-decanethiol SAM, (C) a methyl-terminated undecanethiol SAM, and (D) a bare Au substrate showed no evidence of patterning by lift-off lithography. Scale bars are 10 μm. This figure is adapted with permission from reference 132.

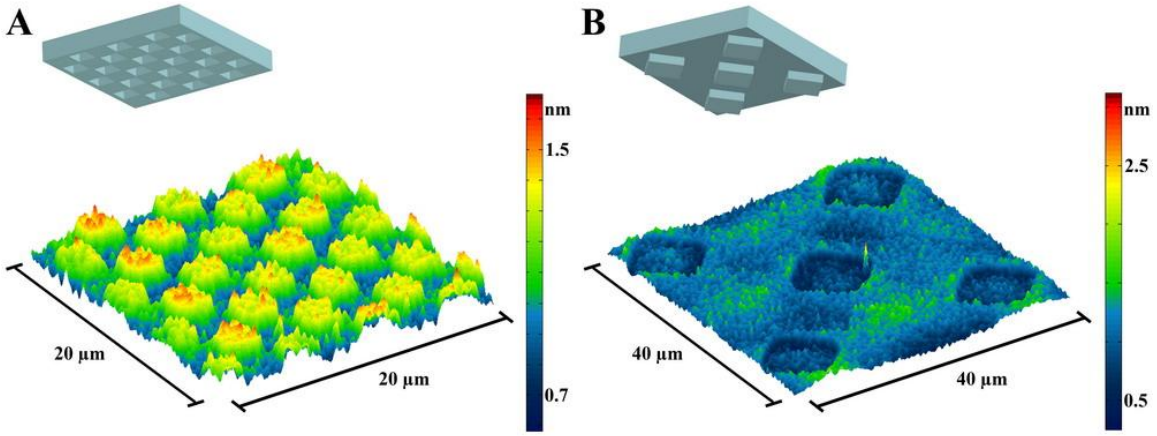

Figure 5-4. Atomic force microscope topographic images of substrates patterned by chemical lift-off lithography. Self-assembled monolayers of hydroxyl-terminated tri(ethylene glycol)alkanethiol on Au substrates were patterned using chemical lift-off lithography and (A) a PDMS stamp with 2-µm × 2-µm depressed wells or (B) a PDMS stamp with 10-µm × 10-µm protruding posts. Stamp geometries are illustrated above the images. Contact dwell time was 5 min. AFM topographical heights are shown in the scale bars to the right of each image. This figure is adapted with permission from reference 132.

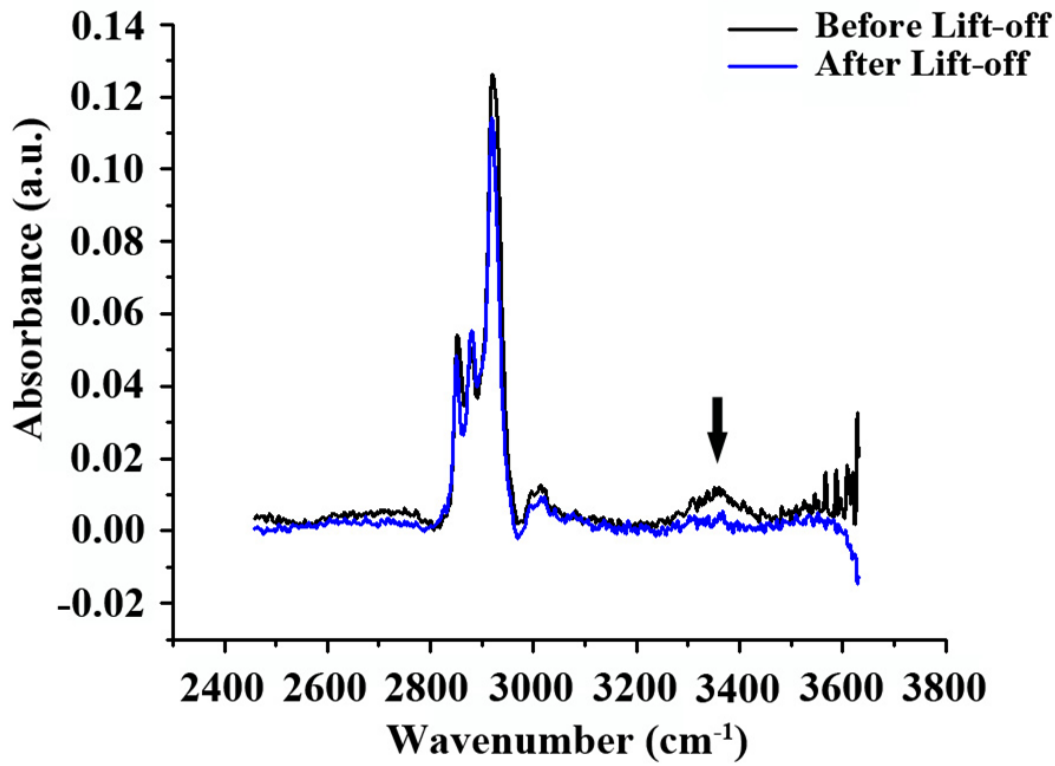

Figure 5-5. Fourier-transform infrared reflection-absorption spectra of a hydroxyl-terminated SAM-coated Au substrate before and after the lift-off process. The broad hydroxyl stretch band (indicated by the black arrow) arising from the hydroxyl-terminated SAM molecules decreases in relative peak area, indicating 75-80% removal of alkanethiols after lift-off. This figure is adapted with permission from reference 132.

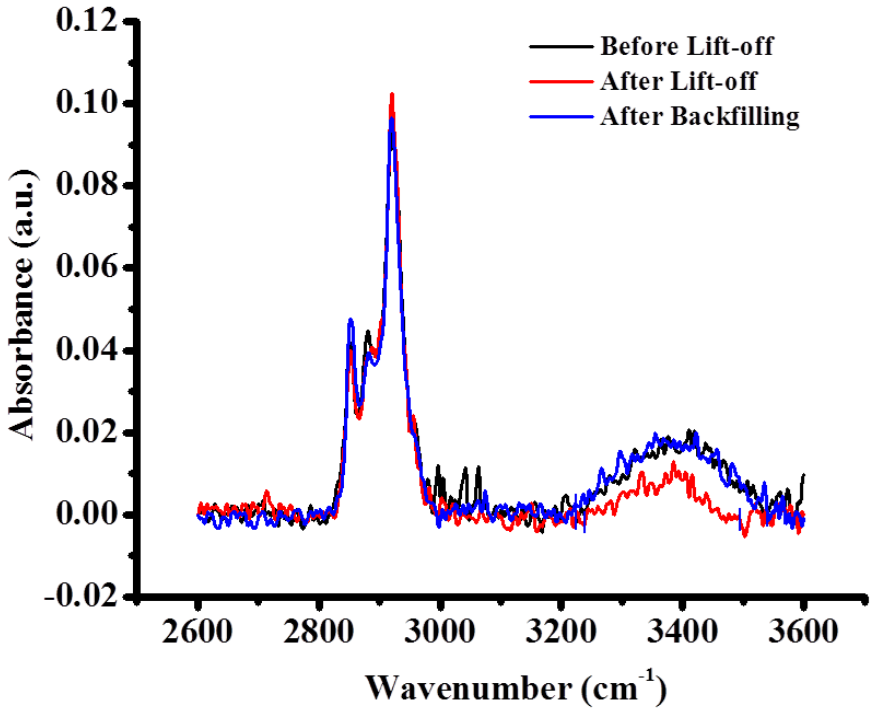

Figure 5-6. Polarization-modulation infrared reflection-absorption spectra of a hydroxyl-terminated SAM-coated Au substrate before/after lift-off and after backfilling. The broad hydroxyl stretch centered around 3400 cm^{-1} of the hydroxyl-terminated alkanethiol SAM decreases after lift-off, due to the removal of hydroxyl-terminated alkanethiols and increases after backfilling, indicating hydroxyl-terminated alkanethiol refilling. By contrast, the C-H stretching modes stay constant, within experimental error. This figure is adapted with permission from reference 132.

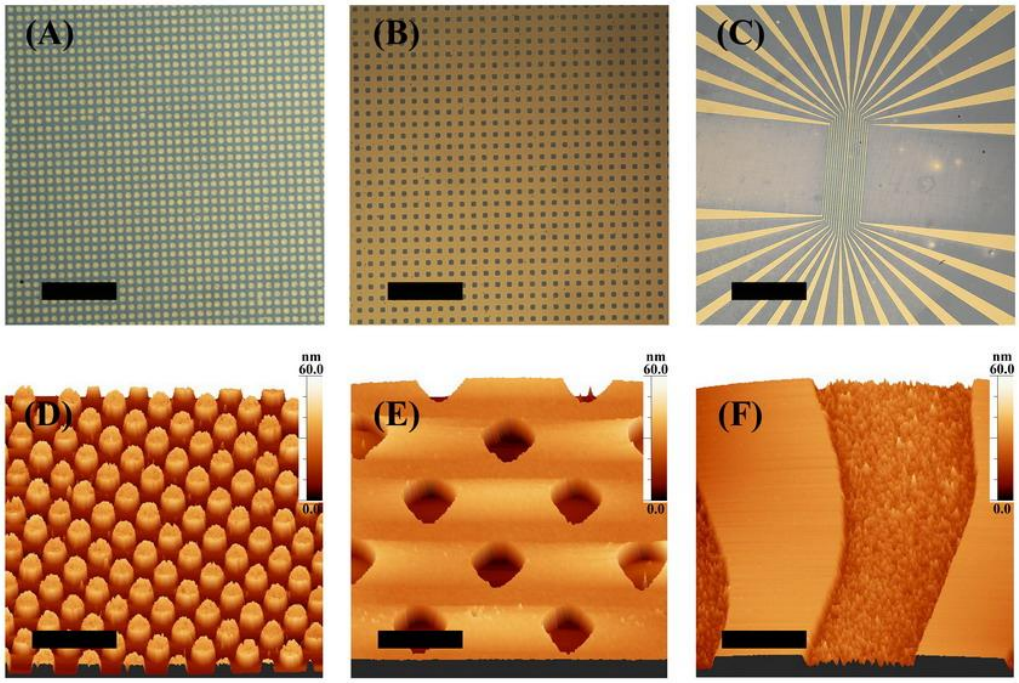

Figure 5-7. Patterning underlying gold substrates by lift-off lithography. Hydroxyl-terminated tri(ethylene glycol)undecanethiol was self-assembled on Au substrates. Lift-off lithography via activated PDMS stamps was used to produce a variety of patterns. Substrates were then chemically etched (Fe^{3+}/thiourea) to pattern the underlying metal by removing additional gold in the exposed regions. The SAM molecular resist was intact during imaging with bright-field microscopy and AFM. Patterns transferred by the molecular-resist lift-off process include (A, D) pillars, (B, E) wells, and (C, F) channels. Bright-field microscope images are shown in A-C. Corresponding AFM topography images are shown in D-F. Scale bars are 18 μm, 130 μm, 1325 μm, 5 μm, 15 μm, and 17.5 μm in A-F, respectively. AFM topographic heights are shown in the upper right corners of D-F. This figure is adapted with permission from reference 132.

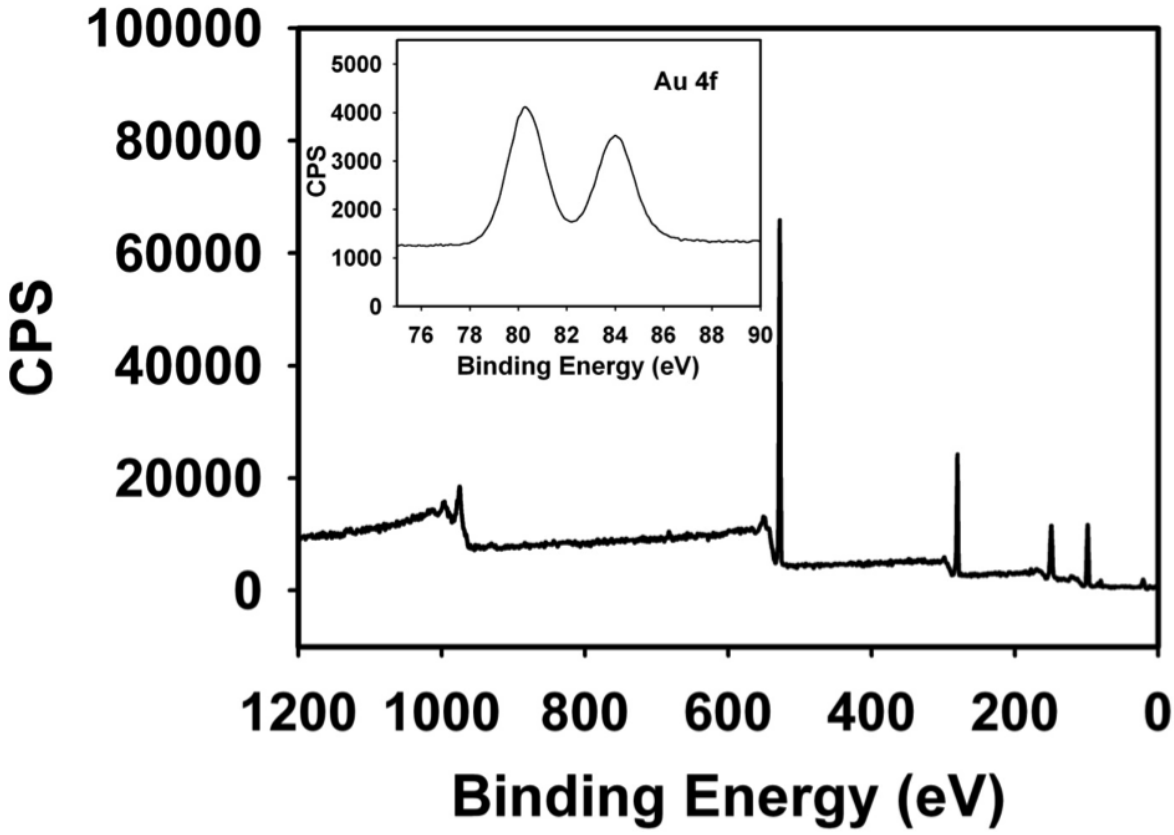

Figure 5-8. X-ray photoelectron spectrum after lift-off from a hydroxyl-terminated SAM. An oxygen plasma-treated PDMS stamp was subjected to the contact reaction followed by the lift-off process. Peaks (Au 4f) indicate the presence of Au on the stamp surface after lift-off and are shown in the inset. This figure is adapted with permission from reference 132.

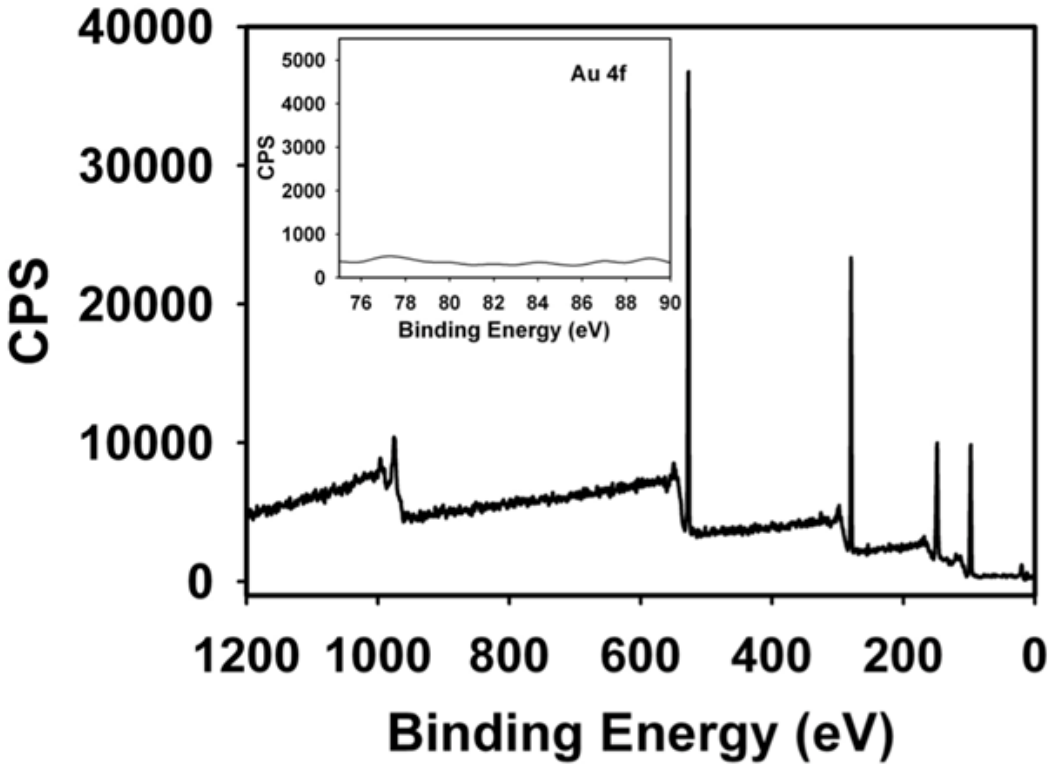

Figure 5-9. Oxygen-plasma treatment is necessary for lift-off. Here, a PDMS stamp was not treated with oxygen plasma prior to the contact reaction and lift-off processes. No Au 4f peaks are observed in the XPS spectrum, as shown in the inset, demonstrating that stamp activation is needed to observe lift-off of the molecular resist and removal of Au adatoms. This figure is adapted with permission from reference 132.

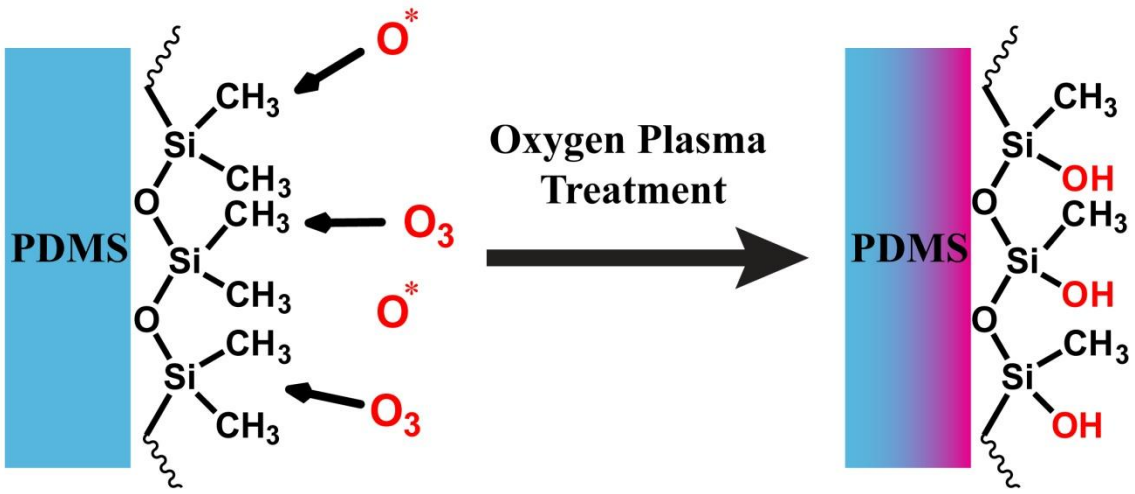

Figure 5-10. Schematic of a PDMS stamp before and after oxygen plasma treatment. After mold casting, a PDMS surface, containing methyl groups (Si-CH_3), is hydrophobic. When treated with oxygen plasma, which consists of reactive oxygen radicals, the methyl groups on the PDMS surface are substituted by silanol groups (Si-OH), resulting in a hydrophilic surface. The silanol groups on the treated PDMS stamp can react with many functional groups, such as silyl cholride, hydroxyl, and carboxyl groups, through condensation reaction.

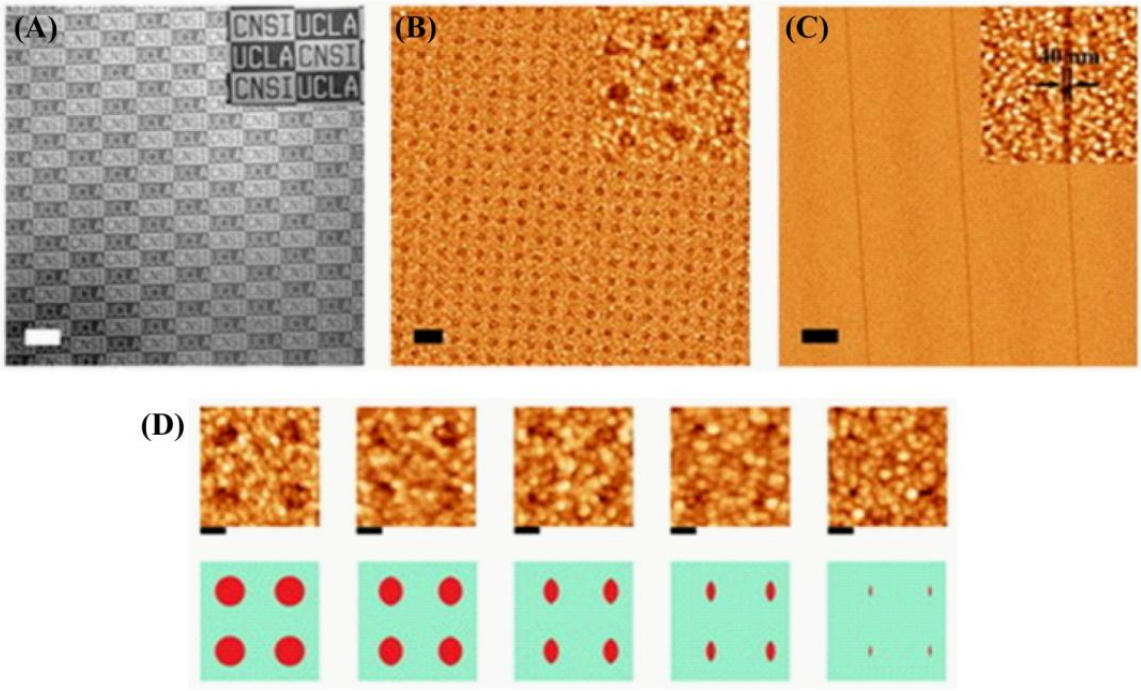

Figure 5-11. Large-area patterning of microscale and nanoscale features via chemical lift-off lithography. (A) a PDMS stamp having "UCLA" characters as positive (protruding) features and "CNSI" characters as negative (depressed) features was used to lift off a TEG SAM. After patterning, a new monolayer of 90% TEG/10% BEG (nominal solution ratio) was self-assembled on the exposed Au regions ("UCLA" characters and areas surrounding the "CNSI" characters). Bright areas indicate fluorescence associated with FITC-labeled anti-streptavidin antibody recognition of streptavidin bound to biotin. Dark areas display minimal fluorescence due to the protein-resistant characteristics of TEG. The fluorescent pattern is sharp and extends over a large substrate area (>3 mm^2). Scale bar is 250 μm for the main image. (B) a PDMS stamp with 90-nm-diameter holes was used to lift off a TEG SAM. After patterning, a new monolayer of 100% biotin-terminated oligo(ethylene glycol)alkanethiol was self-assembled on the exposed Au regions (areas surrounding the resulting pillar features). The inset shows a high-

resolution AFM image of biospecific 90-nm circular features. Scale bar is 400 nm. (C) AFM images display biotin streptavidin recognition areas separated by narrow line features. The inset shows a detailed AFM image of an individual line feature whose width is 40±2 nm made using a stamp with 40-nm channels. Scale bar for the large area AFM image is 1 μm. (D) Topographic AFM images display decreasing feature sizes (from left to right): 90±5 nm, 80±3 nm, 50±2 nm, 30±3 nm, and 15±5 nm. Protruding (lighter) areas indicate biotin-streptavidin recognition. Shallow (darker) areas comprise intact TEG SAM. Scale bars are 100 nm. This figure is adapted with permission from reference 132.

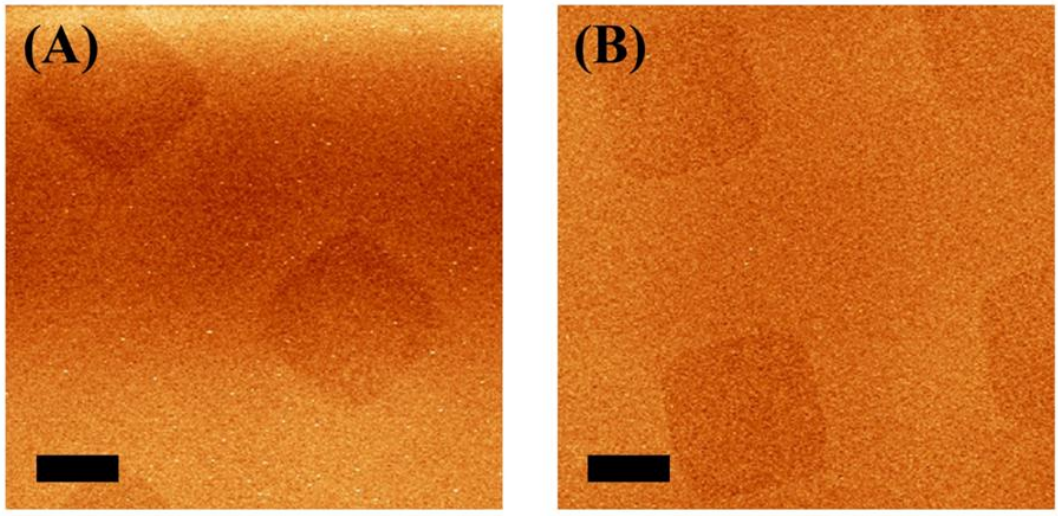

Figure 5-12. Atomic force microscope topographic images of TEG SAM hole features created by chemical lift-off lithography. PDMS stamps with 10 μm × 10 μm protruding posts were used to lift-off areas of a TEG SAM on a Au substrate. (A) Freshly lifted-off TEG SAM hole features. (B) Lift-off TEG SAM features two days after storing under ambient conditions. Scale bars are 5 μm. This figure is adapted with permission from reference 132.

5.6 References

1. Gates, B. D., Xu, Q. B., Stewart, M., Ryan, D., Willson, C. G., and Whitesides, G. M. New Approaches to Nanofabrication: Molding, Printing, and Other Techniques. *Chem. Rev.* **2005**, *105*, 1171-1196.
2. Willson, C. G., and Roman, B. J. The Future of Lithography: Sematech Litho Forum 2008. *ACS Nano* **2008**, *2*, 1323-1328.
3. Saavedra, H. M., Mullen, T. J., Zhang, P. P., Dewey, D. C., Claridge, S. A., and Weiss, P. S. Hybrid Strategies in Nanolithography. *Rep. Prog. Phys.* **2010**, *73*, 036501.
4. Shim, W., Braunschweig, A. B., Liao, X., Chai, J. N., Lim, J. K., Zheng, G. F., and Mirkin, C. A. Hard-Tip, Soft-Spring Lithography. *Nature* **2011**, *469*, 516-521.
5. Piner, R. D., Zhu, J., Xu, F., Hong, S. H., and Mirkin, C. A. "Dip-Pen" Nanolithography. *Science* **1999**, *283*, 661-663.
6. Xu, S., Laibinis, P. E., and Liu, G. Y. Accelerating the Kinetics of Thiol Self-Assembly on Gold - a Spatial Confinement Effect. *J. Am. Chem. Soc.* **1998**, *120*, 9356-9361.
7. Xu, S., and Liu, G. Y. Nanometer-Scale Fabrication by Simultaneous Nanoshaving and Molecular Self-Assembly. *Langmuir* **1997**, *13*, 127-129.
8. Xia, Y. N., and Whitesides, G. M. Soft Lithography. *Angew. Chem. Int. Ed.* **1998**, *37*, 551-575.

9. Li, X. M., Peter, M., Huskens, J., and Reinhoudt, D. N. Catalytic Microcontact Printing without Ink. *Nano Lett.* **2003**, *3*, 1449-1453.

10. Rogers, J. A., and Nuzzo, R. G. Recent Progress in Soft Lithography. *Mater. Today* **2005**, *8*, 50-56.

11. Wilbur, J. L., Kumar, A., Kim, E., and Whitesides, G. M. Microfabrication by Microcontact Printing of Self-Assembled Monolayers. *Adv. Mater.* **1994**, *6*, 600-604.

12. Chou, S. Y., Krauss, P. R., and Renstrom, P. J. Imprint Lithography with 25-Nanometer Resolution. *Science* **1996**, *272*, 85-87.

13. Loo, Y. L., Hsu, J. W. P., Willett, R. L., Baldwin, K. W., West, K. W., and Rogers, J. A. High-Resolution Transfer Printing on GaAs Surfaces Using Alkane Dithiol Monolayers. *J. Vac. Sci. Technol. B* **2002**, *20*, 2853-2856.

14. Childs, W. R., and Nuzzo, R. G. Decal Transfer Microlithography: A New Soft-Lithographic Patterning Method. *J. Am. Chem. Soc.* **2002**, *124*, 13583-13596.

15. Kumar, A., and Whitesides, G. M. Features of Gold Having Micrometer to Centimeter Dimensions Can Be Formed through a Combination of Stamping with an Elastomeric Stamp and an Alkanethiol Ink Followed by Chemical Etching. *Appl. Phys. Lett.* **1993**, *63*, 2002-2004.

16. Christman, K. L., Enriquez-Rios, V. D., and Maynard, H. D. Nanopatterning Proteins and Peptides. *Soft Matter* **2006**, *2*, 928-939.

17. Vaish, A., Shuster, M. J., Cheunkar, S., Weiss, P. S., and Andrews, A. M. Tuning Stamp Surface Energy for Soft Lithography of Polar Molecules to Fabricate Bioactive Small-Molecule Microarrays. *Small* **2011**, *7*, 1471-1479.

18. Shuster, M. J., Vaish, A., Cao, H. H., Guttentag, A. I., McManigle, J. E., Gibb, A. L., Martinez, M. M., Nezarati, R. M., Hinds, J. M., Liao, W. S., Weiss, P. S., and Andrews, A. M. Patterning Small-Molecule Biocapture Surfaces: Microcontact Insertion Printing vs. Photolithography. *Chem. Commun.* **2011**, *47*, 10641-10643.

19. McLellan, J. M., Geissler, M., and Xia, Y. N. Edge Spreading Lithography and Its Application to the Fabrication of Mesoscopic Gold and Silver Rings. *J. Am. Chem. Soc.* **2004**, *126*, 10830-10831.

20. Srinivasan, C., Mullen, T. J., Hohman, J. N., Anderson, M. E., Dameron, A. A., Andrews, A. M., Dickey, E. C., Horn, M. W., and Weiss, P. S. Scanning Electron Microscopy of Nanoscale Chemical Patterns. *ACS Nano* **2007**, *1*, 191-201.

21. Braunschweig, A. B., Huo, F., and Mirkin, C. A. Molecular Printing. *Nat. Chem.* **2009**, *1*, 353-358.

22. Xu, S., Miller, S., Laibinis, P. E., and Liu, G. Y. Fabrication of Nanometer Scale Patterns within Self-Assembled Monolayers by Nanografting. *Langmuir* **1999**, *15*, 7244-7251.

23. Tiberio, R. C., Craighead, H. G., Lercel, M., Lau, T., Sheen, C. W., and Allara, D. L. Self-Assembled Monolayer Electron-Beam Resist on GaAs. *Appl. Phys. Lett.* **1993**, *62*, 476-478.

24. Loo, Y. L., Willett, R. L., Baldwin, K. W., and Rogers, J. A. Interfacial Chemistries for Nanoscale Transfer Printing. *J. Am. Chem. Soc.* **2002**, *124*, 7654-7655.

25. Lahiri, J., Ostuni, E., and Whitesides, G. M. Patterning Ligands on Reactive SAMs by Microcontact Printing. *Langmuir* **1999**, *15*, 2055-2060.

26. Delamarche, E., Geissler, M., Bernard, A., Wolf, H., Michel, B., Hilborn, J., and Donzel, C. Hydrophilic Poly (Dimethylsloxane) Stamps for Microcontact Printing. *Adv. Mater.* **2001**, *13*, 1164-1167.

27. Kaufmann, T., and Ravoo, B. J. Stamps, Inks and Substrates: Polymers in Microcontact Printing. *Polym. Chem.* **2010**, *1*, 371-387.

28. Pan, S., Belu, A. M., and Ratner, B. D. Self Assembly of 16-Mercapto-1-Hexadecanol on Gold: Surface Characterization and Kinetics. *Mat. Sci. Eng. C-Bio. S.* **1999**, *7*, 51-58.

29. Saavedra, H. M., Thompson, C. M., Hohman, J. N., Crespi, V. H., and Weiss, P. S. Reversible Lability by in Situ Reaction of Self-Assembled Monolayers. *J. Am. Chem. Soc.* **2009**, *131*, 2252-2259.

30. Liao, W.-S., Chen, X., Chen, J., and Cremer, P. S. Templating Water Stains for Nanolithography. *Nano Lett.* **2007**, *7*, 2452-2458.

31. Geissler, M., Wolf, H., Stutz, R., Delamarche, E., Grummt, U. W., Michel, B., and Bietsch, A. Fabrication of Metal Nanowires Using Microcontact Printing. *Langmuir* **2003**, *19*, 6301-6311.

32. Wasserman, S. R., Biebuyck, H., and Whitesides, G. M. Monolayers of 11-Trichlorosilylundecyl Thioacetate - a System That Promotes Adhesion between Silicon Dioxide and Evaporated Gold. *J. Mater. Res.* **1989**, *4*, 886-891.

33. Stranick, S. J., Parikh, A. N., Allara, D. L., and Weiss, P. S. A New Mechanism for Surface-Diffusion-Motion of a Substrate-Adsorbate Complex. *J. Phys. Chem.* **1994**, *98*, 11136-11142.

34. Stranick, S. J., Atre, S. V., Parikh, A. N., Wood, M. C., Allara, D. L., Winograd, N., and Weiss, P. S. Nanometer-Scale Phase Separation in Mixed Composition Self-Assembled Monolayers. *Nanotechnology* **1996**, *7*, 438-442.

35. Skulason, H., and Frisbie, C. D. Detection of Discrete Interactions Upon Rupture of Au Microcontacts to Self-Assembled Monolayers Terminated with -S(Co)CH_3 or -SH. *J. Am. Chem. Soc.* **2000**, *122*, 9750-9760.

36. Liu, M., Amro, N. A., and Liu, G.-y. Nanografting for Surface Physical Chemistry. *Annu. Rev. Phys. Chem.* **2008**, *59*, 367-386.

37. Poirier, G. E., and Tarlov, M. J. The C(4x2) Superlattice of N-Alkanethiol Monolayers Self-Assembled an Au(111). *Langmuir* **1994**, *10*, 2853-2856.

38. Poirier, G. E., and Tarlov, M. J. Molecular Ordering and Gold Migration Observed in Butanethiol Self-Assembled Monolayers Using Scanning-Tunneling-Microscopy. *J. Phys. Chem.* **1995**, *99*, 10966-10970.

39. Maksymovych, P., Sorescu, D. C., and Yates, J. T., Jr. Gold-Adatom-Mediated Bonding in Self-Assembled Short-Chain Alkanethiolate Species on the Au(111) Surface. *Phys. Rev. Lett.* **2006**, *97*, 146103.

40. Yu, M., Bovet, N., Satterley, C. J., Bengio, S., Lovelock, K. R. J., Milligan, P. K., Jones, R. G., Woodruff, D. P., and Dhanak, V. True Nature of an Archetypal Self-Assembly System: Mobile Au-Thiolate Species on Au(111). *Phys. Rev. Lett.* **2006**, *97*, 166102.

41. Moore, A. M., Mantooth, B. A., Donhauser, Z. J., Yao, Y., Tour, J. M., and Weiss, P. S. Real-Time Measurements of Conductance Switching and Motion of

Single Oligo(Phenylene Ethynylene) Molecules. *J. Am. Chem. Soc.* **2007**, *129*, 10352-10353.

42. Han, P., Kurland, A. R., Giordano, A. N., Nanayakkara, S. U., Blake, M. M., Pochas, C. M., and Weiss, P. S. Heads and Tails: Simultaneous Exposed and Buried Interface Imaging of Monolayers. *ACS Nano* **2009**, *3*, 3115-3121.

43. Gou, H. L., Xu, J. J., Xia, X. H., and Chen, H. Y. Air Plasma Assisting Microcontact Deprinting and Printing for Gold Thin Film and Pdms Patterns. *ACS Appl. Mater. Interfaces* **2010**, *2*, 1324-1330.

44. Schueller, O. J. A., Duffy, D. C., Rogers, J. A., Brittain, S. T., and Whitesides, G. M. Reconfigurable Diffraction Gratings Based on Elastomeric Microfluidic Devices. *Sens. Actuat. A-Phys.* **1999**, *78*, 149-159.

45. Duffy, D. C., Schueller, O. J. A., Brittain, S. T., and Whitesides, G. M. Rapid Prototyping of Microfluidic Switches in Poly(Dimethyl Siloxane) and Their Actuation by Electro-Osmotic Flow. *J. Micromech. Microeng.* **1999**, *9*, 211-217.

46. Pale-Grosdemange, C., Simon, E. S., Prime, K. L., and Whitesides, G. M. Formation of Self-Assembled Monolayers by Chemisorption of Derivatives of Oligo(Ethylene Glycol) of Structure $HS(CH_2)_{11}(OCH_2CH_2)_mOH$ on Gold. *J. Am. Chem. Soc.* **1991**, *113*, 12-20.

47. Dameron, A. A., Hampton, J. R., Smith, R. K., Mullen, T. J., Gillmor, S. D., and Weiss, P. S. Microdisplacement Printing. *Nano Lett.* **2005**, *5*, 1834-1837.

48. Stranick, S. J., Kamna, M. M., and Weiss, P. S. Interactions and Dynamics of Benzene on Cu(111) at Low-Temperature. *Surf. Sci.* **1995**, *338*, 41-59.

Chapter 6

Conclusions and Future Prospects

6.1 Conclusions

The works presented in this dissertation have focused on utilizing self-assembled monolayers as molecular building blocks to create small-molecule-functionalized surfaces and nano- and microscale patterned platforms for biological investigations and engineering applications. Chapter 1 provided basic knowledge of self-assembled monolayers and experimental techniques necessary for all studies. Chapter 2 described the significance of small molecules in cell signaling, neuroscience, and pharmacological developments. The requirements and challenges of immobilizing small molecules on substrates for biomolecular recognition were discussed. In this chapter, initiative works from our group to develop methods for small-molecule-derivatized surfaces capable of selective capturing large-biomolecule partners were reviewed. Serotonergic neurotransmission was an initial target system for directing the development of functionalized substrates. Selectivity, accessibility, and bioactivity of immobilized molecules were addressed based on insertion-directed self-assembled chemistry of oligo(ethylene glycol)alkanethiols and surface chemical functionalization using neurotransmitters and their biological precursors. The functionalized surfaces exhibit specific biorecognition to biological targets, including antibodies and native membrane-associated receptors.

In chapter 3, small-molecule-functionalized surfaces were utilized to study the interactions of bound-ligands, mimicking endogenous 5-HT neurotransmitters, and their G-protein-coupled receptors in a real-time, label-free manner. The interactions of 5-HT_{1A} receptors with 5-HTP-functionalized surfaces were examined by QCM to extract key binding parameters, including equilibrium dissociation constants and binding rate constants. These values are comparable to previous literatures in other GPCR systems. This binding information demonstrates that this platform is a suitable alternative for receptor binding studies, which are conventionally carried out by labeling methodologies. Moreover, this strategy can be extended to other neurotransmitters or related molecules containing an auxiliary carboxylic moiety for anchoring reactions for better understanding of cell signaling mechanisms and discovering new drugs for clinical trials.

Chapter 4 presented an experimental strategy to tune the wettability of PDMS stamp surface energies by precisely controlling oxygen plasma treatment times. This enables the use of microcontact insertion printing with polar ink molecules, notorious to hydrophobic PDMS stamp, inserted into hydrophilic host SAMs. The fabricated 5-HTP-functionalized microarrays by this strategy were able to capture serotonin-specific receptors. The result illustrates that on-chip functionalization produces low-density bioactive small-molecule patterned surfaces by microcontact insertion printing. Nonetheless, this finding suggest that printing, whether by microcontact printing, microcontact insertion printing, or other techniques, using inks and substrates having a wide range of different chemistries will benefit from careful control of PDMS surface properties to optimize ink transfer.

Chapter 5 introduced chemical lift-off lithography, a novel hybrid chemical patterning, for fabricating micro- and nanoscale resolution features. The limitations from conventional soft lithography, such as molecular ink diffusion and pattern dissolution, were overcome. Instead of direct contact printing, oxygen-plasma-treated patterned stamps remove hydroxyl-terminated oligo(ethylene glycol)alkanethiolates from preformed SAMs at the conformally contact area, creating subtractive featured SAMs. The covalent linkages between hydrophilic stamps and hydroxyl terminal groups on surfaces were anticipated to cause this physical phenomenon. Based on this hypothesis, alkanethiols containing different terminal groups, including biotin, methoxy, methyl, and amine, were tested. With this method, conventional nanolithography techniques are only required for the fabrication of stamp master molds. Once individual masters are produced, CLL can be implemented as a strategy for high-resolution, high-throughput, low-cost pattern fabrication.

6.2 Future Prospects

6.2.1 Nonspecific Adsorption Minimization

Small-molecule-functionalized surfaces in this dissertation were used as platforms to capture large-biomolecule targets and study their biomolecular interactions in a complex biological mixture. In chapter 3 and 4, nonspecific adsorption on surfaces contributes approximately 20 to 40% (in some cases) of the total binding (QCM measurements). This problem occurs especially when functionalized surfaces are used for "fishing" the target brain proteins that are embedded in lipid membranes [*1*]. The biological specimens containing heterogeneous membrane components may cause unwanted adsorption. This may partly attribute to the structural similarity of lipid bilayers and SAMs of oligo(ethylene glycol)alkanethiols. Interestingly, self-assembled monolayers have been employed as supporting layers to facilitate phospholipid leaflet formations on solid substrates [*2, 3*]. Polar phospholipid groups of lipid bilayers could have attractive dipole-dipole interactions with hydroxyl-terminated SAMs. Furthermore, the hydrocarbon backbone components of these molecules could lead to non-polar interactions. Therefore, minimizing nonspecific adsorption from these biological samples is prerequisite to avoid binding from either non-target receptors or other membrane components that do not have affinity for immobilized molecules. This is an open question for further investigations on surfaces resisting lipid membranes.

In addition to common OEG SAMs, methoxy -terminated OEG alkanethiols have been known for their better bio-resistant properties [*4-6*]. The methoxy groups exhibit the long-range repulsive electrostatic forces with fibrinogen-coated AFM tips. More

importantly, monolayers containing methoxy groups, prepared by the hydrosilylation reactions, show not only protein resistance but also cellular debris [*7*]. However, methoxy-coated SAMs have not been reported on preventing lipid bilayers or cell membranes. It is therefore promising to investigate their membrane-repellant properties.

6.2.2 Studies of Allosteric Modulation of GPCRs and LGICs via Small-Molecule-Functionalized Surfaces

In chapter 2, the allosteric modulation of GPCRs and LGICs by small molecule drugs (allosteric ligands) was mentioned. The ligands are designed to bind selectively to target receptors at allosteric sites, resulting in either potentiating or inhibiting endogenous ligand binding at orthosteric sites (Figure 6-1). Investigating the effects of allosteric modulation is a mandatory process in drug discovery. Instead of conventional radioligand binding assays, small-molecule-functionalized surfaces offer an opportunity to study such effects with a label-free manner. The orthosteric ligands can be tethered on surfaces and their binding affinity, influenced by allosteric modulators, can be evaluated by measuring the change in transducer signals (*i.e.*, QCM, SPR) as a function of modulator concentrations [*8*].

In the ternary model on a surface (Figure 6-2), the equilibrium dissociation constant (K_d) of a surface-bound ligand (L^S) and a receptor (R) can be modulated by the binding of an allosteric ligand (A) in solution at an allosteric site, resulting in either positive ($\alpha < 1$) or negative ($\alpha > 1$) cooperativity. Since our developed methods can be

extended to other small molecule systems, analyzing drug candidates with this strategy can support the fast-growing need in modern drug developments.

6.2.3 Investigating Chemistry and Physics of Chemical Lift-Off Lithography

In chapter 5, self-assembled monolayers were patterned by selectively removing alkanethiolates from preformed SAMs using oxygen-plasma-treated PDMS stamp. We initially hypothesized that the contact reactions at stamp-SAM interfaces are sufficiently strong to lift off not only molecules in the monolayers but also one layer of gold atoms from the substrates. We anticipated that silanol groups on activated-PDMS stamps and hydroxyl terminal groups on SAMs form strong covalent bonds with nucleophilic substitution reactions and water condensations. To test this hypothesis, we performed a systematic study by using alkanethiols containing nucleophilic terminal groups. Preliminary results show that oxygen-plasma-treated stamps can also remove amine-terminated oligo(ethylene glycol)alkanethiolates as shown by AFM topographic image (Figure 6-3). Based on this convincing data, further detail investigations of the types of chemical bonds at interfaces is necessary to elucidate the actual mechanisms of chemical lift-off processes. Techniques for investigations at interfacial regions include sum frequency generation spectroscopy, PM-IRRAS, and attenuated total reflection spectroscopy.

Since a layer of Au atoms is removed by this process, it is essential to deeply understand the roles of surface lattices, surface defects, and surface roughness on Au-Au bond breakage. Finally, the chemical and physical parameters, including SAM

crystallinity, pH, temperature, alkyl-chain length, different metal substrates are also open for full-detail investigations.

6.3 Appendix A

6.3.1 Kinetic Derivation of Ligand Binding

By considering the simplest case of 1:1 stoichiometry, the binding rate of surface-bound ligand (L^s) and receptor (R) as a function of time (t) can be described as:

$$R + L^s \underset{k_{off}}{\overset{k_{on}}{\rightleftharpoons}} R - L^s \tag{6-1}$$

$$\frac{d[R - L^s]_t}{dt} = k_{on}[R][L^s]_t - k_{off}[R - L^s]_t, \tag{6-2}$$

where k_{on} and k_{off} are the association and dissociation rate constants, respectively.

$$[L^s]_t = [L^s]_0 - [R - L^s]_t \tag{6-3}$$

Substituting Eq. 6-3 (mass balance) in Eq. 6-2 yields Eq. 6-4, which can be rearranged to the form of Eq. 6-5.

$$\frac{d[R - L^s]_t}{dt} = k_{on}[R]\{[L^s]_0 - [R - L^s]_t\} - k_{off}[R - L^s]_t \tag{6-4}$$

$$\frac{d[R - L^s]_t}{dt} = k_{on}[R][L^s]_0 - \{k_{on}[R] + k_{off}\}[R - L^s]_t \tag{6-5}$$

We can define a new term, called observed binding rate (k_s), as described in Eq. 6-6.

$$k_s = k_{on}[R] + k_{off} \tag{6-6}$$

Solving Eq. 6-5 gives the concentration of ligand-receptor complexes as a function of time, which can be described as:

$$[R - L^s]_t = \frac{k_{on}[R][L^s]_0}{k_s}(1 - e^{-k_s t}). \tag{6-7}$$

The first term of Eq. 6-7 is called equilibrium binding of receptor concentration, which can be defined as:

$$[R - L^s]_{eq} = \frac{k_{on}[R][L^s]_0}{k_{on}[R] + k_{off}}. \tag{6-8}$$

In a binding experiment, $[R - L^s]_t$ refers to the change in the transducer signal (ΔX) due to the binding events and $[R - L^s]_{eq}$ refers to the change in the signal at equilibrium (ΔX_e), as shown in Eq. 6-9.

$$\Delta X = \Delta X_e(1 - e^{-k_s t}) \tag{6-9}$$

Rearranging Eq. 6-8 also gives Scatchard equation (Eq. 6-10) and Langmuir isotherm (Eq. 6-11), where K_d is the dissociation equilibrium constant (k_{off}/k_{on}).

$$\frac{[R - L^s]_{eq}}{[R]} = -\frac{1}{K_d}[R - L^s]_{eq} + \frac{1}{K_d}[L^s]_0 \tag{6-10}$$

$$\frac{[R - L^s]_{eq}}{[L^s]_0} = \frac{[R]}{K_d + [R]} \tag{6-11}$$

6.4 Figures

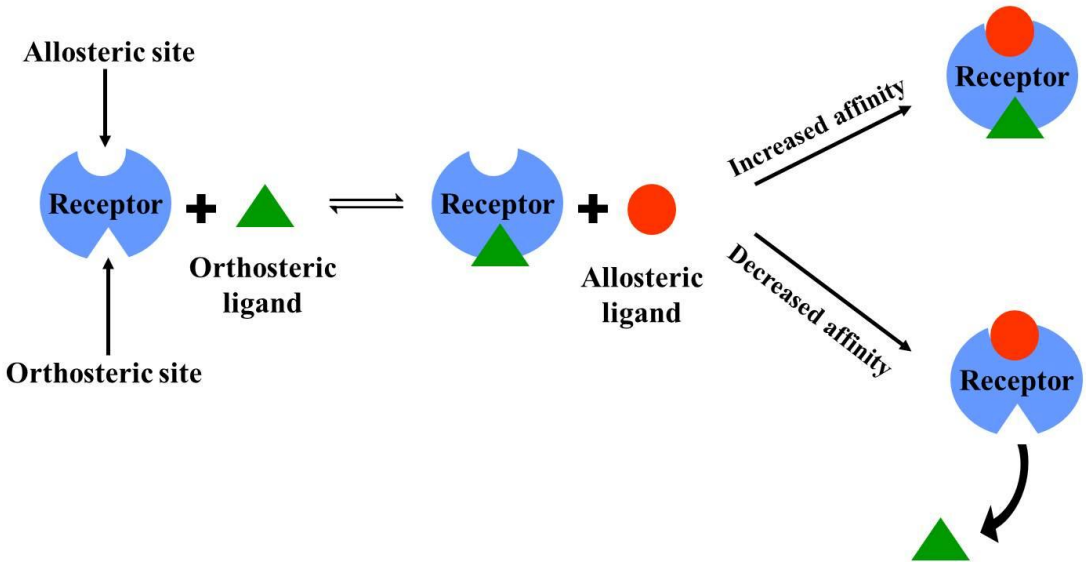

Figure 6-1. **Schematic representation of the allosteric modulation of a receptor.** The interactions of an allosteric ligand (red circle) at an allosteric site can either increase or decrease the binding affnity of an endogenous ligand (green triangle) and a receptor (blue shape) at an orthosteric site.

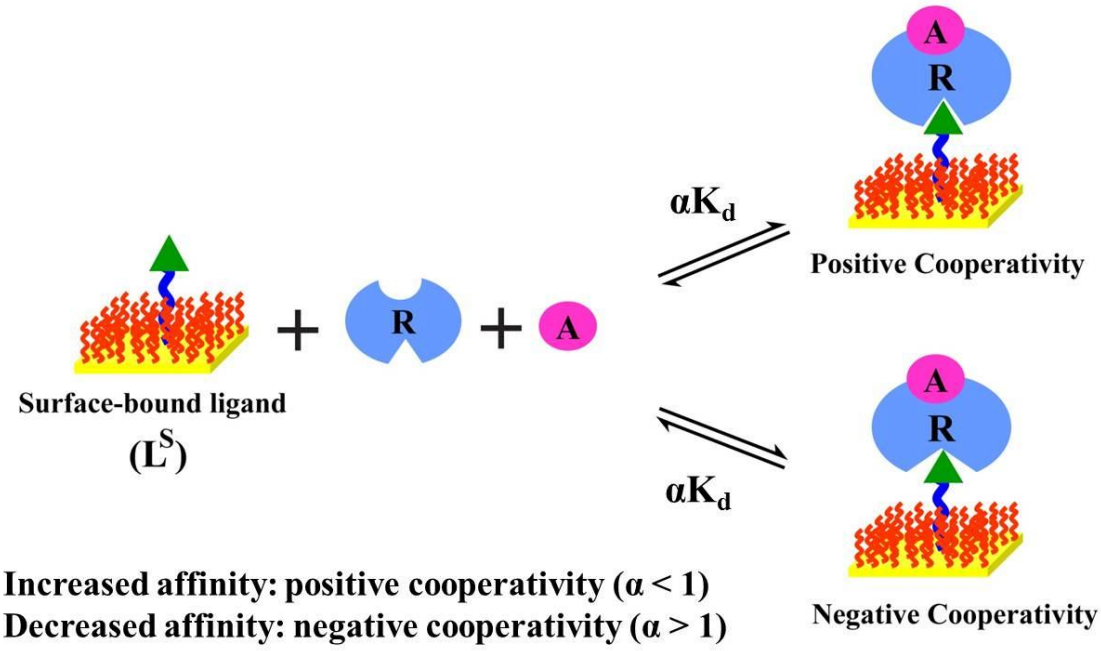

Figure 6-2. **The ternary model of a surface-bound ligand (L^s) and a modulated receptor (R).** Small-molecule-functionalized surfaces can be utilized as platforms to investigate the allosteric modulation. Changing in the binding affinity (K_d) of a receptor and a surface-bound ligand due to an allosteric ligand can be monitored by transducer biosensors, resulting in an evaluation of positive ($\alpha < 1$) and negative ($\alpha > 1$) cooperativities.

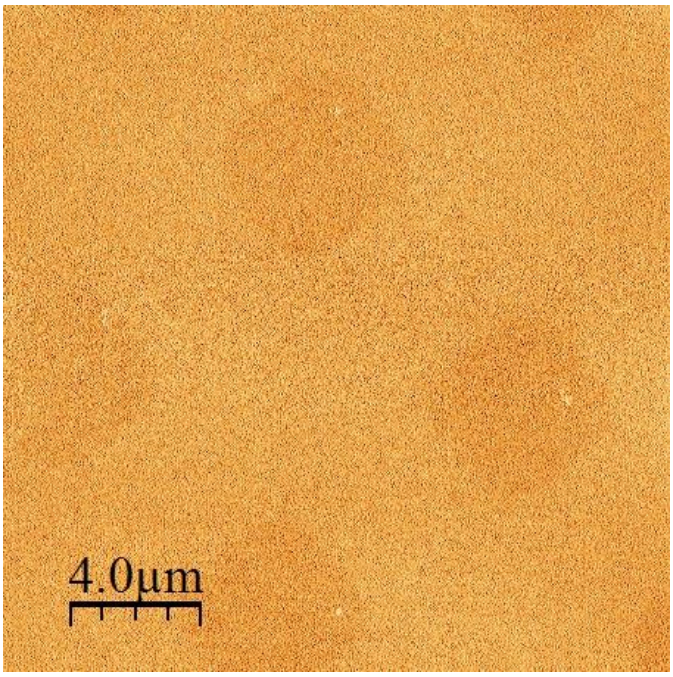

Figure 6-3. **Atomic force microscope topgraphic image of chemical lift-off lithography on amine-terminated oligo(ethylene glycol)alkanethiolate (AEG) SAMs.** Self-assembled monolayers of AEG on Au substrates were investigated using chemical lift-off lithography and oxygen-plasma-treated stamps with 5-µm x 5-µm protuding posts.

6.5 References

1. Kroger, D., Hucho, F., and Vogel, H. Ligand Binding to Nicotinic Acetylcholine Receptor Investigated by Surface Plasmon Resonance. *Anal. Chem.* **1999**, *71*, 3157-3165.
2. Castellana, E. T., and Cremer, P. S. Solid Supported Lipid Bilayers: From Biophysical Studies to Sensor Design. *Surf. Sci. Rep.* **2006**, *61*, 429-444.
3. Strulson, M. K., and Maurer, J. A. Mechanistic Insight into Patterned Supported Lipid Bilayer Self-Assembly. *Langmuir* **2012**, *28*, 13652-13659.
4. Hoffmann, C., and Tovar, G. E. M. Mixed Self-Assembled Monolayers (SAMs) Consisting of Methoxy-Tri(Ethylene Glycol)-Terminated and Alkyl-Terminated Dimethylchlorosilanes Control the Non-Specific Adsorption of Proteins at Oxidic Surfaces. *J. Colloid Interface Sci.* **2006**, *295*, 427-435.
5. Feldman, K., Hähner, G., Spencer, N. D., Harder, P., and Grunze, M. Probing Resistance to Protein Adsorption of Oligo(Ethylene Glycol)-Terminated Self-Assembled Monolayers by Scanning Force Microscopy. *J. Am. Chem. Soc.* **1999**, *121*, 10134-10141.
6. Skoda, M. W. A., Schreiber, F., Jacobs, R. A. J., Webster, J. R. P., Wolff, M., Dahint, R., Schwendel, D., and Grunze, M. Protein Density Profile at the Interface of Water with Oligo(Ethylene Glycol) Self-Assembled Monolayers. *Langmuir* **2009**, *25*, 4056-4064.
7. Yam, C. M., Lopez-Romero, J. M., Gu, J. H., and Cai, C. Z. Protein-Resistant Monolayers Prepared by Hydrosilylation of Alpha-Oligo(Ethylene Glycol)-

Omega-Alkenes on Hydrogen-Terminated Silicon (111) Surfaces. *Chem. Commun.* **2004**, 2510-2511.

8. Nieba, L., Krebber, A., and Pluckthun, A. Competition Biacore for Measuring True Affinities: Large Differences from Values Determined from Binding Kinetics. *Anal. Biochem.* **1996**, *234*, 155-165.

CURRICULUM VITAE

Sarawut Cheunkar

Education

Ph.D., in Chemistry, The Pennsylvania State University May 2013
University Park, Pennsylvania, United States
Advisors: Professors Anne M. Andrews and Paul S. Weiss
Dissertation Title: Molecular Self-Assembly for Biological Investigations and Nanoscale Lithography

B.S., in Chemistry (2nd Class Honor), Mahidol University March 2004
Bangkok, Thailand
Advisors: Professors Sauvarop Bualek-Limcharoen and Toemsak Srikhirin
Undergraduate Project: Spectroscopic Study of Photoinduced Isomerization of a Homopolymer and a Copolymer Based on 4'-(6-acryloxy)hexyloxy-4-methoxyazobenzene and acrylic acid

Professional Experiences

Staff Research Associate, University of California, Los Angeles 2010-2012
Advisors: Professors Anne M. Andrews and Paul S. Weiss

Graduate Research Assistant, The Pennsylvania State University 2006-2009
Advisors: Professors Anne M. Andrews and Paul S. Weiss

Teaching Assistant, The Pennsylvania State University 2007-2008
Analytical Instructional Laboratories

Teaching Assistant, Mahidol University 2004-2005
Physical Chemistry Laboratory

Awards and Honors

Royal Thai Government Scholarship 2006-2011